Coastal and Estuarine Morphology Changes Induced by the 2011 Tsunami and Its Recovery Process

Coastal and Estuarine Morphology Changes Induced by the 2011 Tsunami and Its Recovery Process

(2011 年東日本大震災津波による海浜・河口の地形変化と回復過程)

by

Vo Cong Hoang

Supervisor

Professor Hitoshi Tanaka

A dissertation submitted in partial fulfillment of the requirements for the degree of Doctor of Engineering

Graduate School of Engineering

Tohoku University

Japan

August 2016

Abstract

Coastal and Estuarine Morphology Changes Induced by the 2011 Tsunami and Its Recovery Process

Vo Cong Hoang

The 8.9 magnitude earthquake, which happened on March 11, 2011, triggered the huge tsunami approaching the northern coast of Japan. The tsunami, the maximum height of which was reported to be 40 m, caused significant changes to the coastal area in northeastern Japan. This study attempts to clarify the damages of morphology along Sendai Coast in Miyagi Prefecture and its recovery process through analyses of the aerial photographs, the analytical solutions of one-line model, and the Empirical Orthogonal Function (EOF). The recovery of morphology is presented in terms of temporal scale (short-term and long-term) and spatial scale (small area and large area). Results of this study indicate that the tsunami caused severe damages of morphology, the coast was significantly eroded and the sand barriers in front of lagoons and the sandspits at the river mouths were swashed. The breaching of sandy coasts was observed at several places. Due to the existing of breaching, concave shorelines were observed commonly along the affected coast right after the tsunami. The recovery of morphology has different aspects, fast recovery at places with sufficient long adjacent sandy coasts, and very slow or no recovery at places without adjacent sandy coasts. At the fast recovery places, during the recovery process the sandy coasts adjacent to breaching were eroded. The erosion was propagating along the coast with the propagated distance proportional to the square root of elapsed time. A new approach determining value of the diffusion coefficient from measured data and analytical solution of one-line model is introduced. Moreover, in the subsequent recovery, the intrusion into river mouths of sandspit was observed. The scouring river mouth bed deeper than the depth of closure has been pointed out as the main cause of the sandspit intrusion after the tsunami. Results from EOF analysis indicate that during the subsequent recovery process, the recovery of morphology at the places where were significantly damaged by the tsunami, was the most dominant process. A new analytical solution of one-line model, which can describe the evolution of concave

shoreline in case of rigid boundaries at both ends, is introduced. This equation reveals the effects of coastal structures that are considered as rigid boundaries on the recovery process. When the value of dimensionless total length of the adjacent sandy coast bounded by the rigid boundaries to the concave width, L_S*, gets larger, the value of dimensionless recovery time, t*, gets smaller. Discussion on the evolution of shoreline position described by the analytical solutions of one-line model for cases without and with rigid boundaries, has been also given. When the value of dimensionless length of the sandy coast bounded by the rigid boundaries, L*, gets larger, the dimensionless shoreline position, y*, given by the solution with rigid boundaries is asymptotic to the one given by the solution for case without rigid boundaries. In addition, a new analytical solution that can evaluate the proportional backfilled area in the concave portion is also given. The introduced solutions are not only the findings and interests in research activities, but also important in the engineering application (e.g., beach nourishment). The investigation on long-term morphological recovery indicates that the dominant processes, which were carried out in the study on subsequent recovery, are still remained. However, their contribution rates (the level of importance) have been changed. The littoral system of the northern part of Sendai Coast has changed significantly between before and after the tsunami, and between the short-term and the long-term recovery after the tsunami. The recommendations of the present study have been also given. The approach of classification small and large area, short-term and long-term in this study would be useful to apply in the areas which have similar characteristics. For engineering application, the fresh-sea water boundary moves upstream once happening the sandspit intrusion, hence the external wave forces need to be taken into account when implementing design of structures at river mouth area. In addition, the estimated values of diffusion coefficient would be useful for engineering application too. However, several things need to be improved in the future studies. Firstly, the introduced analytical solutions, which can deal with case of concave shoreline with symmetric rigid boundaries, need to be extensionally developed. So, they can be applied for the cases with asymmetric adjacent sandy coasts, or non-constant depth of closure, or non-uniform shape of concave portion. Moreover, the evolution shoreline position during the recovery process and the connections with bathymetry change and the sediment budget need to be evaluated. Last but not least, a numerical model is also necessary to be developed for predicting the evolution of shoreline evolution in the future.

Acknowledgements

I would like to express my deepest gratitude to my supervisor Professor Hitoshi Tanaka for his knowledges, valuable advices and encouragements throughout the period of my studying at Tohoku University. He has provided me invaluable insights and precious guidance. Without his helps in both academic and personal concerns during my stay in Japan, this research could not have been completed.

I would like to extend my sincere gratitude and acknowledgements to the members of my dissertation committee, Professor So Kazama, Associate Professor Makoto Umeda and Associate Professor Keiko Udo for their patient reading, and great suggestions and comments.

I would also like to convey my special thanks to Assistant Professor Yuta Mitobe for his great support during my time at the Hydrodynamics Environmental Laboratory, especially the analysis of aerial photograph and programing.

I would also like to take this opportunity to acknowledge the Government of Japan for awarding me MEXT scholarship. Without this financial support, my studying in Japan and this study would not become true.

Last but not least, I would like to dedicate this dissertation to my parents with great respect for their immense love and spiritual supports through my education life, to my parents in law for their encouragements and great support before and after 2009 when I left Vietnam for studying abroad. Finally, to my beloved wife Nguyen Lan Anh, for her endless loves, encouragements, great supports and taking care alone the family and children in such many years, to lovely daughter Vo Ngoc Minh who I left when she was only six months old, to lovely son Vo Minh Hoang, who I was first time meeting him at the exist gate of Narita Airport, when he has already been almost five months old.

Aobayama, Sendai, August 8, 2016

Vo Cong Hoang

To my family,

Lan Anh,
Ngoc Minh, and Minh Hoang

Table of Contents

CHAPTER 3

STUDY AREAS, DATA COLLECTION AND METHODOLOGIES

CHAPTER 4

MORPHOLOGICAL CHANGES AND SUBSEQUENT RECOVERY AT THE RIVER MOUTHS AND BREACHING OF SANDY COASTS

CHAPTER 5

SUBSEQUENT RECOVERY OF MORPHOLOGY ON THE NORTHERN PART OF SENDAI COAST

CHAPTER 6

LONG-TERM RECOVERY OF TSUNAMI-INDUCED CONCAVE SHORELINE

CHAPTER 7

LONG-TERM RECOVERY OF MORPHOLOGY ON THE NORTHERN PART OF SENDAI COAST

CHAPTER 8

CONCLUSIONS AND RECOMMENDATIONS

List of Figures

List of Tables

CHAPTER 1

INTRODUCTION

1.1 Background

On March 11, 2011, the 8.9-magnitude Tohoku Earthquake triggered giant tsunami waves which reached heights of 40 m above sea-level in Iwate Prefecture, Japan (Mori et al., 2012). The tsunami not only caused severe damages to the infrastructures along the northeast coast of Japan but also resulted in massive changes of coastal and estuarine morphology. After the 2011 tsunami, there have been studies on the changes and recovery process of morphology in Sendai Bay area, e.g., Tanaka et al. (2012, 2014a, b), Tappin et al. (2012), and Udo et al. (2012). Among these studies, Tanaka et al. (2012) reported the significant changes of coastal and riverine morphology in Miyagi Prefecture such as erosion of sandy beaches, disappearance of sand barriers in front of lagoons, flushing of sandspits in front of river mouths and the breaching of sandy beaches at the locations of old river mouths. As a result, concave shorelines were observed at several places after the tsunami (Tanaka et al., 2012). One of the important factors leading to the fast or slow recovery of morphology in these areas is the sediment supply from adjacent sandy coasts. The recovery of morphology at the river mouths (Kitakami, Naruse, Natori, Abukuma), which have insufficient sediment supply from adjacent sandy coasts, was very slow. In contrast, concave shorelines at the Nanakita River mouth, at breaching of sandy coasts at Akaiko and Yamamoto, which have sufficient sediment supply from adjacent sandy coasts, recovered comparatively fast. However, the erosion of sandy coasts on both sides of the concave portion was also observed during the recovery process. Sediment from adjacent coasts was transported into the concave portion, and led to the accretion of shoreline in this area. The erosion firstly happened on the parts of the coasts which are next to the concave portion. Subsequently, it was propagating along the coast. Moreover, the intrusion of sandspit into the river mouth area was also observed during the recovery

process. The above phenomenon reveals the sink effect at river mouth areas after the severe damages induced by the tsunami.

Several years have passed since the tsunami occurrence, the damages of morphology after such huge tsunami at the river mouths of many areas are still remaining, while at some other river mouths morphology has largely recovered. Thus, several questions were prompted. How were the detailed damages of morphology of the coast in Miyagi Prefecture induced by the tsunami? How were the behaviors of morphology in short-term and in long-term recovery after the tsunami? Last but not least, how were the effects of coastal structures on the recovery process?

1.2 Objectives of study

1.2.1 Main objective

The frequency of occurrence of such 2011 tsunami is extremely low, and so far the understanding of the morphological recovery after such severe damages is insufficient. Hence, findings from the study on the recovery of morphology will provide key information for the preparation and recovery planning for future similar disasters. Moreover, these findings on the recovery of riverine morphology and relevant phenomenon are not only important for coastal and riverine management in short-term or long-term periods but also very useful for many other human activities such as navigation, fishery, river mouth environmental concerns, especially the ones adjacent to lagoon.

Taken together, this study clarifies the changes of coastal and estuarine morphology on Sendai Coast, Miyagi Prefecture, Japan induced by the 2011 tsunami and its recovery process.

1.2.2 Specific objectives

The main objective of this study can be specified into details as following,

1. Revealing the changes of coastal and estuarine morphology (damages) induced by the tsunami using aerial photographs.
2. Clarifying the subsequent recovery process of morphology at particular severely damaged areas such as river mouths or breaching of sandy coasts and relevant phenomenon raised during the recovery process like sandspit intrusion into river mouth, erosion propagation of sandy coast based on the analysis of aerial photographs and analytical solutions of one-line model.

3 Analyzing the behavior of subsequent recovery process of morphology in a large scale area, from Sendai Port to Natori River mouth, including severely damaged areas and coastal structures, etc. using aerial photographs and EOF analysis.

4 Revealing the recovery of concave shoreline at river mouths and breaching of sandy coasts with considering the role of coastal structures as rigid boundaries using aerial photographs and analytical solutions of one-line model.

5 Extending the analyzation on the long-term recovery of morphology in the large scale area using extracted shoreline positions and EOF analysis. Making the comparative study on the evolution of morphology before and after the tsunami, and between the short-term and long-term recovery after the tsunami.

1.3 Classification on the temporal and spatial scales of recovery

The tsunami induced significant changes of morphology along the northeast coast of Japan. If only a particular area is emphasized, then the river mouths, lagoons and breaching of sandy coasts were among the most severely damaged areas. In addition, along the affected area, there are sandy coasts that are bounded by coastal structures and they include the above mentioned river mouths, lagoons and breaching of sandy coasts. Therefore in this dissertation, the recovery of morphology will be clarified in terms of temporal and spatial scales. The classification is schematically represented by the matrix in Fig. 1.1.

On the temporal scale, there are recoveries in short-term and long-term, whereas on the spatial scale, there are small area and large area. More quantitative explanations on this classification will be given in Section 4.5.

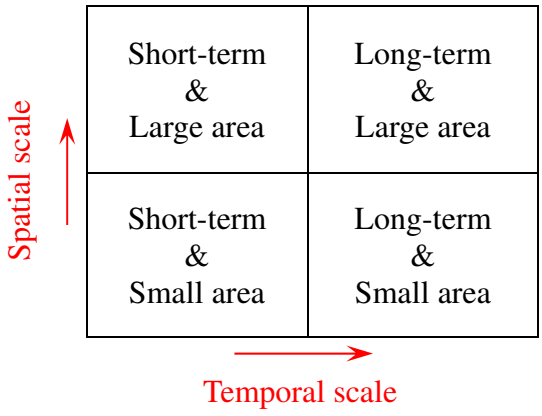

Fig. 1.1 Schematic classification of recovery of morphology in terms of temporal and spatial scales

With respect to the above classification, the recovery of morphology will be presented in terms of small area and short-term (Chapter 4); large area and short-term (Chapter 5); small area and long-term (Chapter 6); and large area and long-term (Chapter 7).

1.4 Outline of the dissertation

The framework of this dissertation is shown in Fig. 1.2. The dissertation comprises eight chapters. Briefings on these chapters are presented as following,

Chapter 1: This chapter introduces the background, the necessities as well as the aims of this study.

Chapter 2: This chapter reviews the existing literature on topics relevant to coastal morphological changes and recovery in normal conditions including tidal inlet, estuary, and in relating to the natural disaster such as tsunami; shoreline change analysis using aerial photograph, satellite image as well as video-monitoring camera system; EOF analysis; Even and Odd analysis; sediment budget analysis; shoreline change modeling based on one-line theory.

Chapter 3: This chapter provides information about study areas including the river mouths, the breaching of sandy coasts and sandy beach along the coast of Miyagi Prefecture; and data collection as well as the methodologies of aerial photograph analysis, EOF analysis and obtaining analytical solution of one-line model.

Chapter 4: This chapter reveals the changes of morphology at the river mouths and breaching of sandy coasts along the Miyagi Prefecture. Moreover, the erosion propagation along the beaches adjacent to concave shorelines and the sandspit intrusion into river mouths, whose phenomenon has been raised up during the subsequent recovery of morphology, are also investigated.

Chapter 5: In this chapter, the EOF analysis is utilized to reveal the behavior of subsequent morphology recovery in a larger area which includes the severely damaged areas such as river mouths and sandy coast (the coast from Sendai Port to the Natori River mouth).

Chapter 6: This chapter clarifies the long-term recovery of morphology at a small area. The existing and new developed analytical solutions of one-line model are utilized to present the evolution of concave shorelines after the tsunami.

Chapter 7: In this chapter, the long-term recovery of morphology on the large area is analyzed. The EOF analysis is employed again to extensionally evaluate and reveal the behavior of morphology recovery.

Chapter 8: This chapter presents the overall conclusions of this study and the recommendations for engineering applications as well as future studies.

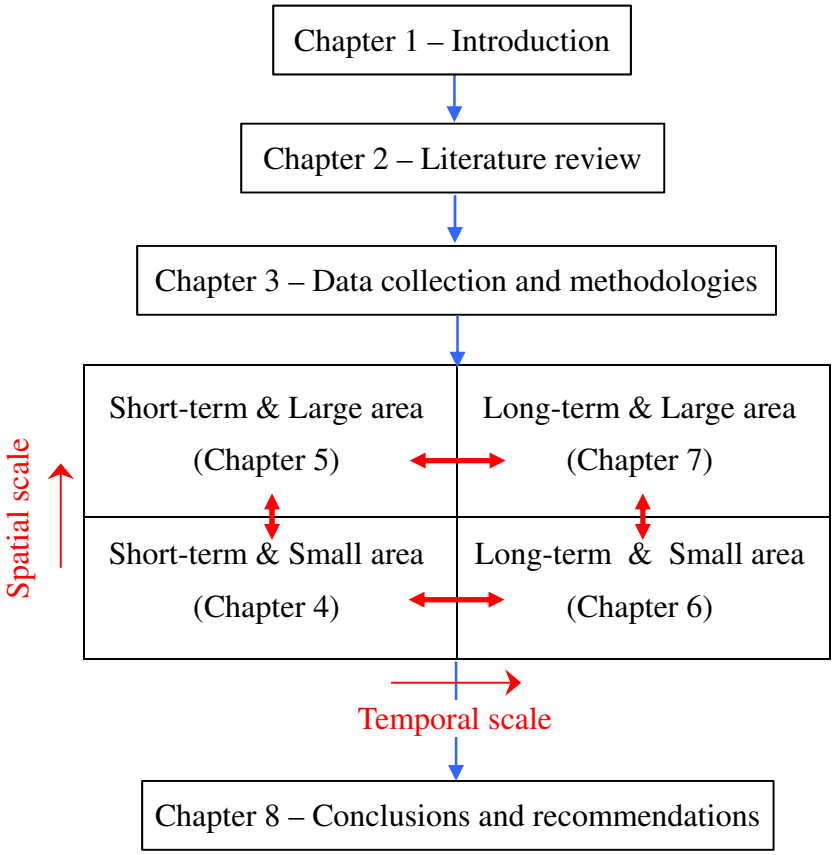

Fig. 1.2 Framework of the dissertation

In Fig. 1.2, the red double-headed arrow lines represent interrelationships between the chapters. More descriptions on these interrelationships will be given in Section 4.5.

CHAPTER 2

LITERATURE REVIEW

2.1 Coastal morphology changes

Coastal geomorphology (or morphology) is the study of the morphological development and evolution of the coast as it acts under the influence of winds, waves, currents, and sea level changes (Leatherman, 1994). Besides, the evolution driven by natural processes, coastal morphology could be extremely changed induced by coastal hazards such as tsunami, storm, and others (Masselink and Gehrels, 2014). With almost haft (44 %) of the 1994's world population live 100 km of a coastline, and approximately 44% (2.45 billions) within 150 km of a coastline (Tobler et al., 1995; Cohen et al., 1997). The rate of population growth in coastal area is accelerating, hence studying the evolution of coastal morphology driven by natural processes or coastal hazards would be very important and useful.

2.1.1 Tidal inlet morphology

A tidal inlet is a short, narrow waterway connecting a bay, estuary, or similar body of water with a larger water body such as a sea or ocean. Tidal currents maintain the main channel of a tidal inlet (FitzGerald, 2005; Kraus, 2010). In order to maintain the cross-sectional area, location, and orientation of the channel, the activities such as channel dredging, construction of jetty, breakwater for disrupt natural sediment transport, need to be conducted. There have been studies on the evolution of tidal inlets due to its importance in navigation, especially the tidal inlets in the U.S. such as (e.g., Oertel 1975; Hubbard 1975; Hayes 1980; Kana et al. 1999). It is common to observe the sand deposition landward of the delta driven by the flood-tidal currents (flood-tidal deltas) and seaward sides of the inlet driven by the ebb-tidal currents (ebb-tidal delta).

Figure 2 sketches the features of a natural tidal inlet that has been given by Kraus (2010). The morphology of tidal inlet has several components (FitzGerald, 2005).

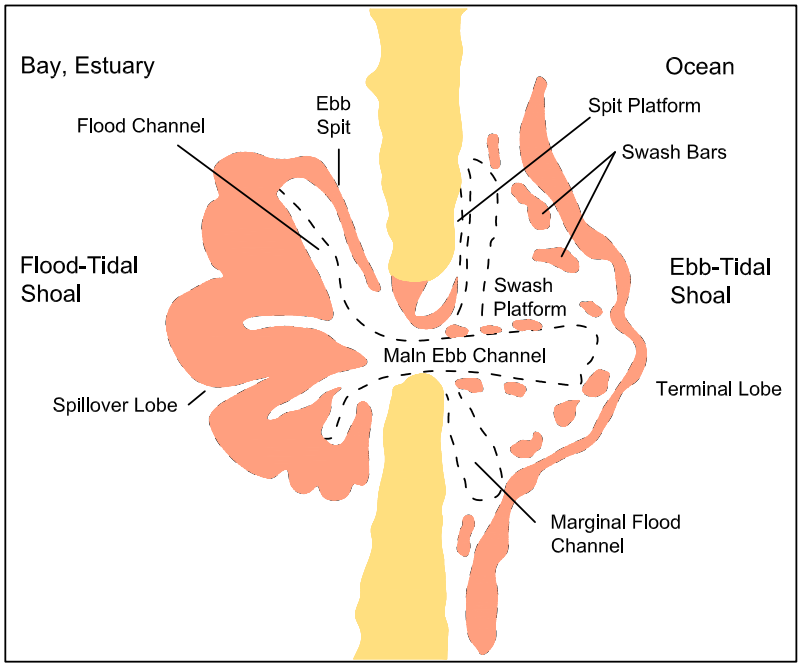

Fig. 2.1 Definition sketch for tidal inlet morphology (Kraus, 2010)

- Flood-tidal deltas: Flood ramp, flood channels, ebb shield, ebb spits, spillover lobes.
- Ebb-tidal deltas: Main ebb channel, terminal lobe, swash platform, swash bars, marginal-flood channels.

2.1.2 Estuary morphology

Estuary is formed at the mouth of river. It is the boundary zone between the sea and the land. The estuary is controlled by a combination of hydrodynamics conditions, the sedimentary environment and sediment supply and the underlying geology (Moore et al, 2009). In some cases, river mouth has the same characteristics with tidal inlet. The distinct difference between tidal inlet and estuary is that river mouth is supplied with sediment from river discharge, while tidal inlet is supplied with limited sediment from the longshore sediment (ebb tide delta). The supplement of sediment from river has been leading to the developing of river delta toward the sea. The estuary can be classified into several types based on different schemes. The most three common classification schemes are geomorphology, vertical structure of salinity and tidal range (Fairbridge, 1980).

Figure 2.2 presents the types of estuaries based on the scheme of geomorphology given in Valle-Levinson (2010).

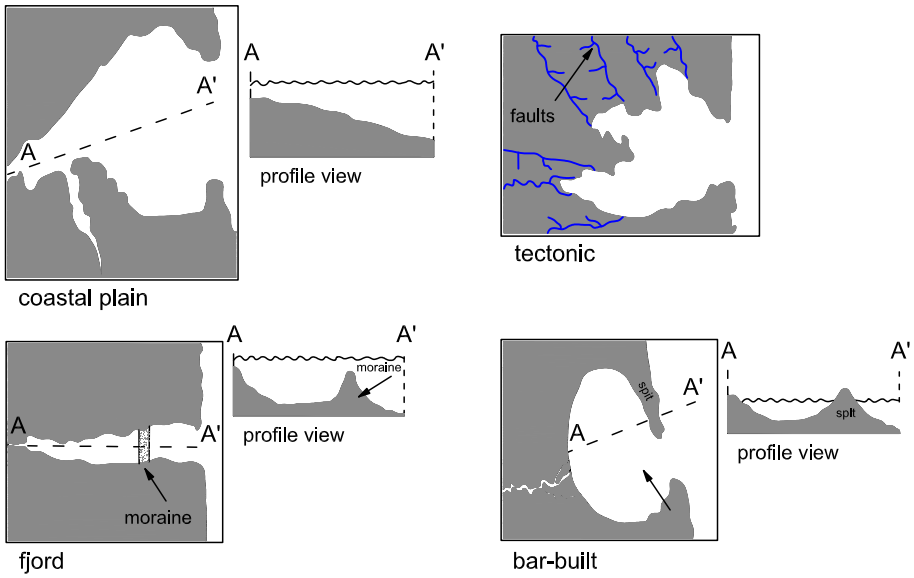

Fig. 2.2 Classification of estuaries on the basic of geomorphology (Valle-Levinson, 2010)

Wright (1976) presented about the evolution of morphology at the Shoalhaven River mouth from observed data. This river mouth is dominated by wave action. Figure 2.3 shows the morphology of the Shoalhaven River mouth in Wright (1976). This is a typical type of wave dominated river mouth morphology.

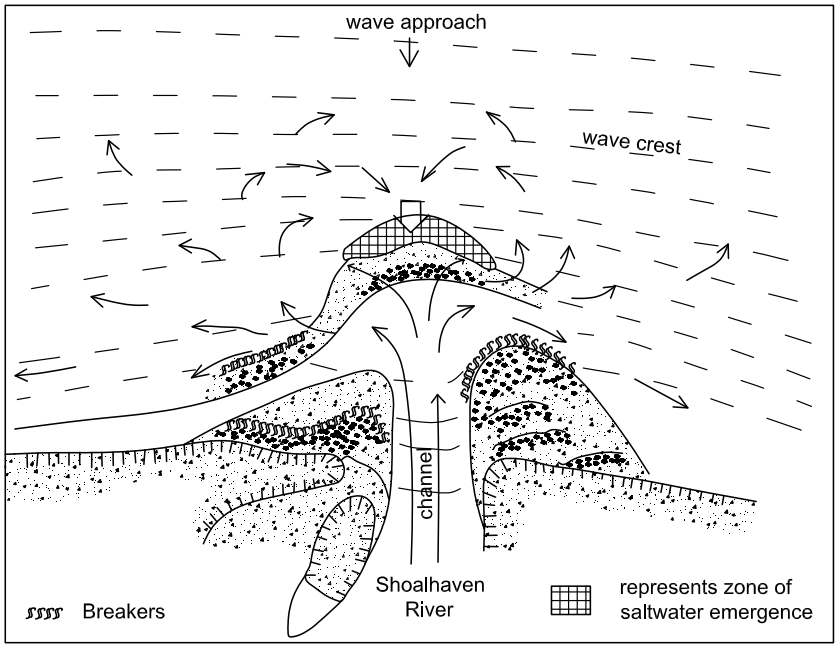

Fig. 2.3 Horizontal surface outflow patterns and plan-view morphology at the Shoalhaven River mouth (dominated by wave) (Wright, 1976)

Deguchi and Sawaragi (1988) experimentally investigated the influences of coastal structures on a discharged flow and a depositional pattern of discharged sediment from a river. A numerical model for the prediction of depositional pattern of discharged sediment was also developed based on the experimental results.

Moore et al. (2009) studied the spatial distribution of tidal distortion and asymmetry in the Dee estuary, U.K. The influence of the asymmetry in the tide (unequal ebb and flood duration) to the residual sediment transport and morphological changes in estuaries has been presented. In addition, a 3-dimensional numerical model has been developed to investigate that. High resolution LIDAR surveys were used to underpin and explain the numerical modelling.

2.1.3 Morphology change induced by the tsunami and its recovery process

Tsunami, which is a Japanese word for "harbor wave", is also known as a seismic sea wave. It is a series of sea waves which can be generated by any significant displacement of water in ocean or large lake. Besides, the significant displacement created by volcanic eruptions, landslides, etc., the movement of tectonic plates under the ocean floor during an earthquake is the most commonly abrupt disturbance to generate tsunami. There is a long history of tsunami on earth, there have been many tsunamis in the past (ITIC, NCEI). The tsunami wave height when reaching the shore and tsunami run-up of ancient tsunamis now can be approximately estimated from sediment deposition layers (e.g., Goto et al., 2014; Takashimizu et al., 2012; Minoura et al. 2001), while the recent tsunamis have been well recorded. The most destructive tsunamis in the past two decades are The 2004 Indian Ocean tsunami followed by the magnitude 9.1 (Mw) earthquake, The 2010 Chile tsunami generated by the magnitude 8.8 (Mw) earthquake, and The 2011 Tohoku tsunami triggered by the 9.0 (Mw) earthquake. The reoccurrence frequencies of these tsunamis are extremely low. Giant tsunamis not only knock down infrastructure, destroy human life but also cause significant changes of coastal morphology. The significant changes and recovery process of coastal and estuarine morphology after a huge tsunami have attracted attention of researchers. After The 2004 Indian Ocean Tsunami, which occurred on December 26, 2004 and has been one of the largest and deadliest tsunamis in recorded human history so far, there have been several works by such researchers such as Ali and Narayana (2015), Choowong et al. (2009), Liew et al. (2010) and Paris, et al. (2009). They presented the significant changes such as erosion, deposition or

disappearance of sandy coasts, river mouths, sandspit and recovery process both in short-term and long-term of affected areas in Andaman and Nicobar Islands of India, Indonesia and Thailand. Most of studies utilized yearly satellite images with intermediate spatial resolution and field survey data. The results indicate that fast recovery of coastline and beaches can be observed, whereas sand barriers, river mouths and coastal lagoons were slower. Following the occasion of The 2010 Chile tsunami, which happened on February 27, 2010, there have been few works on the field of morphological recovery. Villagran et al. (2014) investigated two typical kinds of morphological damages, disappearance of sandspit at the Mataquito River mouth and barely change at Duao beach. The recovery of morphology at these two areas after three year has been reported to be rapid. However, the post-tsunami configurations are different with the pre-tsunami ones. Next, Catalán et al. (2014) qualitatively and descriptively assessed the sudden changes induced by the tsunami and consequent recovery process of coastal area in central Chile. They presented that strong waves have driven to very fast recovery capacity. Another study, Cienfuegos, et al. (2014) deployed a video monitoring system for continuous and long-term monitoring the evolution of river mouth and sandspit reforming after the tsunami. In addition, the monitoring on the migration of beach cusp was also implemented. Similarly, there have been studies on the damages and recovery process of morphology on Sendai Coast and surrounding areas after the 2011 tsunami. Tanaka et al. (2012) reported the significant changes of morphology at river mouths and breaching of sandy coasts in Miyagi Prefecture and its recovery process. Tanaka et al. (2014) investigated the recovery of morphology at the Nanakita River mouth and its relevant phenomenon such as closure or re-opening based on the analysis of continuously measured data of water level and aerial photographs. Tappin et al. (2012) identified influences of the tsunami on the low-lying coastal zone in Sendai Coast through using the time-series satellite imagery, helicopter-borne video footage and field observation data. The comparison on the changes of coast with and without seawall protection has been made. Udo et al. (2012) gave the overview of morphology changes induced by the tsunami in Sendai Plain. In that study, several data sets of laser-scanned DEM (digital elevation model) and aerial photographs of the northern part of Sendai before and just after the tsunami were utilized to reveal the changes of morphology caused by the tsunami. They revealed that the elevation of about 60% of the northern part of Sendai Coast was degraded by 0.2 – 0.5 m, mainly due to land subsidence. Udo et al. (2015) investigated the morphological changes of the southern part of Sendai Coast. That study analyzed topography and aerial photograph data sets to

report the characteristics of morphological damages such as the erosion behind the along seawall, landward and seaward depositions. In addition, the evolution of morphology after the tsunami has been also revealed.

2.2 Shoreline change analysis using photograph

2.2.1 Shoreline position

An idealized definition of shoreline by Dolan et al. (1980) is that it coincides with the physical interface of land and water. However, this simple definition leads to big challenge in application. In reality, the position of shoreline is a temporal subject because of the dynamic nature of water levels at the coastal boundary (e.g., tides, wave run-up, etc.). Boak and Turner (2005) summarized three types of shoreline indicators that have been utilized in shoreline detection. They also indicated that one of the most common shoreline indicators was used is the high-water line (HWL). Usually, HWL is the line which is marked by left debris along the beach face by maximum run-up from a preceding high tide. This kind of indicator has been utilized in notable research works, especial widespread application for the US coasts (e.g., Anders and Byrnes, 1991; Crowell, 1991; Leatherman, 1991; Smith and Zarillo, 1988). However, this shoreline representation is sometime difficult to identify on the image because there is not debris for visible or the beach becomes dry quickly during the summer season. Another indication of shoreline position, the wet/dry line, was also popularly selected. This line is defined as the line to be the rising maximum run-up limit on a flooding tide, and the landward extent of the falling ‘‘wetted’’ beach during tidal ebb. Some studies (e.g., Dolan et al., 1978, 1980; Overton et al., 1999) have applied this term in the studies about coast in the U.S. The HWL and the wet/dry line are among the most common shoreline indicator features used as proxies for the shoreline position determination.

Coastal areas are dynamic in nature with changes in shoreline through processes of accretion and erosion over many time scales. With high-density population in the coastal zone, the increasing of coastal hazards, the study of changing shorelines is not only a pure scientific topic but also is useful for various activities of human life. Shoreline positions of the past and present measured in time periods can be used to calculate the change rates. These change rates can be utilized for further understanding on the magnitude and timing of shoreline changes. Several resources, historical map, Global Positioning System (GPS) survey data, aerial photograph, satellite image and video monitoring system, are available

for both extracting shoreline positions and quantifying shoreline changes. Hereafter, due to the popular and highly application, the literatures on shoreline position extracted from the latter three sources mentioned above will be reviewed.

2.2.2 Aerial photograph analysis

Aerial photography and satellite imaging are remote sensing. Aerial photography is any photograph taken from camera mounting on airborne vehicle (aircraft, helicopter, balloons, and so forth), whereas satellite imaging is digital image recorded by electronic scanner mounting on satellite or spacecraft. Aerial photograph is the most commonly used data source in shoreline mapping. It has been used extensively to determine shoreline position and erosion rate. This kind of photograph was taken and used widely in developed countries like the U.S., Japan, and so forth since the late 1930s and early 1940s (Anders and Byrnes, 1991).

Traditionally, aerial photograph was taken with film camera. Since 2008, digital photograph has been primarily used in the U.S. Digital aerial camera increases the speed of availability of aerial photograph because photograph is already in electronic form. The quality in term of resolution of this kind of aerial photograph has been improved a lot. In recent years, aerial photograph from Light Detection and Ranging (LIDAR) technology has been introduced. It has higher resolution compared to the traditional aerial photograph. One more advantage of LIDAR photograph is that height of objects on the ground can also be provided with extreme accuracy.

There are two major types of aerial photograph, the vertical and the oblique. These two types are classified depending on the attitude of the camera with respect to the earth's surface when the photograph is taken.

A vertical aerial photograph is a photograph that is taken with the camera pointed as straight down as possible. Relationship of aerial photograph with the ground is presented in Fig. 2.4(a). While, there are two types of oblique photograph, low and high. A low oblique photograph is the photograph that is taken with the camera inclined about 30^{O} from the vertical. Relationship of aerial photograph with the ground is presented in Fig. 2.4(b).

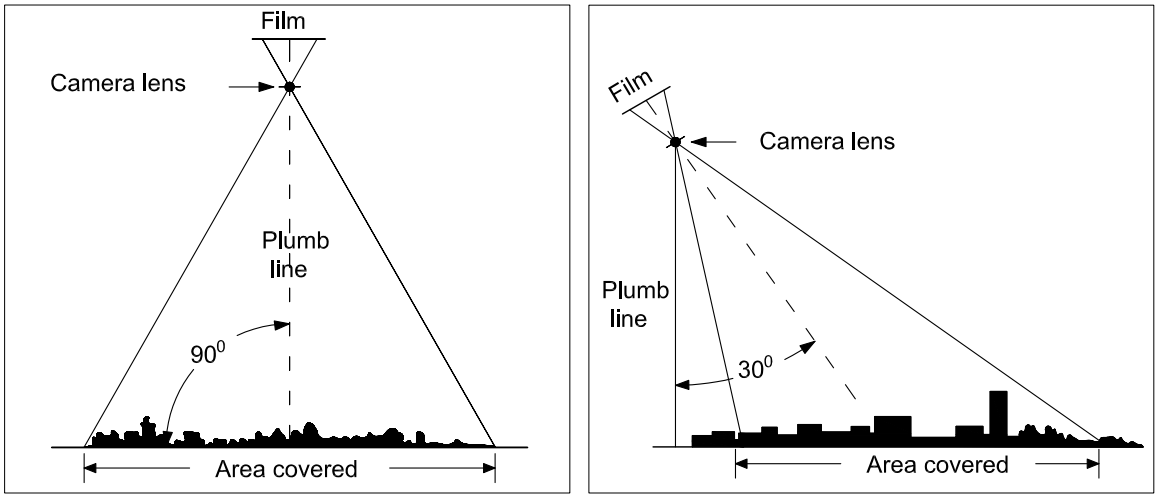

a. Vertical aerial photograph b. Oblique aerial photograph

Fig. 2.4 Relationship of aerial photograph with the ground (U.S. Army Corps of Engineers, 2006)

According to U.S. Army Corps of Engineers (2006), a vertical photograph has the following characteristics,

- The lens axis is perpendicular to the surface of the earth.
- It covers a relatively small area.
- The shape of the ground area covered on a single vertical photo closely approximates a square or rectangle.
- Being a view from above, it gives an unfamiliar view of the ground.
- Distance and directions may approach the accuracy of maps if taken over flat terrain.
- Relief is not readily apparent.

and, a low oblique has the following characteristics,

- It covers a relatively small area.
- The ground area covered is a trapezoid, although the photo is square or rectangular.
- The objects have a more familiar view, comparable to viewing from the top of a high hill or tall building.
- No scale is applicable to the entire photograph, and distance cannot be measured.
- Parallel lines on the ground are not parallel on this photograph; therefore, direction (azimuth) cannot be measured.
- Relief is discernible but distorted.

- It does not show the horizon.

The high oblique is a photograph taken with the camera inclined about 60^{O} from the vertical. This kind of photograph is somewhat similar to the photograph taken from video camera monitoring system which will be presented later in Section 2.2.4.

Aerial photograph needs to be rectified preceding the extracting shoreline position. The rectification process transforms the imagery to a map projection and corrects or minimizes map distortions such as tilt, scale differences, relief displacement, and radial lens distortion. The output image from rectification process is called rectified image. Shoreline position is extracted from this kind of image. Regarding to that, there various mapping techniques have been introduced. Moore (2000) reviewed the availability techniques and its reliability which were presented in various studies (e.g., Stafford (1971); Dolan et al. (1978); Leatherman (1983); Thieler and Danforth (1994); and Overton et al. (1996)). Later on, a few more techniques have been discussed too in Boak and Turner (2005); and Hanslow (2007).

There are several errors which can influence the result of shoreline position. The errors, which cannot be solved, will become the uncertainty of the aerial photograph analysis. According to Underwood and Anders (1991) and Moore (2000), the errors in image analysis can be categorized into two groups: errors from data sources (aerial photograph) and errors from measurement methods. The major errors, which are introduced by the data source itself, are image space distortions; object space displacements and ground control points, whereas the one from measurement methods are interpretation of shoreline proxy and annotation.

Recent advances in aerial photograph taking and rectification process have improved the accuracy of shoreline mapping by significantly reducing the number of ground control points that are required for an individual photograph. The errors only become notable when the scale of aerial photograph is small (Thieler and Danforth, 1994).

2.2.3 Satellite image analysis

Satellite imagery is digital image recorded by electronic scanner mounting on satellite or spacecraft which orbits around the earth. Satellite image can be classified into several categories as below

- Spatial resolution: High-resolution and low-resolution.
- Types of light source: Passive and active.

- Types of spectral bands: Pancromatic and multispectral.
- Special purposes: Earth-observing, meteorological and thermal-infrared

Currently, there are a wide range of sensors in space. They are Landsat TM/ETM, SPOT, RADAR, SAR, IKONOS, ASTER, QuickBird, WorldView, and others. Satellite images have been used in various fields of study. In studying of morphological change, there have been studies such as Ryu et al. (2002); Choowong et al. (2009); Liew et al. (2010); Kuleli al. (2011); Ford (2013); Feyisaa et al. (2014); García-Rubio, G. et al. (2015).

2.2.4 Video-based image analysis

Video-based image is the oblique image extracted from the video monitoring system mounting on high point at site of coastal area interest. In a few past decades, the development of this kind of image system has created powerful and reliable means for the monitoring the evolution of coastal morphology. The operation of video monitoring system is continuous; hence it can provide data covering timescales from seconds to years and spatial scales from meters to kilometers. It reduces the time and cost for beach morphology data collection which was the big challenge before the availability of this technology. This technology is nowadays becoming very popular and widely utilized by researchers in studying the evolution of beach morphology as well as dominant factors governing evolution in the nearshore area. Holland et al. (1997); Lippmann and Holman (1989, 1990) developed the approach using video imagery to quantify a number of natural nearshore processes in terms of both spatial and temporal scales. Several applications of the camera model, which are the measurement of nearshore fluid processes, sand bar length scales, foreshore topography, and drifter motions, are discussed. Aarninkhoff et al. (2003, 2005) presented the details and validation of a video-based method for monitoring morphological changes at the intertidal beach. The quantification of intertidal beach bathymetry is achieved by mapping multiple shorelines during a tidal cycle. Furthermore, there are many other literatures on the application of video-based image for the investigation of morphological evolution, the nearshore process (e. g. Holman and Stanley, 2007; Armaroli and Ciavola, 2011). Besides, the advantages of this technique in the coastal monitoring and studying, its cost-effective would be an important factor that could lead to widely applicability of this technique in developing countries (e. g., Thanh et al., 2015).

2.3 Empirical Orthogonal Function (EOF) analysis

The Empirical Orthogonal Function (EOF) analysis is a method to extract the dominant patterns from data sets. In coastal morphology, it can extract the significant components of shoreline variability from shoreline data sets. It has been applied widely in coastal morphology. There have been several versions of EOF analysis. Winant et al. (1975) firstly applied the EOF analysis to study the variation of beach profile shape (cross-shore variability). They could explain the physical processes reflected by the first three components. They are the mean beach profile, the bar-berm exchange and the low tide terrace. Miller and Dean (2007a) applied EOF analysis to investigate the characteristics of longshore shoreline variability and relationship with nearshore conditions. Uda and Hasumoto (1982); and Hsu et al. (1994) applied EOF analysis to study the two-dimensional beach variability. In the study area of present study, the technique has been applied by Kang and Tanaka (2005). They applied EOF analysis to the shoreline data sets on the northern part of Sendai Coast from 1996 to 2003. The cross-shore variability of shoreline position was indicated as the most dominant component, while the variation of shoreline position driving by the longshore sediment was the second dominant component.

2.4 Even and Odd analysis

Even and Odd Function analysis is a direct and easily applied method to determine effects of natural features, such as an inlet or coastal structure that influences on the longshore sediment transport, on shoreline (or volumetric change) data (Dean and Dalrymple, 2002). It can break down the shoreline position and volume changes into symmetric (even component) and anti-symmetric (odd component). Rosati and Kraus (1997) defined that the shoreline (or volume) change, $f(x)$, between two time periods at some alongshore position, x, can be represented by the even (symmetric), $f_e(x)$, and the odd (anti-symmetric), $f_o(x)$, functions

$$f(x)=f_e(x)+f_o(x) \tag{2.1}$$

where the even and odd functions are given as below

$$f_e(x)=\frac{f(x)+f(-x)}{2} \tag{2.2}$$

$$f_o(x)=\frac{f(x)-f(-x)}{2} \tag{2.3}$$

Based on the above definition, the even function does not change sign if its argument changes sign ($f_e(-x)=f_e(+x)$), whereas the odd function is opposite ($f_o(-x)=-f_o(+x)$).

Work and Dean (1990) and Dean and Work (1993) applied the even/odd analysis to assess the effects of several inlets and coastal structures on the eastern coast of Florida to adjacent shorelines. The results of odd component have been verified with the results of analytical and numerical predictions of shoreline response. Another notable application, Walton (2002), that even/odd analysis was utilized to separate the components for a complex shoreline set having longshore sediment transport gradient. The paper also discussed a more complex case that man-made effects of beach nourishment and natural effects of longshore historical gradients in accretion have been taken into account.

2.5 Sediment budget analysis

Sediment budget analysis is fundamental in coastal science and engineering which is a estimation of sediment gains and losses, or sources and sinks, within a specified control volume (or cell), or in a series of connecting calculation cells, over a given time (Rosati and Kraus, 1999; Rosati, 2005). According to the above definition, the difference between sediment gain (source) and sediment loss (sink) in a cell for the entire sediment budget domain must equal the rate of change in sediment volume occurring within that region. Below equation, which is obtained based on the conservation of mass and given in Rosati and Kraus (1999), can be considered as the sediment budget equation

$$\sum Q_{source} - \sum Q_{sink} - \Delta V + P - R = Residual \tag{2.4}$$

where $Q_{source/sink}$ is the sources and sinks to the control volume; ΔV is the net change in volume within the cell; P and R are the amounts of material placed in and removed from the cell; *Residual* is the degree to which the cell is balanced.

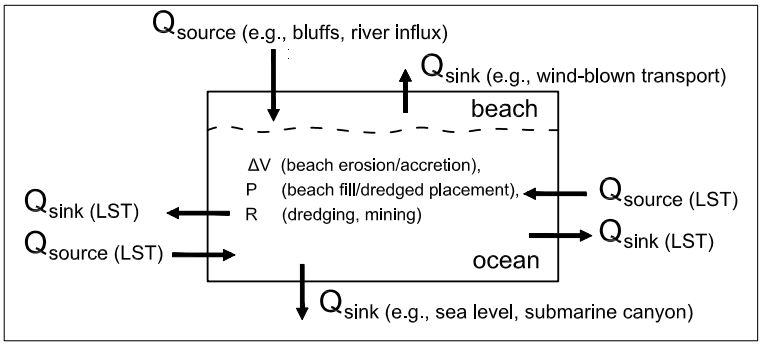

Fig. 2.5 Parameters may appear in Eq. (2.4) (Rosati and Kraus, 1999)

The sediment source includes longshore transport, sea cliff erosion, beach erosion, beach fill, and river flux, whereas the sediment sink relates to longshore sediment transport, dredging and mining of the beach or nearshore, relative sea level rise, and offshore loss. These parameters are schematically expressed in Fig. 2.5.

Rosati (2005) pointed out that the sediment budget analysis can be implemented for a short-term period such as a particular season of the year to longer-term period representing a particular historical time period or existing conditions at the site. As the budget analysis has shown its usefulness in supporting the coastal planning, inlet rehabilitation, harbor navigation maintenance, hence it has been applied by various researchers, for the U.S. coast including Bowen and Inman (1966); Jarrett (1977), Dolan et al. (1987); Patsch (2008); Kaminsky et al. (2010), for the Dutch coast including van Rijn (1997) and for Japanese coast including Kuriyama (2003); Yamada et al. (2010). Rosati (2005) reviewed commonly applied sediment budget analysis concepts and introduced new considerations in order to make the sediment budget process more reliable, streamlined, and understandable. A recent study, Walton (2012), discussed on the problems which are raised when carry out the sediment budget for an inlet. A simple approach for assessing sediment budget, i.e. what is possible, and what is not possible through a matrix equation system and linear algebra, was introduced.

2.6 Shoreline change modeling – one-line model

2.6.1 Overview on the theory of one-line model

One-line shoreline change model was introduced by Pelnard-Considere (1956). It considers that the beach profile move parallel itself out to a limiting depth of closure.

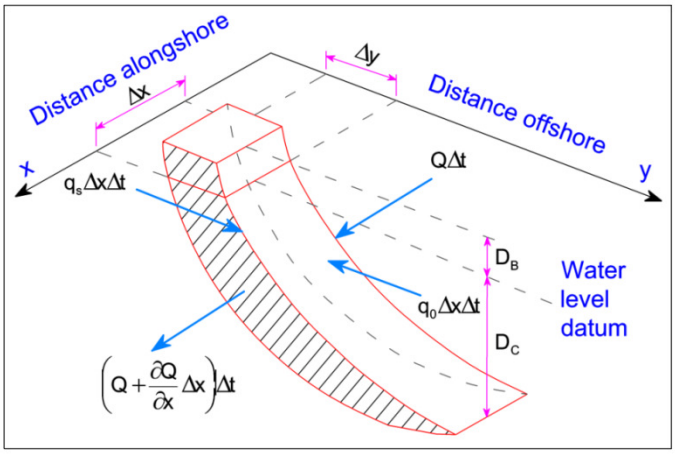

Fig. 2.6 Definition sketch for shoreline change calculation (Hanson, 1989)

Since then, many researchers have made the improvement and modification on this model (e.g., Bakker (1969); Perlin and Dean (1983); Johnson and Kamphuis (1988)).

The governing equation of one-line model is given as

$$\frac{\partial y}{\partial t} = -\frac{1}{D_B + D_C}\frac{\partial Q}{\partial x} \tag{2.5}$$

where Q is longshore sediment transport rate; D_B is the height of berm; D_C is the depth of closure; x is the coordinate along the x-axis which parallels to the trend line of the beach; y is the shoreline position changing on the cross-shore direction; t is the time.

In Eq. (2.5) the variation of shoreline position is balance with the variation of longshore sediment transport rate. If a line source or sink such as river mouth, etc. is considered, Eq. (2.5) will have the following form

$$\frac{\partial y}{\partial t} = -\frac{1}{D_B + D_C}\left(\frac{\partial Q}{\partial x} \pm q\right) \tag{2.6}$$

where q is the source (minus sign) or sink (plus sign) of sand per unit length of beach.

In one-line theory, the beach profile is assumed to displace horizontally without changing its form, hence it is suitable to describe long-term variation of shoreline position. The short-term variations due to storms, seasonal changing of wave conditions, others, cannot be predicted accurately.

Hanson and Kraus (1989) developed GENESIS (GENEralized model for Simulating Shoreline change) model to simulate the long-term shoreline change. The calculated domain and time period can range from 0-100 km and 100 months, respectively. It can represent almost arbitrary numbers and combinations of coastal structures such as groins, detached breakwaters, seawalls, jetties, and beach fills. One of the notable applying of one-line theory for simulating long-term shoreline change for the coast in Japan is Kraus and Harikai (1983). They simulated the evolution of shoreline adjacent to the Oarai Habour, Ibaraki Prefecture. The longshore sediment movement in this area is dominated and interrupted by the breakwater of the port and large groin, respectively. The river flux from Naka River was treated as sediment source.

Thomas and Frey (2013) reviewed the differences and similarities in the most popular and available shoreline change models, GENESIS (GENEralized model for SImulating Shoreline change), UNIBEST (UNIform BEach Sediment Transport), and LITPACK (integrated model for LITtoral Processes And Coastline Kinetics), which were developed based on the one-line theory. Furthermore, Townsend et al. (2014) demonstrated the application of three popular available shoreline change models, GenCade (combination of

the GENESIS and Cascade models, Unibest CL+(Deltares), and LITPACK, which were also developed based on the one-line theory, for various cases with and without coastal structures.

2.6.2 Longshore sediment transport rate

Longshore sediment transport rate, Q, is defined as the littoral drift moving parallel to the shoreline. There have been various formulas to calculate this parameter. Two of the notable formulas are summarized below

CERC formula (SPM, 1984)

This formula is one of the most well-known and widely used formulas. It was documented in U.S. Army Corps of Engineers (1984) (Shore Protection Manual) as below

$$Q=\frac{K}{16\left(\rho_s/\rho-1\right)(1-p)}\left(H^2C_g\right)_b\sin 2\alpha_b \tag{2.7}$$

where H is the wave height; C_g is the wave group celerity; the subscript "b" denotes for the quantity at the breaking line; α_b is the breaking wave angle; ρ_s is the mass density of the sediment grains; ρ is the mass density of water; K is the dimensionless empirical coefficient (more details about this parameter will be presented in the next section).

Kamphuis (1991) formula

In the Kamphuis (1991) formula, the effect of breaking wave height, wave period, grain size, beach slope and wave angle at the breaking point are taken into account as in the below equation

$$Q=6.4\text{x}10^4H_{sb}^2T_p^{1.5}m_b^{0.5}D_{50}^{-0.25}\sin^{0.6}(2\alpha_b) \qquad (\text{m}^3/\text{year}) \tag{2.8}$$

where H_{sb} is the significant wave height at the breaking point; T_p is the peak wave period; D_{50} is the grain size; m is the beach slope at the breaking point.

2.6.3 The dimensionless empirical coefficient in longshore sediment transport rate formula, *K*

The dimensionless empirical coefficient, K, is a key factor in longshore sediment transport rate. There have been various studies on this parameter. U.S. Army Corps of Engineers (1984) proposed a formula to quantify the total longshore sediment transport rate, which is well known as the CERC formula, and widely used. It recommended a

value of K as 0.39 which was derived from the field study data in Komar and Inman (1970). The value of K is associated with whether breaking wave height is specified in term of the significant wave height or the root mean square wave height. The one shown above was carried out based on the computation utilizing the significant wave height, while the value of K corresponding to the root mean square wave height is 0.92. It is important to note that the CERC formula does not include the influence of grain size. The relationship between value of K and the grain size has been documented by Dean (1989) and del Valle et al. (1993) (Fig. 2.7). The increasing of grain size leads to the deceasing value of K.

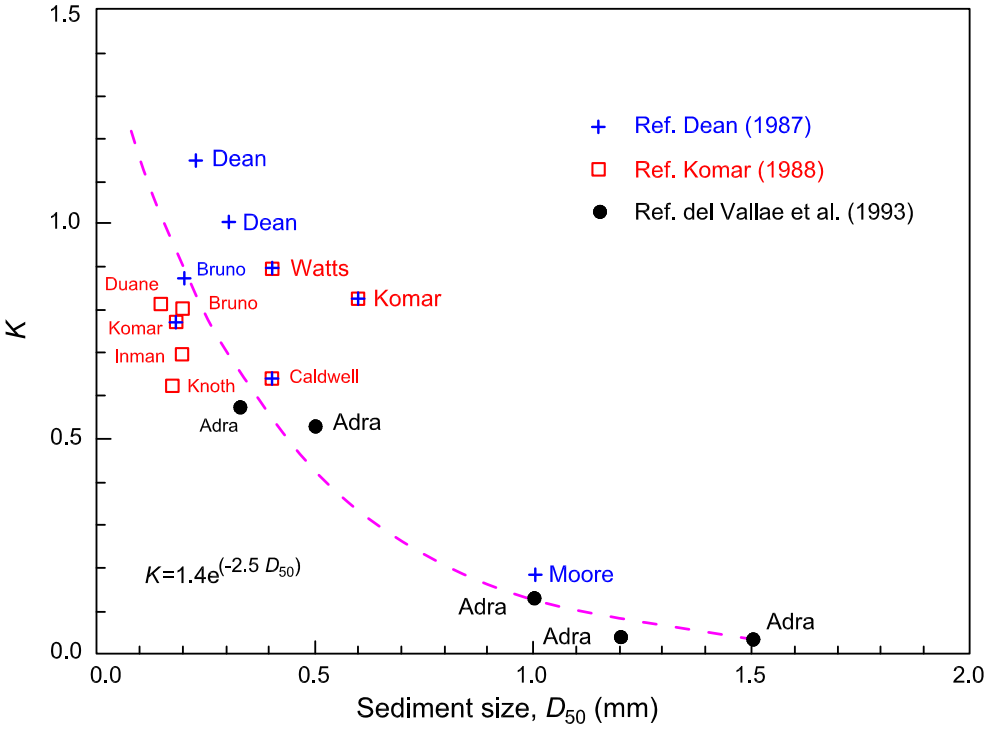

Fig. 2.7 Coefficient, K, versus median grain size, D_{50} (del Valle et al., 1993)

The details on study area, data collection, methodologies and results and discussion are presented in the next chapter.

CHAPTER 3

STUDY AREAS, DATA COLLECTION AND METHODOLOGIES

3.1 Study areas

This study focuses on the recovery process of the coastal and estuarine morphology in Miyagi Prefecture, Japan (Fig. 1) where the tsunami inundation was reported up to 19.5 m (Mori et al., 2012). The recovery process of morphology of five river mouths, the Kitakami, Naruse, Nanakita, Natori, and Abukuma, and three breaching sandy coasts at

Fig. 3.1 Location map of the study area

Arahama, Akaiko and Yamamoto, in order from north to south is investigated.

In addition, the sandy coast located on the northern part of Sendai Coast, from Sendai Port to Natori River mouth is also included.

The rivers in Japan are classified into classes A and B depending on their dimension and importance for land conservation and national economy. Rivers classes A and B are managed by the national government and prefectural government, respectively. The characteristics of the first four river mouths listed in Table 1 were described in terms of river class, river length, catchment area, and river mouth structures by Tanaka et al. (2012). This study supplements the characteristics of the Abukuma River and three breaching.

Table 3.1 Summary of river characteristics

River name	River class (*)	River length (km)	Catchment area (km^2)	River mouth structure
Kitakami	A	249	10150	no structure
Naruse	A	89	1133	2 jetties
Nanakita	B	45	229	1 jetty
Natori	A	55	933	2 jetties
Abukuma	A	239	5400	no structure
Arahama	breaching of sandy coast			old river mouth
Akaiko	breaching of sandy coast			old river mouth
Yamamoto	breaching of sandy coast			old river mouth

(*) Class A: managed by the national government

Class B: managed by the prefectural government

Breaching of three sandy coasts at Arahama, Akaiko and Yamamoto, which were formed by the tsunami waves and return flow at the places used to be river mouths, are also taken as the study areas. Although these areas were not initially river mouths, the breaching of sandy coast made them temporarily convert to river mouth or lagoon.

Another river mouth, Mogami River mouth, which was not subjected to the tsunami damage, is also taken into account for the comparative study on the intrusion of sandspit into river mouth. Mogami River is a river in Yamagata Prefecture which borders the west side of Miyagi Prefecture. It is about 224 km in length with the river basin of about 7040

km^2. This river pours into the Sea of Japan at Sakata City. The sandspit started to intrude upstream after the construction of jetty at the river mouth.

The northern part of Sendai Coast, which is located between Sendai Port and the Natori River mouth, is about 12 km in length. In this coast, there are two river mouths which pour into the Pacific Ocean. The Nanakita River mouth is located about 1.8km south of Sendai Port, while the Natori River mouth is located adjacent to the left side of Yuriage Port. There are two lagoons, Gamo, Idoura, locating on the left sides of the two river mouths, respectively. Along the coast, there are some coastal structures. In Arahama area, central part of the coast, there are six detached breakwaters which were constructed from 1970's to 1980's to prevent the erosion of the beach. At the place, where is about 2 km north of the Natori River mouth, approximately 250 m of wave-dissipating blocks were installed. Due to the severe erosion induced by the tsunami, currently these blocks are located protrusively into the sea water body. They can interrupt the longshore sediment transport and cause the discontinuity of shoreline change. In addition, about 800 m south of the Nanakita River mouth, there is a shore-perpendicular drainage, which is belonged to Minami-gamo Sewage Treatment Plant. After the tsunami, shoreline in this area was still getting retreat, then, currently a part of this drainage is exposed and located protrusively into the sea water body. So, it plays the role as a jetty and can interrupt the longshore sediment transport.

The longshore sediment transport direction in this study area has been reported from the south to the north (bottom to the top in Fig. 1) (Tanaka and Takahashi, 1995). It is blocked at both ends of the coast by the long breakwaters of Yuriage Port and Sendai Port.

3.2 Data collection

3.2.1 Aerial photographs

Aerial photographs of Sendai Coast, including the Nanakita, Natori River mouths and breaching at Arahama, were being taken frequently in every one or two months before and after the tsunami. Those photographs taken from April, 2015 onwards were given in digital form, whereas those taken before then were given in printed form (after that scan to 400 dpi). Besides that many set of aerial photographs and satellite images of study areas were also collected from other sources such as, Geographical Survey Institute (hereafter referred to as GSI), Google Earth, the Kitakami River Lower Reach office, the Ministry of Land, Infrastructure and Transport (hereafter referred to as MILT).

3.2.2 Wave conditions

The characteristics of 20-minute significant waves in the period from January 1, 2009 to December 31, 2015 at Sendai Port are presented in Fig. 3.2. The wave rose indicates that waves most come from the east and south-east direction (90^{O}~150^{O} from the north). The 20-min significant wave heights, which are greater than 1 m, take 25.4 % of all the wave heights. The characteristics of daily average wave data measured at the same location in the period from 1991 to 2009 are shown in Pradjoko and Tanaka (2010).

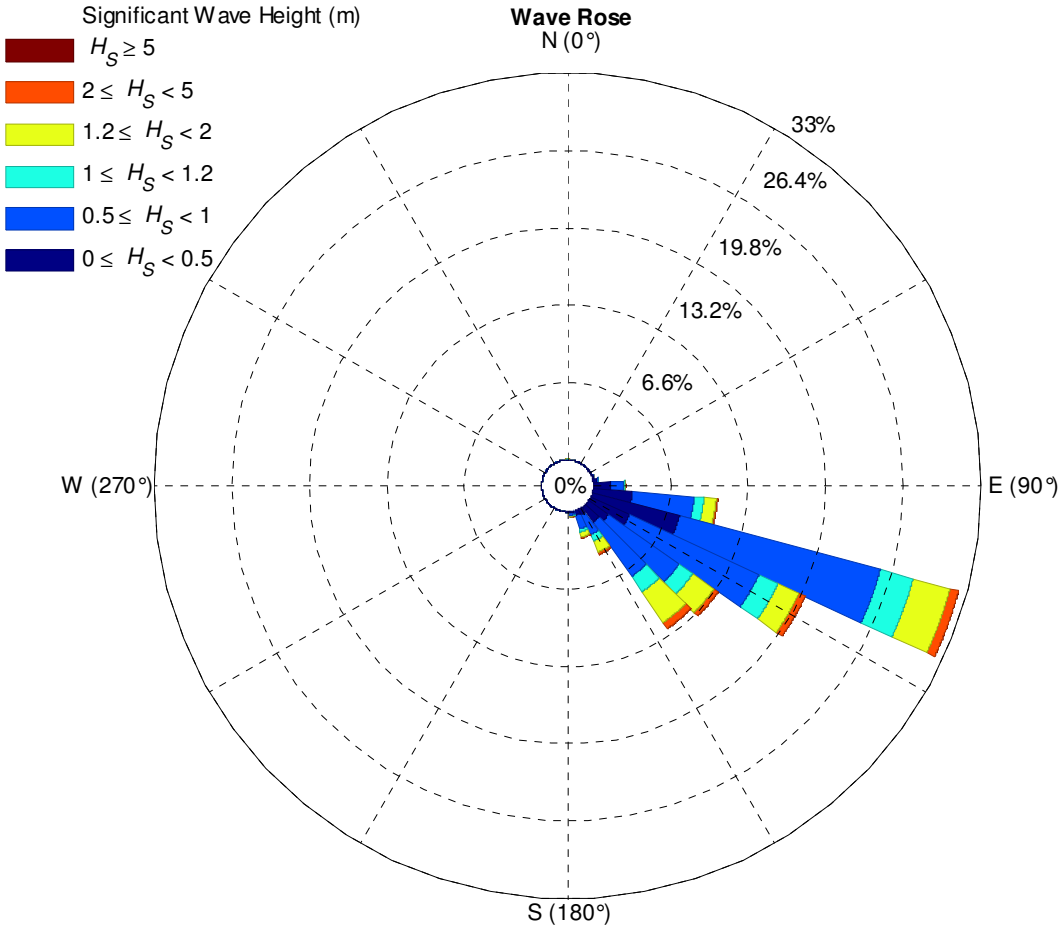

Fig. 3.2 Characteristics of significant waves in the period from January 1, 2009 to December 31, 2015 at Sendai Port

Due to the damages of facility at Sendai Port Station induced by the tsunami, the wave data in the period from after the tsunami to middle of 2012 is not available at this station. Therefore, the wave data at the Central Miyagi Station is employed. The regression, which is presented in Mori et al. (2015), is made in order to use the wave data at that station. All the wave data was downloaded from website of NOWPHAS (The Nationwide Ocean Wave information network for Ports and HArbourS).

3.2.3 Tidal conditions

Due the devastation of measuring stations induced by the tsunami, the tide in Sendai Coast was recommended to use calculated astronomical tide at Sendai Port. This data was downloaded from the website of Japan Meteorological Agency (JMA). The tide at this station is semi diurnal type with about 1.6 m of tidal range as showing in Fig. 3.3. The tidal datum of Sendai Port is T.P. +0.84 m (Tokyo Peil). For more details, an exaggeration of tide in April, 2016 is shown in Fig. 3.4. The tidal data is used in the tidal correction for shoreline positions extracted from aerial photographs.

Shoreline positions extracted from aerial photographs are corrected to the tidal datum of Sendai Port.

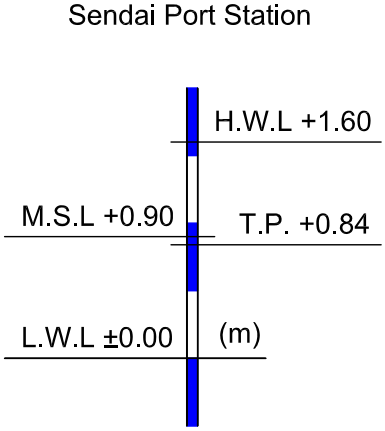

Fig. 3.3. Tidal conditions at Sendai Port

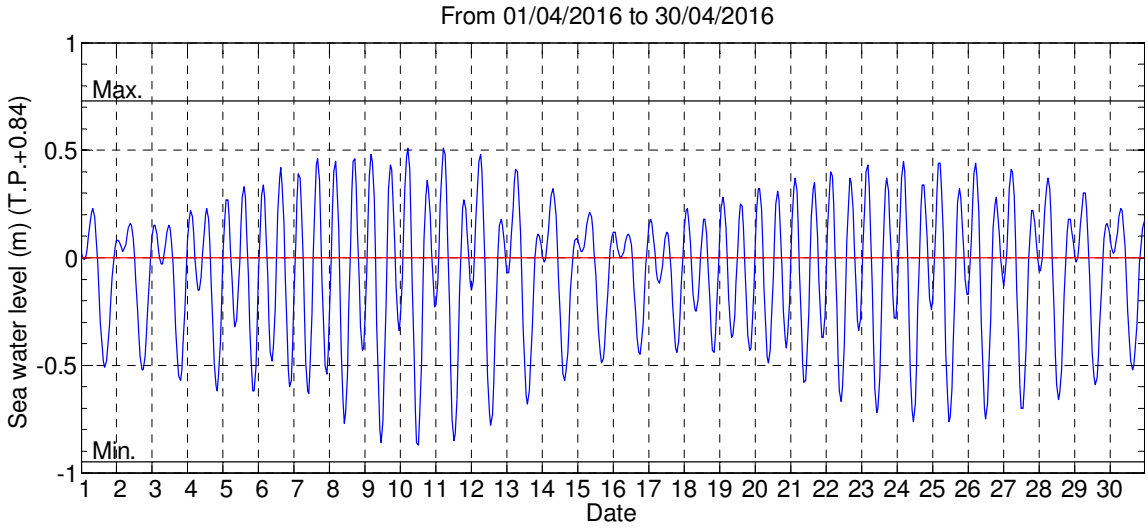

Fig. 3.4 The calculated tide at Sendai Port Station in April, 2016 (Max. and Min. is the maximum and minimum water level in 2016)

3.2.4 Bathymetry data

The bathymetry of the northern part of Sendai Coast before the tsunami was presented in Kang (2006). Udo et al. (2012) analyzed the air borne laser scanned topographic data in 2005 and March 19-24, 2011, and reported that roughly 60 % of the coast was

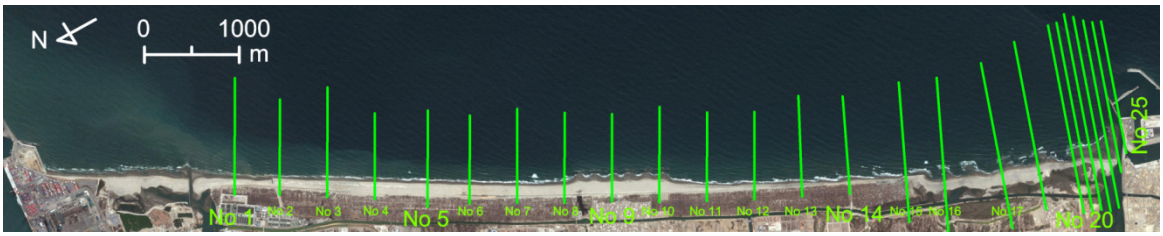

Fig. 3.5 Location map of beach profile serveyed transections (background: April 10, 2012, Google Earth)

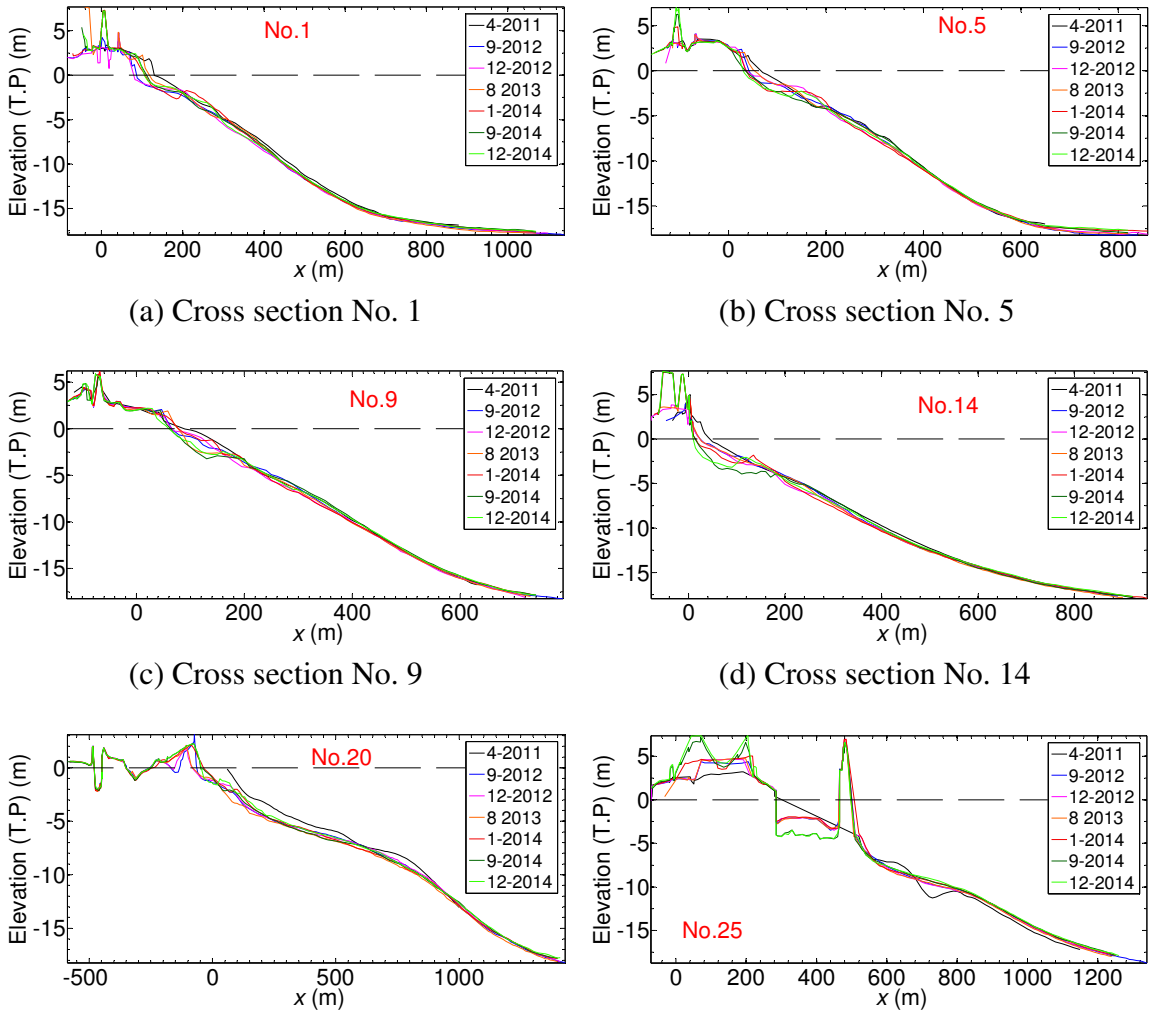

(a) Cross section No. 1

(b) Cross section No. 5

(c) Cross section No. 9

(d) Cross section No. 14

(e) Cross section No. 20

(f) Cross section No. 25

Fig. 3.6. Beach profiles along the northen part of Sendai Coast

degraded about 0.2 to 0.5 m, mainly due to the land subsidence. However, according to a recent GSI's reports, depending to the locations, about 70 % to 90 % of the land subsidence has recovered.

In addition, this study also collected the beach profiles on twenty five transections along the coast (Fig. 3.5). This data was available from Tohoku Regional Bureau, Ministry of Land, Infrastructure and Transport. It was measured in different times after the tsunami. The beach profiles on some transections are shown in Fig. 3.6.

Besides that the cross sections of the Kitakami, Naruse and Natori River mouths utilized in this study were collected from MILT.

3.3 Methodology of image analysis

3.3.1 Image rectification

Image rectification is a transformation process which projects image onto a mapping system. This is done by matching ground control points (GCPs) in the mapping system to points in the image. The GCPs are fixed points in the map system and can also be visible in the image. Road intersections, building corners, solitary trees, and so forth are considered as good GCPs. The number of GCPs needs to be chosen depending on the amount of distortion in photograph and desired level of accuracy. The more control points are selected the more accuracy is obtained. In this study, the control points and their coordinates are chosen in the Google Earth. The base coordinate system is World Geodetic System 1984 (WGS-84).

3.3.2 Shoreline position extraction

The aerial photographs taken before April, 2015 were given in printed form with the size of 9x9 inches and most of them have scale of 1:8000. The sandy coast from Sendai Port to the Natori River mouth is covered by 19 photographs with about 60 % overlapping. The photographs were scanned into 400 dpi JPEG images. Hence, the spatial resolution is about 0.5 m. Since April, 2015, the digital aerial photographs have been available. There are total 45 photographs covering the mentioned sandy coast. Each digital aerial photograph covers a smaller area compared to the printed form aerial photograph; however the spatial resolution has much increased (nearly 0.1 m).

Shoreline positions were extracted from rectified images in the alongshore direction based on the difference of color intensity of wet and dry sand sides. The most wetted line

(wet/dry line) is selected to be the proxy for shoreline position. This line is exampled in Fig. 3.7.

Fig. 3.7 Shoreline position proxy in the aerial photograph (background: Mar 4, 2016)

The wave run-up, R_U, which can be obtained from Hunt (1959), Eq. (3.1), for uniform, smooth, impermeable slopes

$$\frac{R_U}{H_0}=\xi_0 \tag{3.1}$$

where H_0 is the significant deep water wave height; ξ_0 is the surf similarity parameter and calculated from the significant deep water wave height and wave length.

The aerial photographs are taken during the good weather and calm waves, hence the wave run-up effect is considered to be neglected in this study.

A shore-parallel line, which angles clockwise the north direction a certain degree, is taken as the baseline for measurement of shoreline position. Value of the angle is assigned depending on the particular study area (river mouths or breaching or sandy coast) in order to make the shoreline paralleling to the baseline. This value for northern part of Sendai Coast is 210^{O}. Shoreline positions were extracted from aerial photographs in the alongshore direction. Figure 3.8 presents the calculated tidal level at Sendai Port from 2011 to 2016 and the values of water level from the tidal datum (T.P. +0.84 m) for each aerial photograph. The shoreline position correction amount can be obtained when dividing the corrected height in Fig. 3.8 to the beach slope of 0.11 (Pradjoko and Tanaka, 2010).

Detected shoreline positions extracted from aerial photographs and satellite images of the third party were not corrected to tidal level due to the lack of exact time of capture.

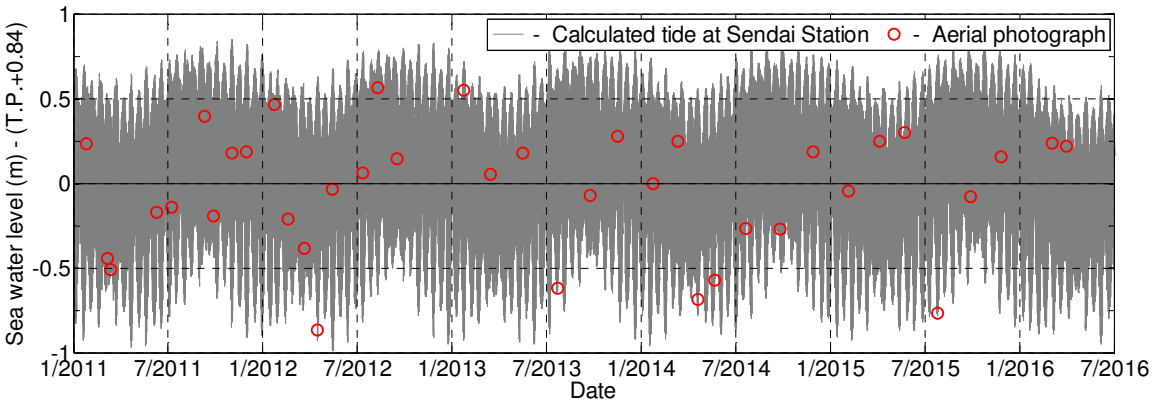

Fig. 3.8 Calculated sea level at Sendai Port from 2011 to 2016 and corrected height for each aerial photograph

3.3.3 Uncertainty of image analysis

According to Moore (2000), there are various kinds of error that would affect to the accuracy of shoreline position analysis. The two notable types of error are the error from data sources themselves (aerial photograph) and error from the measured methods. These errors have been reviewed in Chapter 2. This study utilizes similar method of image rectification in Pradjoko and Tanaka (2010). In the latter study, they have discussed clearly the errors of image analysis. The average error between actual coordinates in base map system and resulted coordinates in rectified image could rise up to 6 m, whereas the averaged RMS error of checked points between the base map system and rectified image is 5.27 m. This is considered as the uncertainty of aerial photograph analysis.

3.4 Methodology of EOF analysis

In the present study, the EOF analysis, which was presented in Kang and Tanaka (2005), is utilized to decompress the dominant processes of shoreline variability along the northern part of Sendai Coast. In EOF analysis, the separation of variables approach is used to isolate the temporal and spatial dependences of shoreline data. Thus, shoreline can be represented by a series of linear combination of corresponding function of time and space, respectively.

$$y(x, t)=\sum_{n=1}^{n_x} e_n(x)c_n(t) \tag{3.2}$$

where $y(x, t)=y_s(x, t) - \bar{y}(x)$; $y_s(x, t)$ is the distance from the baseline to the shoreline position; $\bar{y}(x)$ is the mean shoreline position in the computed period; n_x is the number of

survey section sections along the coast. This parameter will be replaced by n_t, which is the number of survey times, if the value of n_t is smaller than the value of n_x; $c_n(t)$ and $e_n(x)$ are the temporal and spatial eigenfunctions, respectively.

In order to generate $c_n(t)$ and $e_n(x)$, correlation matrix A is obtained as below

$$A=[a_{ij}]=\frac{1}{n_x n_t}\sum_{t=1}^{n_t} y_{it}y_{jt} \tag{3.3}$$

where $(1\leq i\leq n_x)$; $(1\leq j\leq n_x)$

Matrix A represents a set of eigenvalues, λ_n

$$Ae_n=\lambda_n e_n \tag{3.4}$$

where $(1\leq n\leq n_x)$

A series of corresponding eigenfunctions, which are defined by the matrix equation, is obtained as following

$$c_n(t)=\sum_{n=1}^{n_t} y(x,t)e_n(x) \tag{3.5}$$

Contribution rate, R_n, which reveals the importance of data set, is given as below

$$R_n=\frac{\lambda_n}{\sum_{i=1}^{n_x}\lambda_i} \tag{3.6}$$

3.5 Methodology of obtaining analytical solution of one-line model

The analytical solutions of one-line model can be obtained when solving the simplified governing equation of the one-line model (diffusion equation), Eq. (3.11), with corresponded initial and boundary conditions. Equation (3.11) has been simplified from the governing equation of one-line model (Eq. 2.5). Detailed simplification process has been presented in Larson et al. (1987). Hereafter, some main steps are represented.

The longshore sediment change rate in Eq. (2.5) at a local scale is described by the following equation

$$Q=Q_0\sin 2\alpha_b \tag{3.7}$$

where Q_0 is the amplitude of longshore sediment transport rate; α_b is the angle between breaking wave crests and shoreline expressed as

$$\alpha_b=\alpha_0-\arctan\left(\frac{\partial y}{\partial x}\right) \tag{3.8}$$

where α_0 is the angle of breaking wave crests relative to an axis set parallel to the trend of the shoreline; $\partial y/\partial x$ is the local shoreline orientation.

Substituting Eq. (3.8) into Eq. (3.7), the longshore sediment change rate is given as below

$$Q=Q_0\sin\left\{2\left[\alpha_0\text{-}\arctan\left(\frac{\partial y}{\partial x}\right)\right]\right\} \tag{3.9}$$

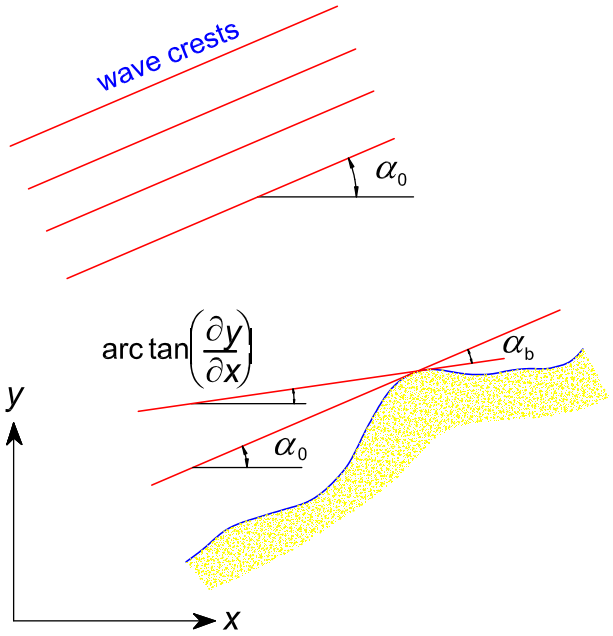

Fig. 3.9 Definition sketch for geometric properties at a specific location as related to shoreline change (Larson et al., 1987)

It is assumed that the angle between breaking wave crests and the local shoreline orientation are small, the truncating to the first order of Taylor series expansion on Eq. (3.9) yields

$$Q=Q_0\left(2\alpha_0\text{-}2\frac{\partial y}{\partial x}\right) \tag{3.10}$$

Another assumption is made. The characteristics of wave are constant along the coast with all time. Therefore, the longshore sediment transport rate is constant along the coast. The simplified governing equation of one-line model can be obtained as below

$$\frac{\partial y}{\partial t}=\varepsilon\frac{\partial^2 y}{\partial x^2} \tag{3.11}$$

where ε is the diffusion coefficient, and is given by the following equation

$$\varepsilon=\frac{K(H^2C_g)_b}{8(\rho_s/\rho\text{-}1)(1\text{-}n)}\frac{1}{D_B+D_C} \tag{3.12}$$

where n is the sediment porosity.

According to Eq. (3.12), the diffusion coefficient is intensely depended on the breaking wave height, H_b, and the dimensionless empirical coefficient in longshore sediment transport rate formula, K. In the computation of shoreline change, the parameter K is usually utilized instead of the parameter ε.

Larson et al. (1987) stated that analytical solution cannot handle the problems which involve complex boundary conditions and wave inputs. Moreover, the fine details of shoreline change cannot be described. In order to solve the complex problems, the numerical method is needed. Therefore, not so many analytical approaches have been published. There have been notable attempts on the analytical solutions of one-line model including Bakker and Edelman (1965); Bakker (1969); Grijm (1961, 1965); Walton and Chiu (1979); Larson et al. (1987), and U.S. Army Corps of Engineers (2002).

In summary from the above literatures, when utilizing the analytical solutions of one-line model, the following assumptions need to be made

1. The beach profile is in equilibrium and moves parallel to it. This assumption is not valid after a strong storm; however it is reasonable for the long-term consideration.
2. Longshore sediment movement takes place uniformly over the beach profile down to the depth of closure.
3. No cross-shore sediment transport is considered.
4. The nearshore circulation is neglected (except the longshore due to wave diffraction from coastal structures).
5. The longshore sand transport rate is proportional to the angle of incidence of breaking wave crests to the shoreline.
6. The angle between the breaking wave crests and the shoreline is small.
7. The angle of the shoreline with respect to the x-axis is small.

Based on the above data collection and methodology of aerial photograph analysis, the rectified images and extracted shoreline positions of river mouths and breaching of sandy coasts along Miyagi Prefecture are utilized in the next chapter to reveal the morphological changes and its recovery process in the short-term after the tsunami.

CHAPTER 4

MORPHOLOGICAL CHANGES AND SUBSEQUENT RECOVERY AT THE RIVER MOUTHS AND BREACHING OF SANDY COASTS

4.1 Introduction

The 2011 tsunami caused significant changes to the coastal areas in northeastern Japan. Tanaka et al. (2012) overviewed the significant changes of coastal and riverine morphology in Miyagi Prefecture and its subsequent recovery. At river mouth areas, it commonly observed the disappearance of river mouth sandspit. At the lagoon areas, the sand barriers in front of lagoons adjacent to river mouth were also severely eroded by the tsunami. Moreover, the breaching of sandy coasts occurred at many places where used to be river mouth such as Arahama, Akaiko and Yamamoto. At these areas, concave shorelines were observed after the tsunami. During the subsequent recovery process, erosion of sandy coasts adjacent to the concave shorelines was observed. The erosion was propagating along the adjacent coasts. Additionally, during the recovery process, intrusion of sandspit into river mouth area was also observed. This phenomenon occurred at various river mouths which were scoured much deeper by the tsunami such as Kitakami, Naruse, Nanakita and Natori.

Altogether, this chapter attempts to present the significant changes and recovery of morphology at the river mouths and breaching of sandy coasts in Miyagi Prefecture, and also the relevant phenomenon that accompanied the recovery process through analysis of aerial photographs, field observation data, and analytical solutions of one-line model.

4.2 Morphological changes at the river mouths, breaching of sandy coasts and its recovery process from aerial photograph analysis

In this section, aerial photographs and sets of river mouth cross profile are analyzed to describe the changes and recovery process of morphology at five river mouths and three breaching of sandy coasts along the coast in Miyagi Prefecture. Some aerial photographs shown here have already been published in Tanaka et al. (2012 and 2014a). However, in

order to make clarification about the changes and introduce the overall recovery as well as to provide a linkage to the next sections, some photographs are re-included.

4.2.1 Kitakami River mouth

Kitakami River is the fourth largest river in Japan and the largest in the Tohoku region. It flows through mostly rural areas of Iwate Prefecture and pours into a small bay in Miyagi Prefectures facing the Pacific Ocean. The mouth area is mostly sandy soil with 0.0001 bed slope, and located on Yokosuka Coast, the northern part of Miyagi Prefecture. The morphology of river mouth and sandy coast was severely destroyed (Fig. 4.1(a)). The farmland adjacent to the river mouth and sandy coast has become river bottom, only a narrow strip of land and a new island remained. The river mouth became much wider than before the tsunami. The recovery of the morphology in this area was rather slow as can be seen in Figs. 4.2(b) and 4.2(c). Tanaka et al. (2012) indicated that the increasing of water depth in the near shore zone due to land subsidence, less availability of sediment supply from surrounding rocky cliffs, and cross-shore sediment movement can be the reasons of slow recovery. Figures 4.2(c) and 4.2(d), which were taken after Tanaka et al. (2012), confirm the slow recovery of morphology in this area. During the recovery process, the intrusion of sandspit into river mouth area was observed (Fig. 4.2(c)). This phenomenon also occurred to other river mouths in this study, however the intrusion distance, L_{SI}, which is the distance between the tips of sandspits before and after the tsunami, is longest for the case of this river mouth. More details on the sandspit intrusion into this river mouth and others will be discussed later in Section 4.3. A project from government to reclaim the morphology at this river mouth is ongoing (Figs. 4.2(c) and 4.2(d)).

Figure 4.3 shows the measured river bed cross-sections at the river mouth before and after the tsunami. According to data measured in March, 2012, which is about one year after the tsunami, the river bed was still much deeper than the river bed before the tsunami. The river mouth bed became much shallower according to the data measured in March, 2013, and that corresponds to the period which sandspit has intruded into river mouth. It had been almost stable in the period from then until August, 2013.

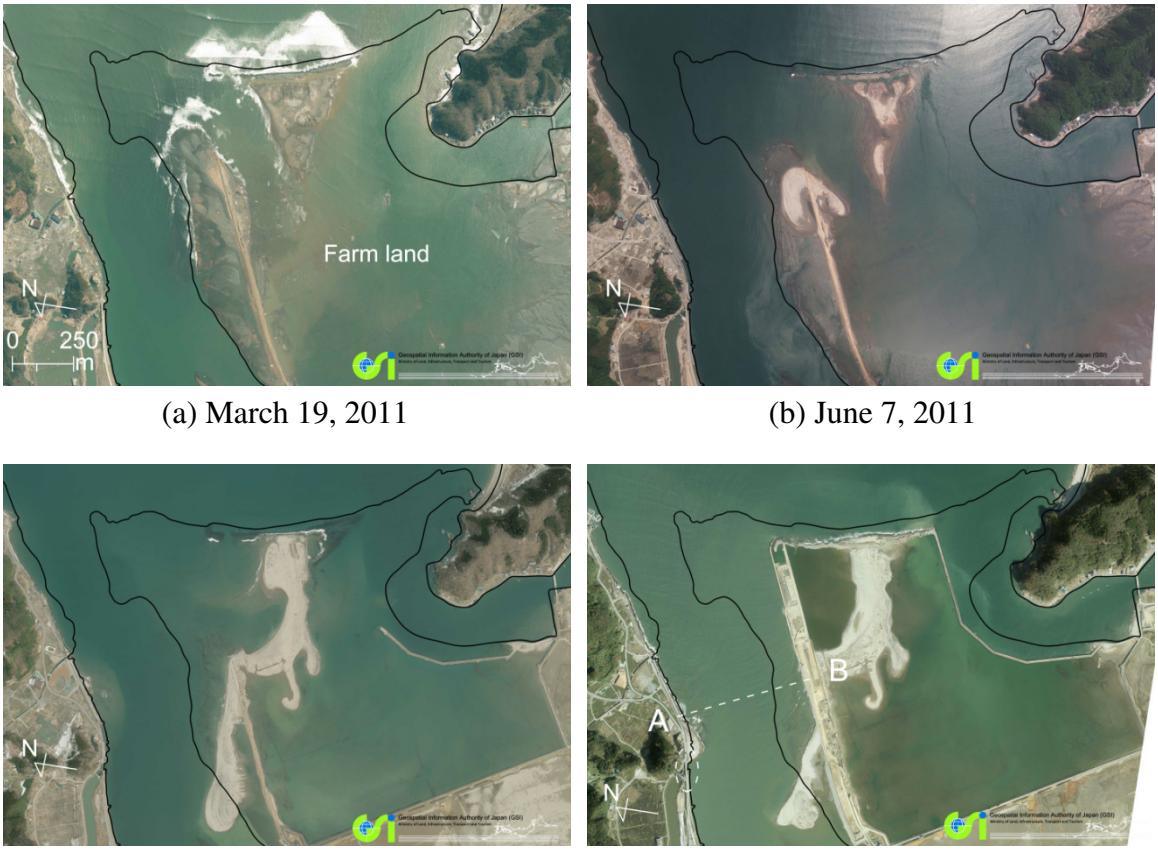

(a) March 19, 2011 (b) June 7, 2011

(c) December 28, 2012 (d) November 2, 2013

Fig. 4.1 Morphological recovery around the Kitakami River mouth (GSI) (black solid line is shoreline position on June 25, 2010)

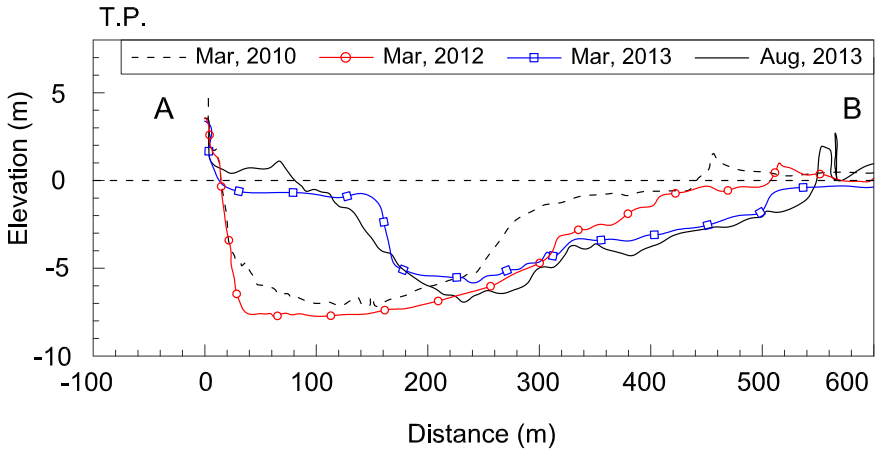

Fig. 4.2 Measured river bed cross-sections (A-B in Fig. 4.1(d)) at the Kitakami River mouth before and after the tsunami (T.P. is the datum level of Tokyo Peil)

4.2.2 Naruse River mouth

Figure 4.3 presents the changes and recovery process of morphology at the Naruse river mouth. The recovery of sandspit on the left bank of river mouth, which was flushed by the tsunami, has not been observed (Figs. 4.3(a) and 4.3(b)). Instead of recovery, the intrusion of sandspit into river mouth area can be seen (Fig. 4.3(c)). Aerial photographs of this river mouth shown in Fig. 4.3 indicate that no significant recovery of morphology has been observed even more than two and haft years since the happening of tsunami. This slow recovery was led by the limited sediment supply from the surrounding sandy coasts. Longshore sediment transport, whose direction is from north to south (left to right), is restricted by the T-headland on the left side of river mouth. Due to the disappearance of sandspit, waves propagate further upstream easier. They scoured the mouth of flooding canal on the left bank of river, transported sediment upstream and formed the sandspit (Fig. 4.3(c)). Moreover, they also caused collapsing of about 50 m long of embankment on the left bank on August 30, 2011 (dashed circle line in Fig. 4.3(c)). Since then the morphology at this river mouth has been almost stable; no further significant recovery has been observed (Fig. 4.3(d)).

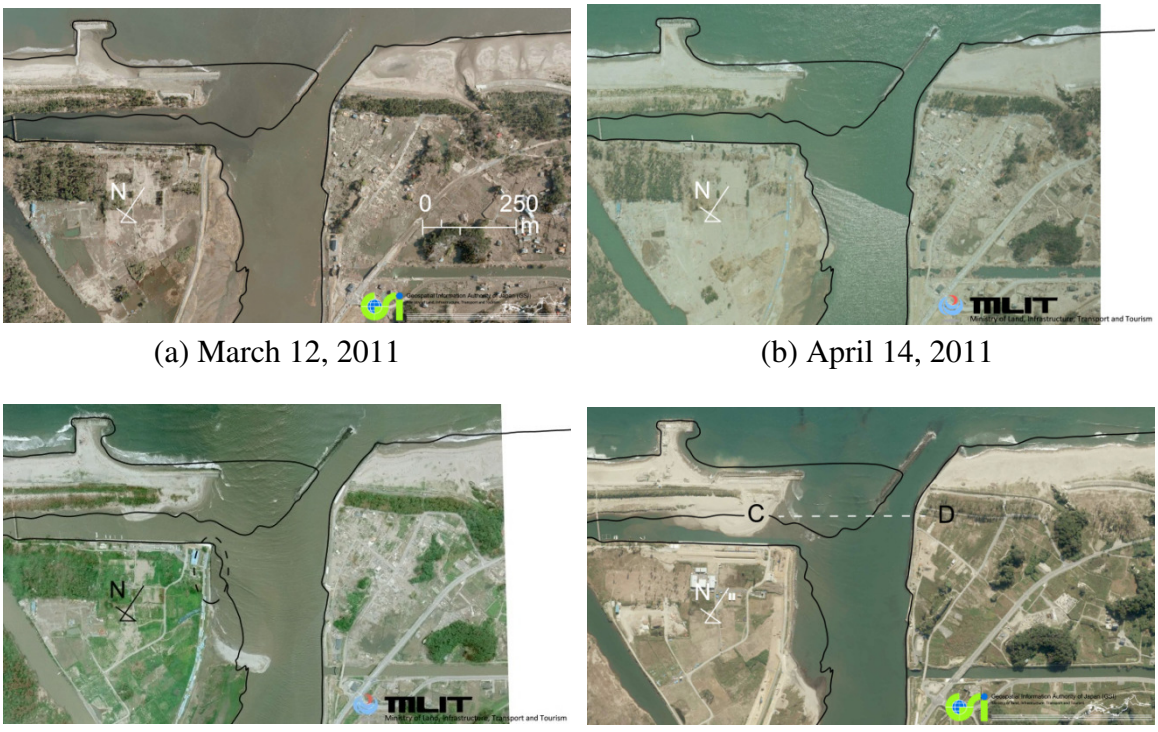

(a) March 12, 2011 (b) April 14, 2011

(c) June 29, 2011 (d) October 14, 2013

Fig. 4.3 Morphological changes and recovery at the Naruse River mouth (black solid line is shoreline position on April 4, 2010)

Figure 4.4 shows the measured river bed cross-sections at the Naruse River mouth. Unfortunately, there is only data for the period after the tsunami. According to data measured in June, 2011, the river bed was very deep. After that it has become shallower, especially on the left bank. Data surveyed in June and September, 2012 indicates that the river bed was almost stable in that period.

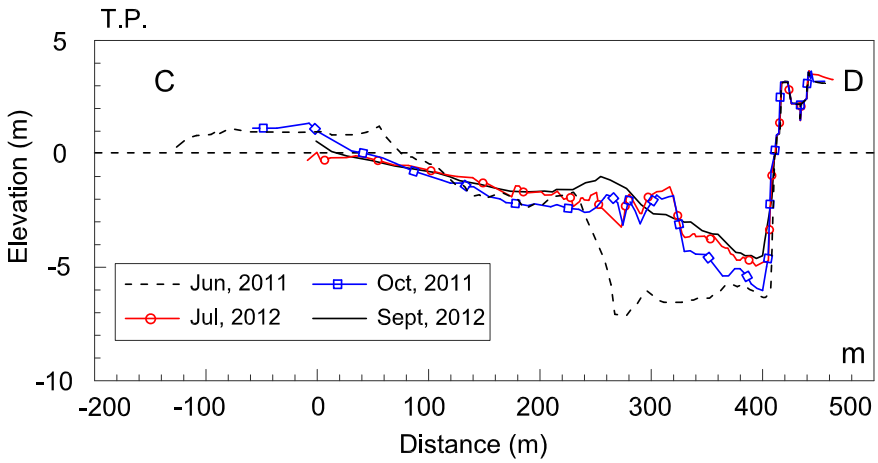

Fig. 4.4 Measured river bed cross-sections (C-D in Fig. 4.3(d)) at the Naruse River mouth after the tsunami

4.2.3 Nanakita River mouth

Figure 4.5 illustrates the recovery process of morphology around the Nanakita River mouth after the tsunami. As can be seen from aerial photographs in Figs. 4.5(a) and 4.5(b), the tsunami caused severe erosion of sandy beach, and flushed off river mouth sandspit and the sandy barrier located in front of Gamo Lagoon. Due to these damages, shoreline at the Nanakita River mouth area became concave shape after the tsunami. This kind of morphology played sink effect and caused erosion of the adjacent sandy coasts. Severe erosion occurred subsequently on both banks of the river mouth (Fig. 4.5(c)). Adityawan et al. (2013) discussed clearly the erosion mechanism of coast on the left side of the Gamo Lagoon. During the recovery process, sediment was transported from the north to the south filling into the concave portion. This direction of sediment movement is contrary with the normal direction of longshore sediment transport in this area which is from south to north. The erosion propagation of coast on the right bank will be presented Section 4.4. During the subsequent recovery process, sandspit intrusion into the river mouth was also observed (Fig. 4.5(c)). Figure 4.5(d) shows the completed closure of the Nanakita River entrance in September, 2011. The mechanism of this closure has been

discussed by Tanaka et al. (2012). In addition, it also shows the opening of a new river mouth on the left bank. Aerial photographs shown in Figs. 4.5(e) and 4.5(f) indicate that the morphology has returned to the shape before the tsunami; however shoreline position still remain far away behind the shoreline position before the tsunami. Detected shoreline positions extracted from some selected photographs are presented in Fig. 4.5(g). The tsunami caused significant retreat of shoreline. The recovery took place after the tsunami. Although the fast recovery was observed in this area, shoreline position in Mar, 2015 still remains about 30 m to 50 m behind the position before the tsunami.

The morphology of Gamo Lagoon had suffered severe damages induced by the tsunami. The morphological recovery process of this lagoon has been discussed specifically in Hoang et al. (2016).

(a) March 6, 2011

(b) March 12, 2011

(c) June 8, 2011

Fig. 4.5 Morphological changes and recovery around the Nanakita River mouth (black solid line is shoreline position on March 6, 2011), (to be continued in the next page)

(d) September 24, 2011

(e) April 8, 2012

(f) February 24, 2014

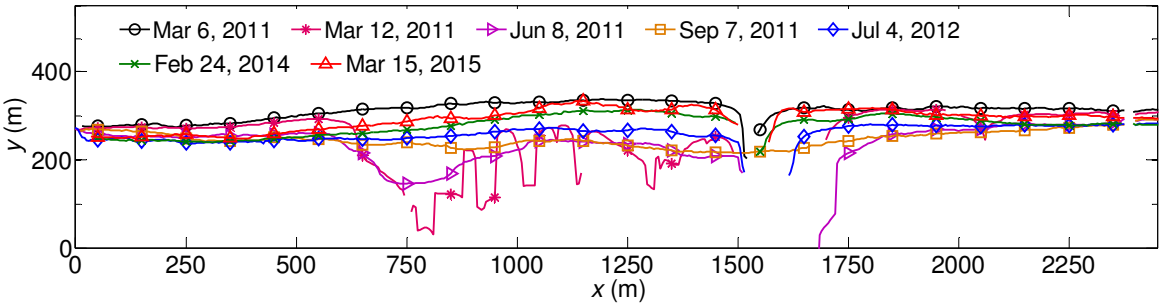

(g) Detected shoreline positions around the Nanakita River mouth

Fig. 4.5 (continued)

4.2.4 Natori River mouth

Figure 4.6 presents the morphological changes and recovery around the Natori River mouth. Similar to the case of the Nanakita River mouth, the tsunami also caused severe damages at this river mouth. Erosion of sandy beach, flushing of sandspit, and disappearance of sand barrier were observed at this river mouth area (Fig. 4.6(b)). However, the recovery of the morphology in this area was in different aspect compared to the recovery at the Nanakita River mouth. Due to the interruption on longshore sediment

transport from the south of breakwater at Yuriage Port and retaining sediment by the wave-dissipating blocks on the left, the recovery around this river mouth was very slow (Figs. 4.6(c) and 4.6(d) and Fig. 4.6(e)). During the subsequent recovery process, the sandspit intrusion into river mouth was also observed (Fig. 4.6(d)). The evolution of shoreline at this river mouth area is revealed more details from detected shoreline positions extracted from aerial photographs in Figs. 4.6(f). It confirms clearly that the recovery process in this area was going rather slow, till March, 2015 shoreline position in this area still remained about 100 m behind the shoreline position before the tsunami.

Figure 4.7 shows the measured river bed cross-sections at the Natori river mouth. Similar to other presented river mouths, this river mouth was scoured much deeper by the tsunami. However, it became much shallower after that when the sand spit intruded into the river mouth.

This case and the case of Nanakita River mouth have similar trend of morphology changes and recovery with cases reported in Liew et al. (2010). That study indicated that the morphology of sandy coast and lagoon has suffered severe damages induced by the 2004 Indian Ocean tsunami. The recovery took place after the tsunami, and the sandy beach was reformed. However, shoreline position still did not resume its position before the tsunami even though many years have passed.

(a) March 6, 2011

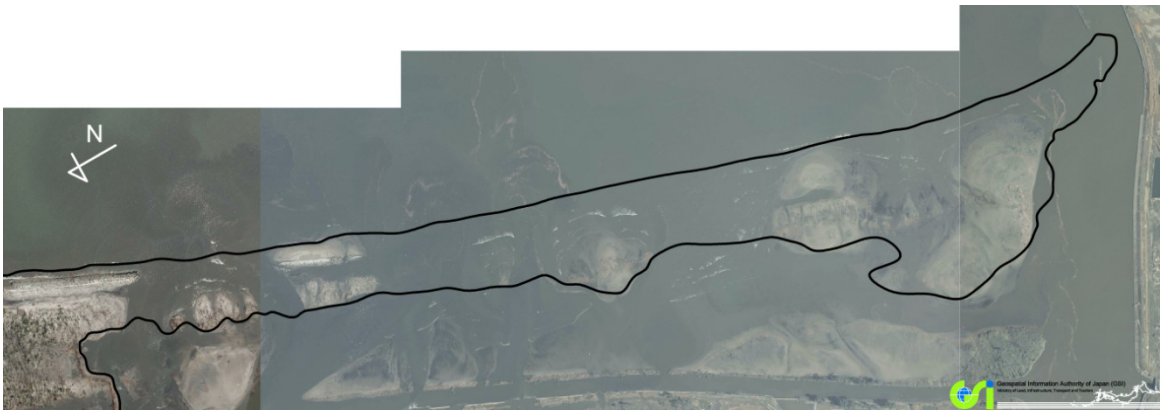

(b) March 12, 2011

(c) June 8, 2011

(d) September 9, 2013

Fig. 4.6 Morphological changes and recovery around the Natori River mouth (black solid line is shoreline position on March 6, 2011), (to be continued in the next page)

(e) February 24, 2014

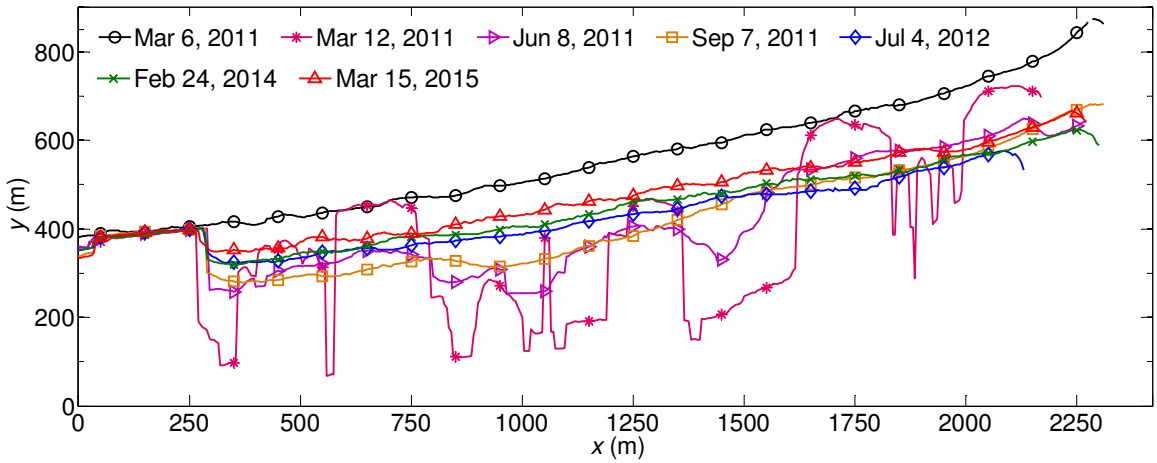

(f) Detected shoreline positions around the Natori River mouth

Fig. 4.6 (continued)

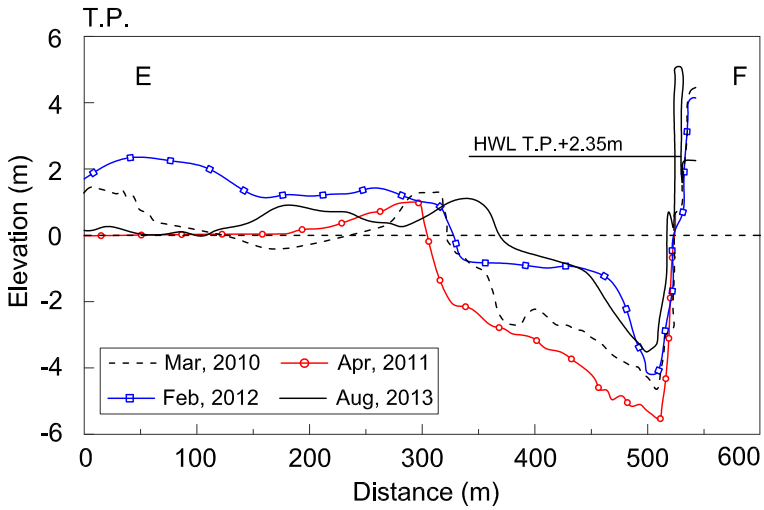

Fig. 4.7 Measured river bed cross-sections (E-F in Fig. 4.6(e)) at the Natori River mouth after the tsunami

4.2.5 Abukuma River mouth

Abukuma River is the sixth longest river in Japan and the second longest in the Tohoku region. It originates from Fukushima Prefecture and pours into the Pacific Ocean on the southern part of Miyagi Prefecture. In order to prevent erosion of sandy beach on the right side of the river mouth entrance, detached breakwaters and groins were constructed in periods 1986-1992 and 1974-1976, respectively. In addition, before 1980 two jetties were installed at the entrance of Torinoumi Lagoon which is located about 800 m south of the right side of river mouth. These structures interrupted the longshore sediment transport whose direction is reported from south to north (Mano et al., 1994).

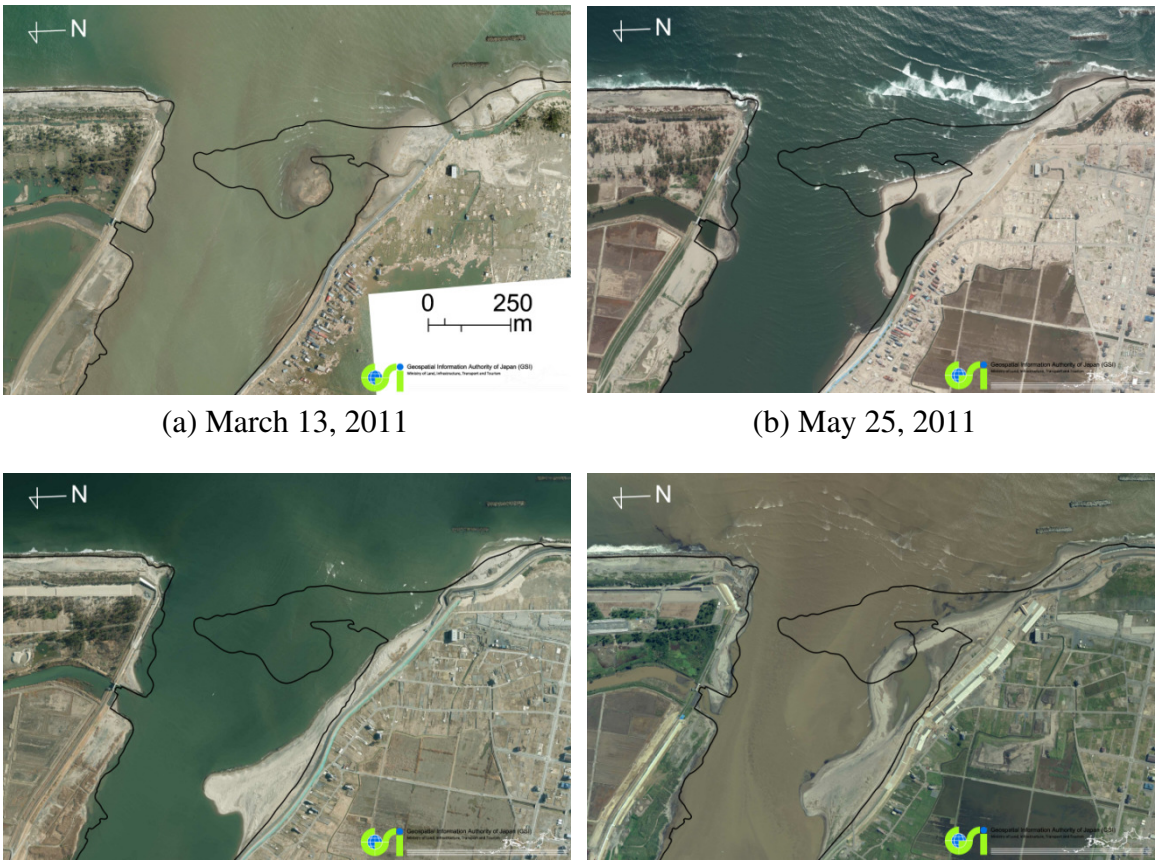

(a) March 13, 2011 (b) May 25, 2011

(c) January 5, 2013 (d) September 18, 2013

Fig. 4.8 Morphological changes and recovery around the Abukuma River mouth (black solid line is shoreline position on December 10, 2009)

Figure 4.8 illustrates the changes and recovery process of morphology at the Abukuma River mouth. The predominant direction of longshore sediment transport is from south to north, therefore a developed sandspit on the right of the river mouth can be seen (shoreline position on December 10, 2009). This sandspit was flushed off by the tsunami.

In addition, slight erosion of sandy coast on both sides of river mouth was observed after the tsunami. Beyond that there were no more significant changes of morphology induced by the tsunami at this river mouth (Fig. 4.8(a)). However, the recovery process in this area was also comparatively slow (Figs. 4.8(b), 4.8(c), and 4.8(d)). Moreover, sandspit intrusion into river mouth area was also observed at this river mouth (Fig. 4.8(c)).

4.2.6 Breaching of sandy coast at Arahama

Tanaka et al., (2014b) pointed out that strong tsunami return flow has formed breaching of sandy beach at the old river mouth area in Arahama Coast. The recovery of morphology at this breaching took place right after the tsunami. Aerial photographs, which show the recovery process of shoreline at the breaching, are presented in Fig. 4.9. According to those photographs, the breaching was connected very quickly within less than a half month after the tsunami. This case has the shortest time of recovery among the river mouths and breaching in this study. The breaching is located behind the detached breakwaters which were constructed from 1970 to 1980 to prevent the erosion in Arahama Coast; hence the recovery process is much faster than other areas.

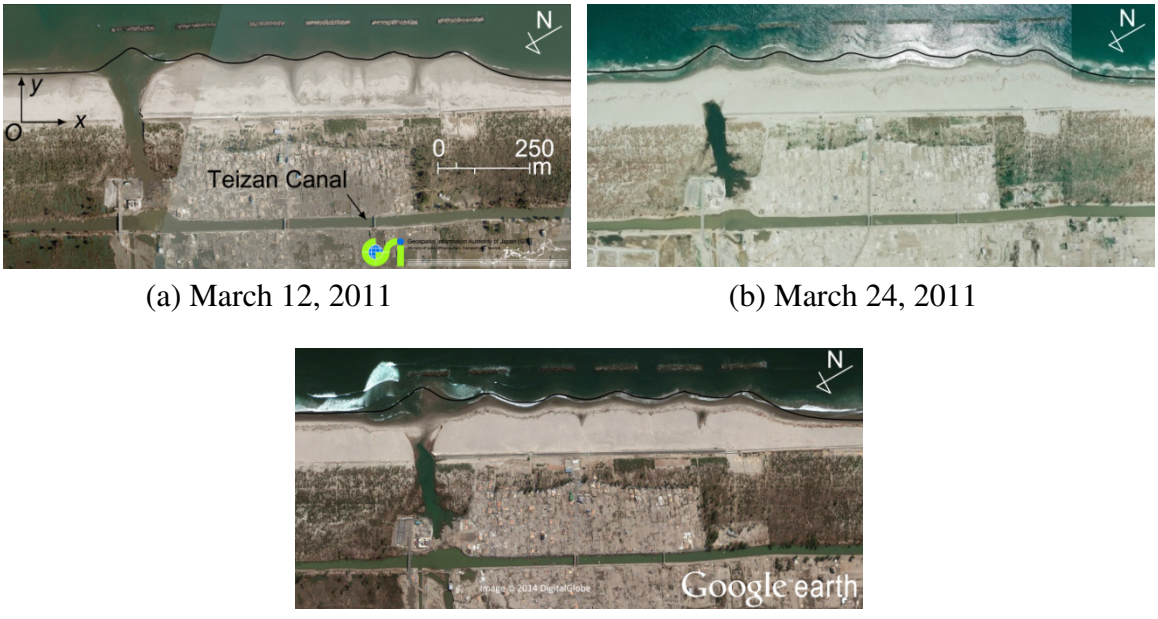

(a) March 12, 2011 (b) March 24, 2011

(c) June 8, 2011

Fig. 4.9 Morphological changes and recovery around the breaching of sandy coast at Arahama (black solid line is the shoreline position on March 6, 2011)

4.2.7 Breaching of sandy coast at Akaiko

The morphological recovery process of breaching at Akaiko is shown in Fig. 4.10. Similar to the case of breaching at Arahama, the tsunami return flow has also formed a breaching of sandy beach at the site of old river mouth (Fig. 4.10(a)). Around the breaching at Akaiko, there are 6.2 km long and 0.8 km long sandy coasts on the left and the right sides of the breaching, respectively. With sufficient sediment supply from both sides has made the recovery process at this breaching comparatively quickly (Figs. 4.10(b), 4.10(c), 4.10(d) and 4.10(e)).

Detected shoreline position around the breaching (Fig. 4.10(f)) indicates that during the recovery process, shoreline position in the concave portion was getting accretion, whereas the ones on adjacent sandy coasts were getting retreat. This behavior is similar to the case of concave shoreline at the Nanakita River mouth.

(a) March 13, 2011

(b) April 6, 2011

(c) May 3, 2011

(d) May 26, 2011

(e) March 13, 2011

Fig. 4.10 Morphological changes and recovery around the breaching at Akaiko (black solid line is shoreline position on August 14, 2009)

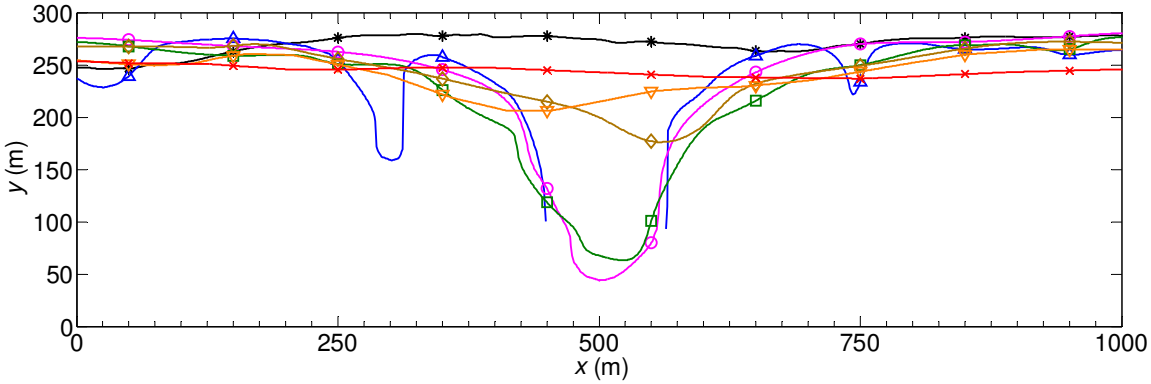

(f) Detected shoreline positions around the breaching at Akaiko

Fig. 4.10 (continued)

4.2.8 Breaching of sandy coast at Yamamoto

Overview of coastal morphology damages and subsequent recovery on entire Yamamoto Coast were presented in Udo et al. (2015, 2016). This study investigates more details on the recovery of the sandy coast of about 1000 m length around the breaching between headlands No. 9 and 11. The location of this breaching used to be a river mouth (Mano et al., 2013). Figure 4.11 shows selected satellite images of sandy beach breaching at Yamamoto. Before the tsunami, the landward part was covered by pine tree forest (Fig. 4.11(a)). Figure 4.11(b) shows the morphology three days after the tsunami. The pine tree forest has been swashed. A longshore canal can be seen clearly from this image. This canal was created due to the erosion behind the seawall (Udo et al., 2015). Breaching of sandy coast can also be observed. Its width was about 110 m. With the existence of the breaching, shoreline in this area had concave form. In addition, according to Udo et al. (2015), due to serious erosion, more than a haft of total amount of eroded sand above the sea level was transported seaward by the return flow. The recovery of morphology of the breaching was rather fast (Figs. 4.11(c), 4.11(d) and 4.11(e)). During the recovery process, the alongshore canal was blocked by the sediment transported into the breaching. Figure 4.11(f) indicates that the recovery of breaching has been completed. The elevating of seawall (T.P. +7.2 m) in this area has been completed. Shoreline positions before the tsunami and during the recovery process, are shown in Fig. 4.11(g). During the recovery process, shoreline position in the concave portion was accreted, while shoreline positions of adjacent sandy coasts was retreated. This behavior is similar to the one of concave shoreline at the Nanakita and breaching at Akaiko.

If consider in broader area, the tsunami and return flow also formed many breaching of sandy coasts along the Yamamoto Coast. During the recovery process, some of them have majorly recovery and some have not. At the breaching, which has no sediment supply from adjacent sandy coasts (no significantly recovery), the formation of tsunami embayment can be observed. More details on this phenomenon can be found in Hoang et al. (2017).

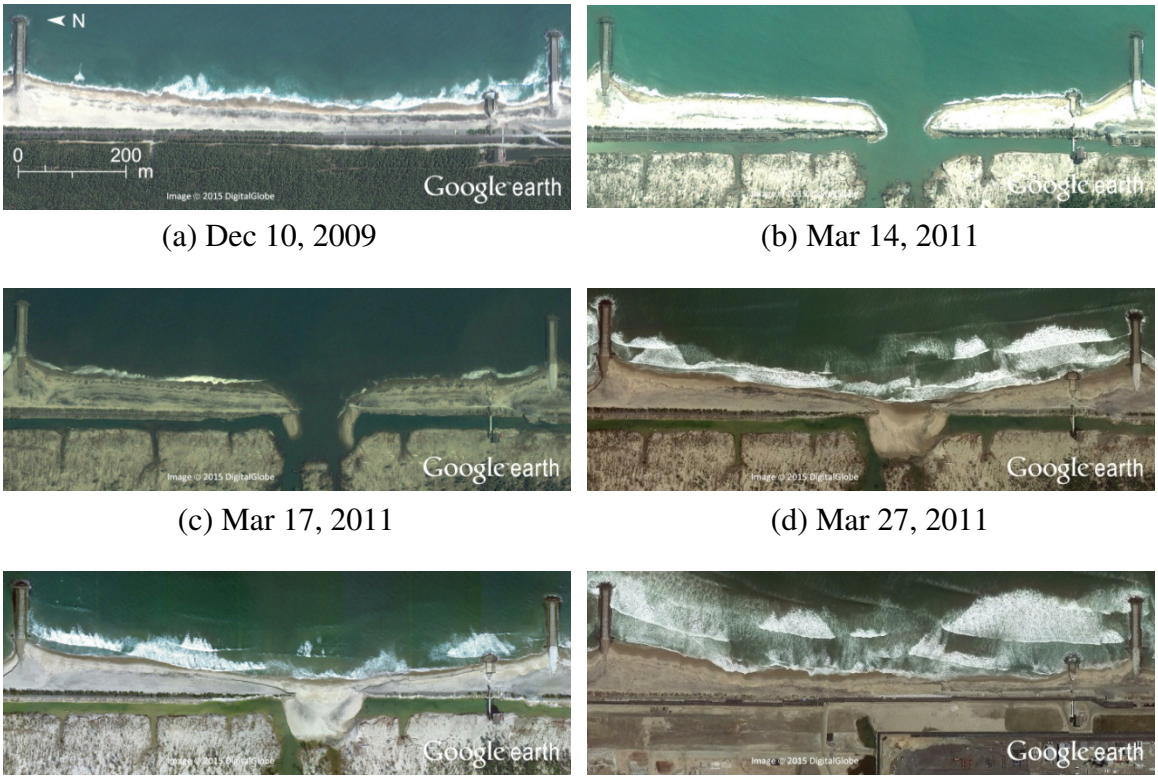

(a) Dec 10, 2009 (b) Mar 14, 2011

(c) Mar 17, 2011 (d) Mar 27, 2011

(e) Apr 06, 2011 (f) Apr 12, 2012

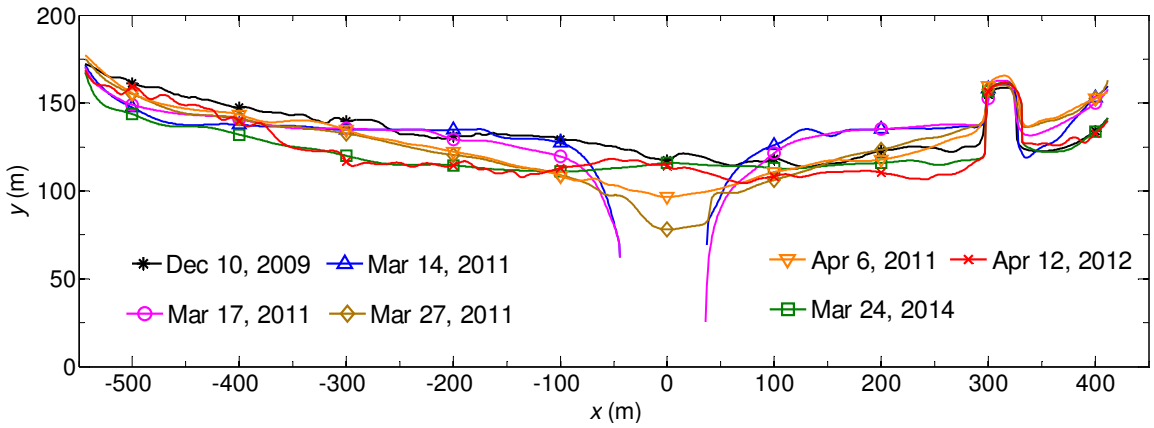

(g) Detected shoreline positions

Fig. 4.11 Morphological changes and recovery around the breaching at Yamamoto (Google Earth)

4.3 Sandspit intrusion into river mouth after the tsunami

4.3.1 Sandspit intrusion distance

As mentioned earlier, during the subsequent recovery process, the sandspit development and intrusion into river mouth was observed at five river mouths presented above. Figure 4.12 illustrates the intrusion of sandspit into each river mouth. Sandspit intrusion distance, L_{SI}, which is the distance between the tip of sandspits before and after the tsunami, can also be obtained from these figures. According to these results, the sandspit intrusion at the Nanakita River mouth has the shortest distance (about 400 m), while the longest is at the Kitakami River mouth (about 1300 m). At the Kitakami River mouth, the narrowest river channel was located upstream, far from the one before the tsunami. Due to this reason, waves can propagate further into the river mouth. They transport sediment toward the river channel. Similar to Naruse River, Kitakami River's structures have traditional design which has been carried out without considering the impact of wave force, therefore the run-up of waves, and sandspit intrusion into river mouth may cause severe problems.

Besides the cases of sandspit intrusion into river mouth regarding to severe morphological changes induced by the tsunami, another case of sandspit intrusion into river mouth after the construction of a jetty at the Mogami River mouth, is also taken into account for comparative study. The intrusion of sandspit into this river mouth was observed right after the construction of a jetty to stabilize the mouth. Maekawa (2010) presented that the sandspit has intruded upstream about 500 m in 12 years (1977-1989) since installing of jetty at the river mouth. An aerial photograph, which shows the morphology of this river mouth in 2010, is also included in Fig. 4.12. Similar to others, the sandspit intrusion distance of this case can be also obtained.

(a) Kitakami River mouth (GSI)

(b) Naruse River mouth (MLIT)

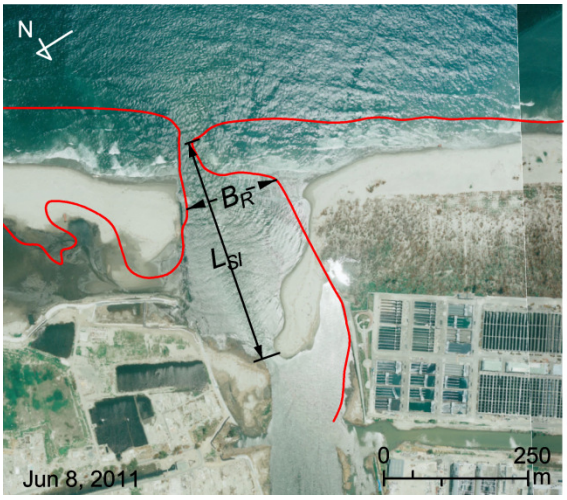

(c) Nanakita River mouth

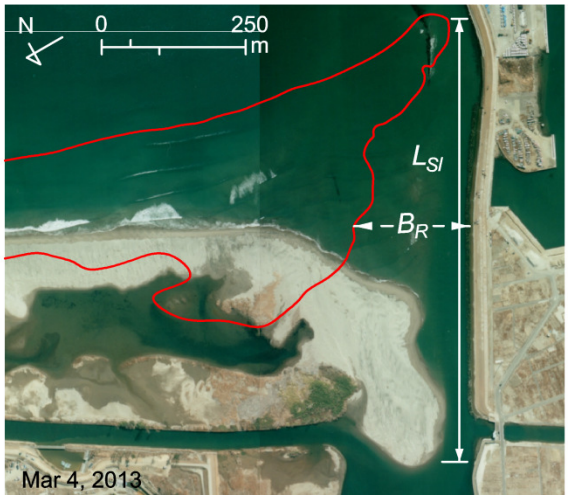

(d) Natori River mouth

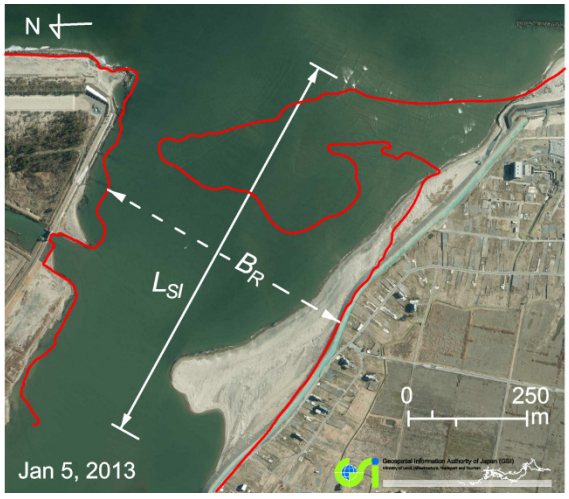

(e) Abukuma River mouth (GSI)

(f) Mogami River mouth (Google Earth)

Fig. 4.12 Sandspit intrusion into river mouths after the tsunami

4.3.2 Relationship between sandspit intrusion distance and river mouth width

Results from aerial photograph analysis indicate that the distance of sandspit intrusion would be proportional to the width of river mouth before the tsunami. Aerial photographs in Fig. 4.12 were also embedded solid lines that present the morphology of each river mouth before the tsunami. Based on these lines, the width of each river mouth before the tsunami, B_R, can be obtained. It was measured on the transection normal to the trend of river. The transection should locate behind the old sandspit and in front of the new sandspit (near the toe of new sandspit). The location, where the river mouth width is measured, is represented by dash line in each photograph. According to these results, the Abukuma River mouth has the widest width (about 500 m), whereas the narrowest is at the Nanakita River mouth (about 160 m).

Figure 4.13 reveals the relationship between the width of river mouth before the tsunami, B_R, and the sandspit intrusion distance, L_{SI}. From these results, a proportional relationship between these parameters is presented in Eq. (4.1) and represented by the black solid line in the figure.

$$L_{SI}=2.5B_R \tag{4.1}$$

The intrusion upstream of sandspit indicates that the boundary of fresh-sea water also moves upstream, therefore external wave forces must be considered when implementing the design of river structures. This is an important finding on the practical problem of this study.

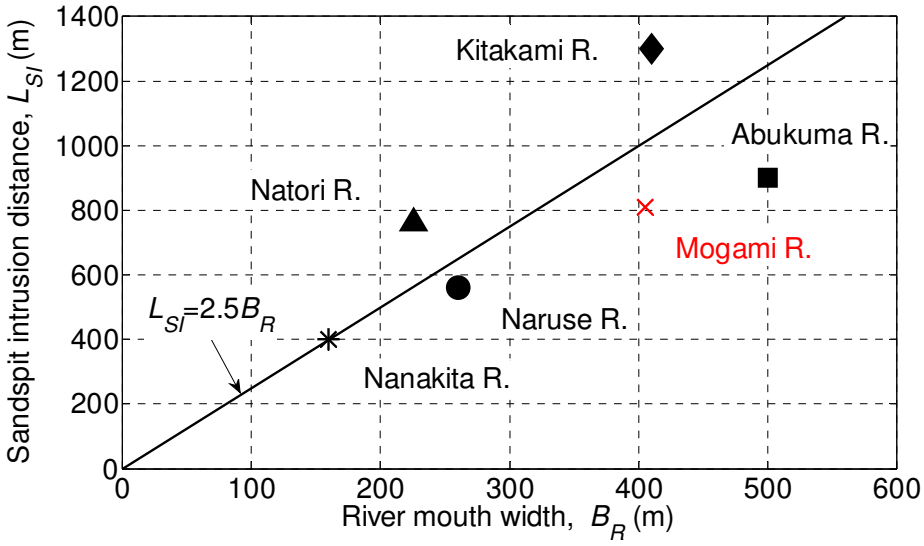

Fig. 4.13 Relationship between sandspit intrusion distance and river mouth width before the tsunami

4.3.3 Relationship between river mouth water depth and sandspit intrusion

Uda and Yamamoto (1992) implemented the experiment in a flat tank to find the relationship between the formation of sandspit and surrounding sea bottom configuration. They aimed to explain the formative process of sandspit at bay mouths based on the results obtained from the experiment. Due to the similarity of characteristics between bay mouth and river mouth, the results of that experiment are also utilized to study the formation and intrusion of sandspit after the tsunami at river mouths in this study. In their experiment, the development of sandspit for two cases of initial shoreline condition is examined. In Case (1), the direction of initial shoreline is abruptly diverted 70^{O} at the center of the test area, and all the bottom contours are set to be parallel to the shoreline. In Case (2), the changing of direction of initial shoreline is same as Case (1), however a flat shallow sea bottom extends along the shoreline. The water depth (from water level to sea bottom) in the area, which initial shoreline is diverted, is 30 cm and 5 cm for Cases (1) and (2), respectively. The initial shoreline position, the beach topography after 8 hours in experiment, and other parameters such as breaker height, breaker angle, and breaker point are presented in Figs. 4.14(a) and 4.14(b). After 8 hours in experiment, for Case (1), the formation of sandspit in the area of diverted initial shoreline is observed (Fig. 4.14(a)), whereas the sandspit is formatted in front of that area in the remained case (Case (2), Fig. 4.14(b)). In Fig. 4.14(b), a dashed line, which represents shoreline at 1 hour, is also included to show the fast formation of sandspit and its location. Results obtained from these two cases in Figs. 4.14(a) and 4.14(b) show consistency with the development of sandspit at the Nanakita River mouth shown in Figs. 4.5(c) and 4.5(a), respectively. Figure 4.15 shows a schematic diagram of the sandspit development from two cases of experiment. In that figure, D_C is the depth of closure corresponding to the average wave, while D_R is the depth of water in the river mouth area. If $D_R > D_C$, Case (1), the formatted sandspit similar to the sandspit at the Nanakita River mouth shown in Fig. 4.5(c) is obtained. In contrast, if $D_R < D_C$, Case (2), the formation of sandspit similar to the sandspit at the Nanakita River mouth as shown in Fig. 4.5(a) is obtained. Before the tsunami, the Nanakita River mouth has almost constant bottom with water depth of 1.5 m (Tanaka and Takahashi, 1995). However, it is assumed that this river mouth was scoured up to 8m water depth similar to the cases shown in Figs. 4.2, 4.4, and 4.7. The depth of closure of Sendai Coast was evaluated as of 8 m by Uda (1997). This value was obtained corresponding to the high waves. Morphological changes at the Nanakita River mouth

presented in Fig. 4.5 was induced by higher frequent waves (H=0.91 m, T=8.5 s, Kang and Tanaka, 2006). Hence, another attempt was made to compute the depth of closure for this area based on the equation proposed by Sato and Tanaka (1962) and above wave characteristics. A value of D_C=2 m was obtained from that computation.

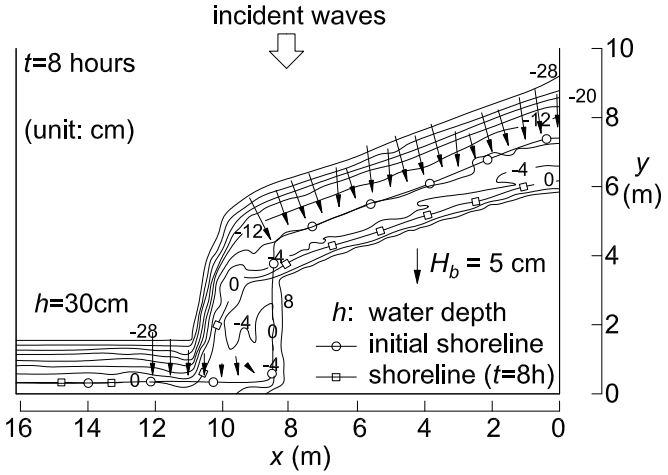

(a) Beach topography at t=8 hours, Case (1)

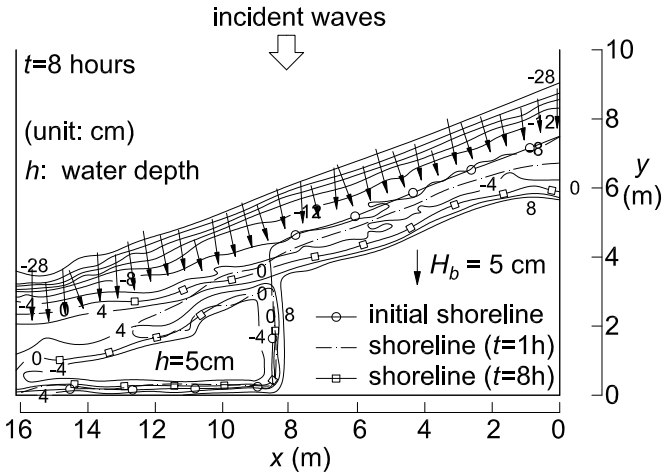

(b) Beach topography at t=8 hours. Dashed line is shoreline at 1 hour, Case (2)

Fig. 4.14 The formation of sandspit (Uda and Yamamoto, 1992). The length and the direction of the vector show the breaker height and the breaker angle, respectively. The tip of the vector is located at the breaking point

The relationship between D_C and D_R from Uda and Yamatomo (1992), and pre-post the tsunami is presented in Fig. 4.16. Results shown in this figure indicate that the scouring deeper of river mouth induced by the tsunami made the correlation of D_R and D_C (D_R>D_C) moving beyond the line of D_R=D_C, and resulted in the morphology change similar to Case (1) of Uda and Yamamoto (1992). It can be concluded that the scouring

deeper of river mouth induced by the tsunami was the cause source of the sandspit intrusion after the tsunami.

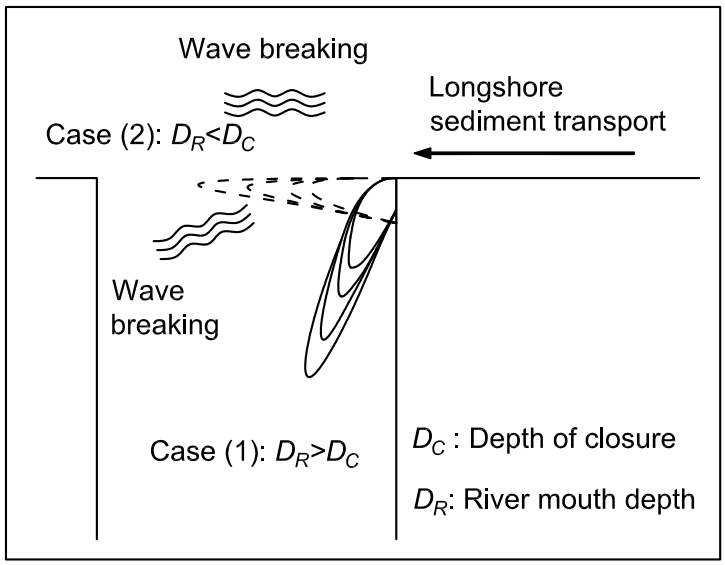

Fig. 4.15 Schematic diagram of sandspit formation

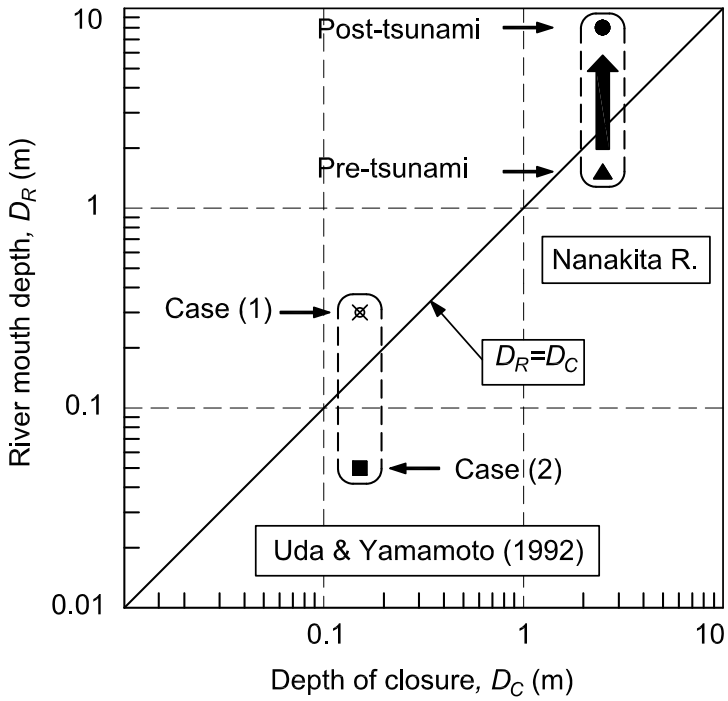

Fig. 4.16 Relationship between D_C and D_R

4.4 Investigating the subsequent recovery by analytical solutions of one-line model

4.4.1 Erosion propagation on beaches adjacent to the Nanakita River mouth

As mentioned previously, concave shoreline was commonly observed at the river mouth area after the 2011 tsunami. A typical case is at the Nanakita River mouth area. Concave shoreline was formed at this area after the eroding of sandy barrier in front of Gamo Lagoon which is adjacent to the left bank of the river mouth, and the flushing of sandspit at the river mouth. The width of concave portion, which is the alongshore length of the concave portion, is about 1050 m. This value is the distance right after the tsunami between the right river bank and left side of Gamo Lagoon. In reality, the shape of concave portion is so complicated, not always truly rectangular, and not uniform bottom elevation. However, in this study, the concave portion is assumed to be rectangular and uniform bottom elevation, and the width is taken as the distance between the left and the right sides of eroded area. Detailed explanation on how to estimate initial conditions of concave shoreline right after the tsunami will be given in Section 6.5. Figure 4.17 shows variation of shoreline position at the Nanakita River mouth area. During the recovery process of morphology, sandy beaches on both sides of the concave portion were being eroded. The erosion of shoreline was propagating from the area bordering concave portion to the far sides of sandy coasts.

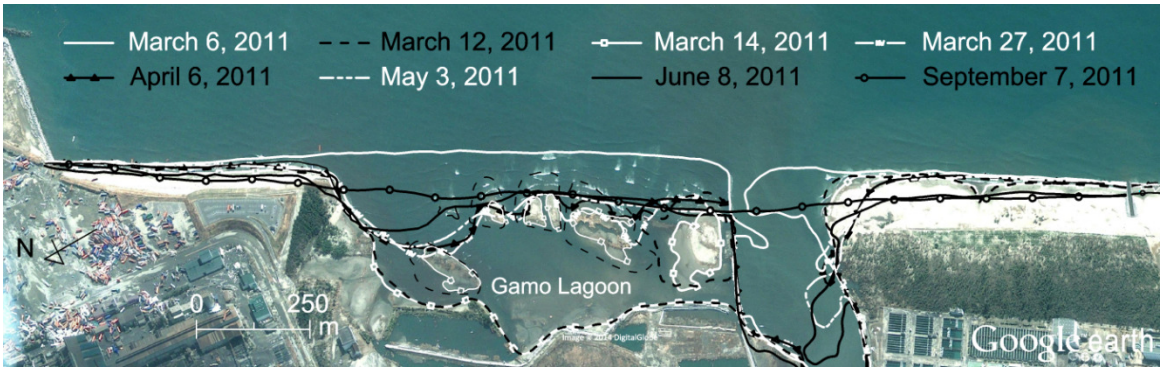

Fig. 4.17 Deformation of beach morphology around the Nanakita River mouth after the tsunami (background: March 14, 2011, Google Earth)

Eroded sediment from adjacent sandy coasts was transported into the concave portion, leading to the accretion of shoreline in this area. This sediment was the main sediment source for the recovery of morphology in the concave portion. Hence, it is considered that the concave shoreline at river mouth area played sink effect on the littoral system. It is similar to the sink effect of river mouth and tidal inlet which have been the topics of

various studies. FitzGerald (1988) and Kraus and Wamsley (2003) examined sink and source effects through the formation of flood shoal in the tidal inlet. Uda (1997) pointed out the sink effect of river mouth after being dredged. That dredging was implemented to reduce sediment deposition in river mouth area in order to avoid river mouth closure. That resulted in severe erosion of adjacent sandy coasts.

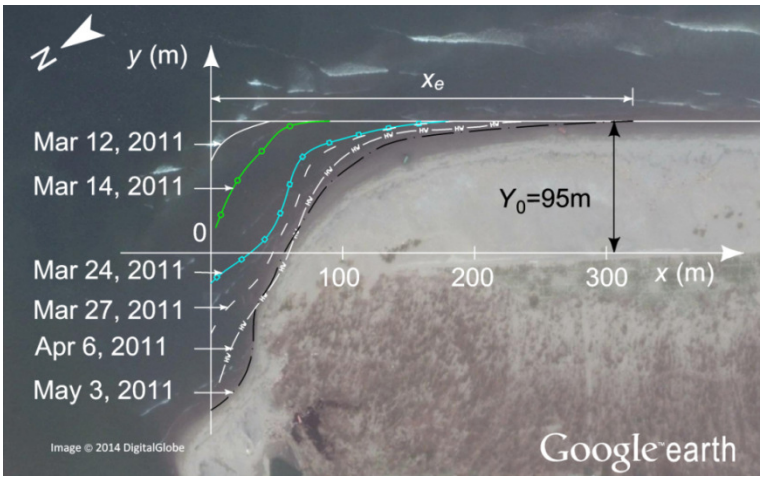

Fig. 4.18 Variation of shoreline position on the right bank of the Nanakita River mouth after the tsunami (background: May 3, 2011, Google Earth)

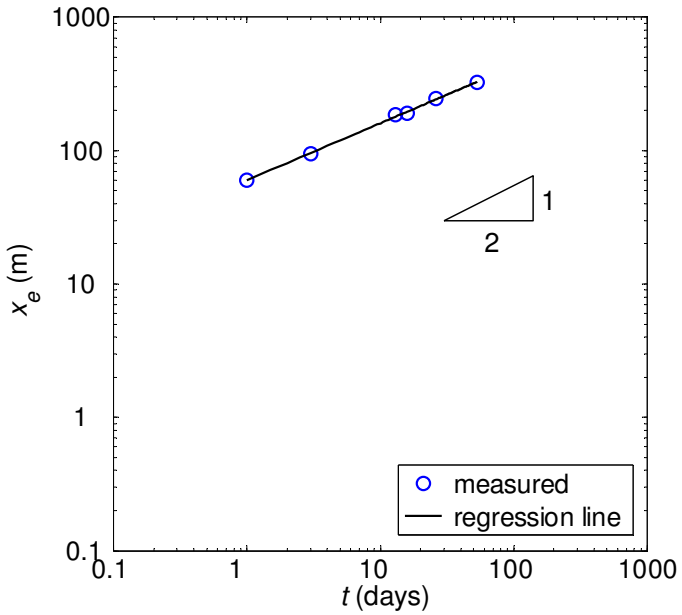

Fig. 4.19 Erosion propagation process on the right bank of the Nanakita River mouth

Figure 4.18 illustrates overlapping shoreline positions right after the tsunami to May, 2011. The erosion propagation of shoreline on the right side of the Nanakita River mouth can be seen from that figure. In order to evaluate the propagation process, which is called

erosion propagation distance, x_e (Fig. 4.18), is utilized. It is defined as the distance from the concave portion to the point where shoreline position becomes 99 % of initial shoreline position. In which, initial shoreline position is the position right after the tsunami. Detailed explanation on how to measure the initial conditions of the concave shorelines after the tsunami will be given in Section 6.5.

Figure 4.19 shows the relationship between erosion propagation distance and elapsed time of the beach on the right bank of the Nanakita River mouth. A regression line is also included in this figure. The results shown in the figure clearly reveal that the distance of erosion propagation increases in proportional to the square root of elapsed time.

Although similar investigation on the erosion propagation of the sandy beach from north side of Gamo Lagoon to breakwater of Sendai Port has been done, clear relationship as founded in Fig. 4.19 was not obtained. The existence of concrete blocks functioning as detached breakwater (Fig. 4.20), which were installed in this area to prevent coastal erosion, is believed to be the main reason.

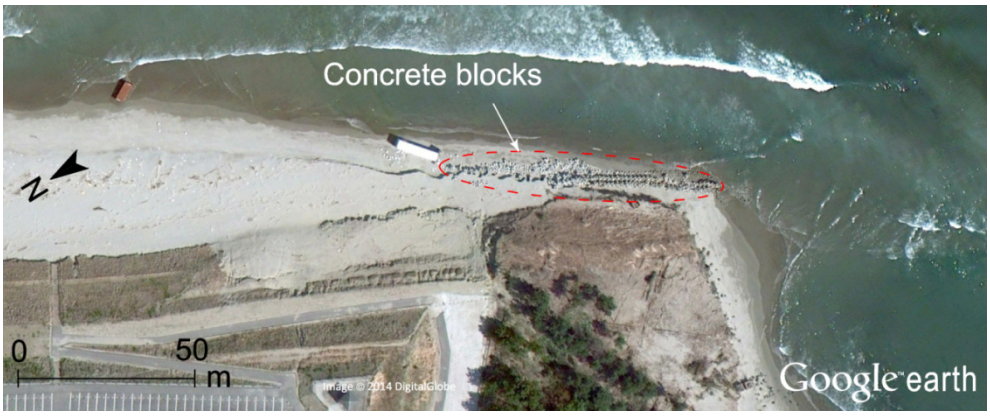

Fig. 4.20 Concrete blocks on the left side of the concave portion at the Nanakita River mouth (background: April 6, 2011, Google Earth)

4.4.2 Erosion propagation on beaches adjacent to the breaching at Akaiko

Figure 4.21 shows the changes of morphology of breaching at Akaiko induced by the tsunami and subsequent recovery. The concave shoreline at this breaching recovered much faster than the one at the Nanakita River mouth. The reason is that its concave portion width is much narrower and its total length of adjacent sandy coasts is longer compared to the case of concave shoreline at the Nanakita River mouth. More details on the relationship between the recovery time and the total length of adjacent sandy coasts

for cases of concave shorelines at the Nanakita River mouth and breaching at Akaiko will be presented in Chapter 6.

The temporal variation of shoreline at the breaching at Akaiko is expanded and shown in Fig. 4.21. According to this figure, on the recovery process, the beaches on both sides of the breaching were eroded. The erosion was extended along the beaches on both sides. This erosion propagation is similar to the erosion propagation at the Nanakita River mouth as shown previously in Fig. 4.18.

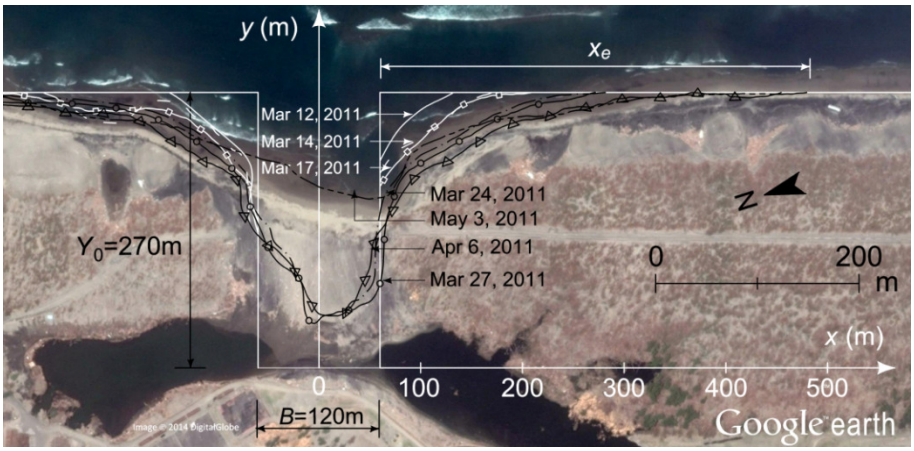

Fig. 4.21 Temporal variation of shoreline position around the breaching of sandy coast at Akaiko after the tsunami (background: May 3, 2011, Google Earth)

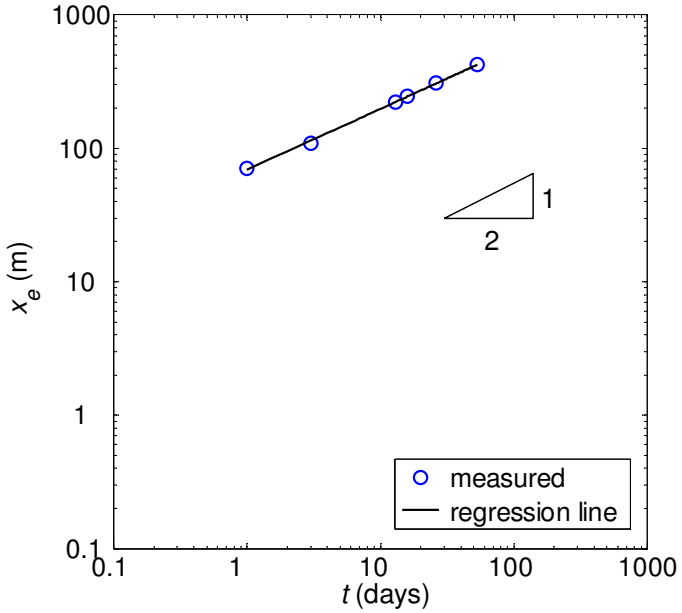

Fig. 4.22 Erosion propagation process around the breaching of sandy coast at Akaiko

Similar process, which was applied for the case of erosion propagation at the Nanakita River mouth, has done for case of the breaching at Akaiko. The relationship between erosion propagation distances, x_e, and the elapsed time, t, for the beach on the right side of the breaching can also be obtained based data in Fig. 4.21. According to the results shown in Fig. 4.22, the erosion propagation distance is proportional to square root of elapsed time. This result confirms the result shown in Fig. 4.19.

Although similar analysis was also done for the beach on the left side of the breaching, similar relationship between the erosion propagation distance, x_e, and the elapsed time, t, to which observed in Fig. 4.21 for the right side was not obtained. The complex initial geometry of the coast after the tsunami, V-shaped channel and the existing of embankment on the left side (Tappin et al., 2012), are considered as the main reasons.

As discussed in previous sections, during the recovery process of morphology, sediment was transported into the concave portion, leading to the accretion of shoreline; however, shoreline positions on adjacent sandy coasts were retreated. In addition, morphology in study areas was highly disequilibrium due the formation of concave shoreline induced by the tsunami; incident waves transported sediment from adjacent beaches to the concave portion. Accordingly, it can be said that during the recovery process of concave shorelines at the Nanakita River mouth and the breaching at Akaiko longshore sediment is predominant. Therefore, the evolution of shoreline can be described by theory of one-line model. More indications proving the dominance of longshore sediment in this coast after the tsunami will be presented in Section 6.2.

Larson et al. (1987) introduced the analytical solutions, Eqs. (4.2) and (4.3), to describe the evolution of shoreline position with initial conditions as shown in Figs. 4.23(a) and 4.23(b) (Cases (A) and (B)), respectively

$$y=\frac{1}{2}Y_0\left[1+\mathrm{erf}\left(\frac{x}{2\sqrt{\varepsilon t}}\right)\right] \tag{4.2}$$

$$y=\frac{1}{2}Y_0\left[\mathrm{erfc}\left(\frac{B-2x}{4\sqrt{\varepsilon t}}\right)+\mathrm{erfc}\left(\frac{B+2x}{4\sqrt{\varepsilon t}}\right)\right] \tag{4.3}$$

where Y_0 is the cross-shore distance of beach cut from the initial shoreline. This distance is estimated based on the actual condition of shoreline right after the tsunami. Detailed estimation of this parameter for the study areas will be given in Section 6.7; erfc is the complementary error function; B is the width of rectangular beach cut (concave portion).

As mentioned in Chapter 3, the analytical solution of one-line model is obtained when solving the simplified governing equation of one-line model, Eq. (3.11), which is derived

from the governing equation of one-line model with the assumptions. One of the assumptions is that the angle between wave crests and shoreline is small. In order to apply the analytical solutions, this assumption needs to be valid. According to the wave conditions shown in Chapter 3, the most dominant waves come from the east and south-east direction (around 100^{O} to 120^{O} from the north direction), whereas shoreline trend, for example the northern part of Sendai Coast (including the Nanakita River mouth), angles clockwise to the north direction about 210^{O}. Hence, the angle between the wave crests and the shoreline trend is small enough. Another assumption is that the wave height is constant along the coast (independence of x and t). Of course, the wave is changing from time to time and place to place due to the difference of bathymetry along the coast. However, on the straight and without diffraction like at the Nanakita River mouth and breaching at Akaiko, the assumption is reasonable.

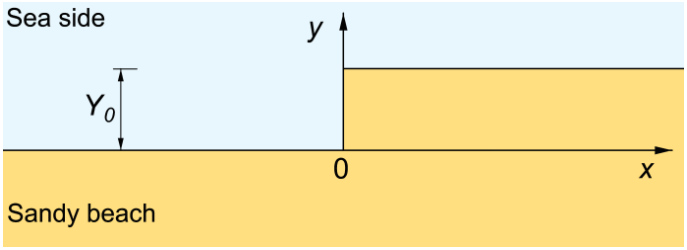

(a) Semi-infinite rectangular beach cut – Case (A)

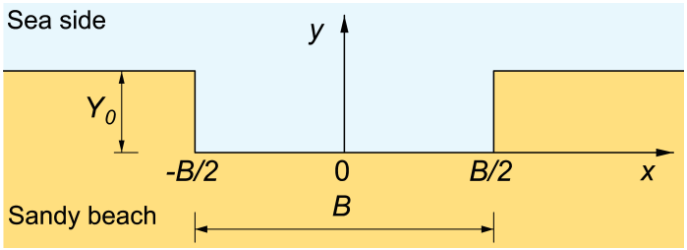

(b) Rectangular cut in an infinite beach – Case (B)

Fig. 4.23 Initial conditions of morphology

Equations (4.2) and (4.3) can be expressed in term of dimensionless parameters as following

$$y^{*}=\frac{1}{2}\left[1+\mathrm{erf}\left(\frac{x^{*}}{2\sqrt{t^{*}}}\right)\right] \tag{4.4}$$

$$y^{*}=\frac{1}{2}\left[\mathrm{erfc}\left(\frac{B^{*}-2x^{*}}{4\sqrt{t^{*}}}\right)+\mathrm{erfc}\left(\frac{B^{*}+2x^{*}}{4\sqrt{t^{*}}}\right)\right] \tag{4.5}$$

where the dimensionless parameters are defined as bellow

$$x^* = \frac{x}{Y_0} \tag{4.6}$$

$$y^* = \frac{y}{Y_0} \tag{4.7}$$

$$t^* = \frac{\varepsilon t}{Y_0^2} \tag{4.8}$$

$$B^* = \frac{B}{Y_0} \tag{4.9}$$

The solution in dimensionless form can describe the evolution of shoreline position in more compact form. The comparison using dimensionless parameters is more significant in relating the results in more general conditions. Therefore, in this study, the dimensionless form is utilized throughout. The dimensional parameters are normalized to the initial beach cut, Y_0. That determines the weight of the dimensional parameters to the initial beach cut. However, when using the dimensionless parameters in the solutions, the physical understanding may be obscured because of the absence of dimensional quantities. For example, when the dimensionless recovery time, t^* (Eq. (4.8)), is large implying that the elapsed time is also large as having constant values of Y_0 and ε. However, it would not be clear and direct meaning as using the dimensional time, t.

Figure 4.24 presents the evolution of shoreline positions from the analytical solutions of one-line model for cases of semi-infinite rectangular beach cut (Case (A)) and rectangular cut in an infinite beach (Case (B)). The evolution of shoreline positions of these two cases are represented by dashed lines with circle markers and solid lines, respectively. An arbitrary value of B^*=2 is selected for the computation of shoreline positions evolution. According to Fig. 4.24, in the early stage the evolution of shoreline positions on the left and the right sides of Case (B) is independent, and shoreline positions obtained from two analytical solutions for two cases are the same. In the longer elapsed time, when the evolution of shoreline positions on both sides has interacted on each other, the positions of shorelines obtained from two analytical solutions are in different trend of evolution; the one of Case (A) tends to advance faster in the beach cut region and retreat earlier on the adjacent beach compared to the one of Case (B).

It is also noted that if the complementary error function, erfc, in Eq. (4.5) is replaced by the error function, erf, it can describe the evolution of rectangular beach fill (convex shoreline) in an infinite beach. Moreover, that modified equation can also be used to evaluate the sediment expansion rate in beach nourishment after a rectangular planform is created, etc. (Dean, 2003).

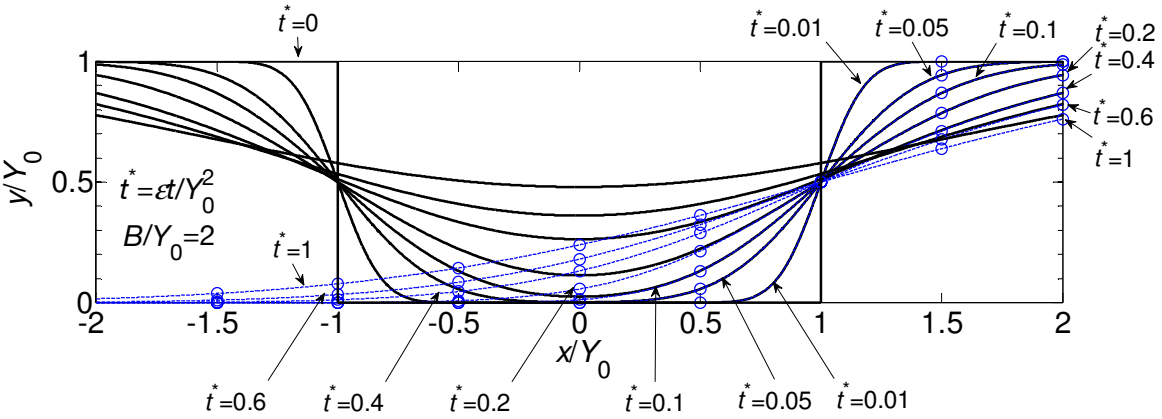

Fig. 4.24 Evolution of shoreline positions from analytical solutions of one-line model for cases of semi-infinite rectangular beach cut (Case (A)) and rectangular cut in an infinite beach (Case (B)). (It is noted that in order to show the evolution of shoreline positions for the Case (1) corresponding to the origin as in this figure, the term x^* in Eq. (4.4) is replaced by the term x^*-$B^*/2$)

Hereafter, the erosion propagation distance, which is shown in Figs. 4.18 and 4.21, is investigated based on the Eqs. (4.2) and (4.3). According to theoretical characteristics of Eqs. (4.2) and (4.3), shoreline positions are described by the error function and error function complementary; hence the erosion propagation distance, x_e is infinite. In order to obtain this value, it is redefined as the distance from beach cut region to the point where shoreline becomes 99 % of Y_0. Similar treatment is also made in the definition of boundary layer thickness of the boundary layer flow which has the similar characteristics (e.g., Sana and Tanaka, 2007).

According to Eq. (4.2) and the definition of erosion propagation distance, x_e, the following equation is obtained

$$0.99=\frac{1}{2}\left[1+\mathrm{erf}\left(\frac{x_e}{2\sqrt{\varepsilon t}}\right)\right] \tag{4.10}$$

or

$$\mathrm{erf}\left(\frac{x_e}{2\sqrt{\varepsilon t}}\right)=0.98 \tag{4.11}$$

by using the error function table for Eq. (4.11), the following equation can be obtained

$$x_e=3.3\sqrt{\varepsilon t} \tag{4.12}$$

Equation (4.12) reveals the relationship between erosion propagation distance and elapsed time. The erosion propagation distance is proportional to the square root of elapsed time.

According to Fig. 4.24, the erosion propagation process is the same with the deposition propagation process in the beach cut region. This is valid for all time for Case (A), while it is valid only in the early stage for Case (B). Hence, if similar definition and procedures, which have been used to determine the relationship between erosion propagation distance and elapsed time, are applied, then the relationship between the deposition propagation distance, x_d, and elapsed time, t, can also be obtained. The time, when the deposition propagation distance excesses $B/2$, is considered as the critical elapsed time point, T_{CR}. If the time has not yet passed beyond T_{CR}, the evolution of shoreline position on the left and the right hand sides of beach cut region has no influence on each other, and analytical solution for case of rectangular cut in an infinite beach can be used for the other case.

Alternatively, above relationship between erosion propagation distance and elapsed time can be expressed in term of dimensionless parameters as following

$$x_e^*=3.3\sqrt{t^*} \tag{4.13}$$

where dimensionless parameter are defined as below

$$x_e^*=\frac{x_e}{Y_0} \tag{4.14}$$

Similar to the case of semi-infinite rectangular beach cut, if analytical solution of one-line model, Eq. (4.3), which describes the evolution of shoreline positions for the case of rectangular cut in an infinite beach, is used, the dimensionless erosion propagation distance on the beaches on both sides of the beach cut region will be given by the following equation

$$\frac{1}{2}\left[\operatorname{erfc}\left(-\frac{x_e^*}{2\sqrt{t^*}}\right)+\operatorname{erfc}\left(\frac{B^*+x_e^*}{2\sqrt{t^*}}\right)\right]=0.99 \tag{4.15}$$

The relationship between the dimensionless erosion propagation distance and dimensionless elapsed time obtained from Eq. (4.15) corresponding to several values of B^* is illustrated in Fig. 4.25(a). According to these results, when the value of B^* is small, the recovery process is completed in a shorter time, thus x_e^* is also shorter than others. When the value of B^* is increasing (e.g., B^*=5, 10, 20 in Fig. 4.25(a)) the dimensionless erosion propagation distance obtained from Eq. (4.15) is asymptotic to the one obtained from Eq. (4.13). Moreover, if the dimensionless elapsed time is small, the dimensionless erosion propagation distance obtained from Eqs. (4.13) and (4.15) are in good agreement. Hence, the measured data of erosion propagation distances, which are shown in Figs. 4.19 and 4.22, indicate high agreement with the theoretical erosion propagation distances, Eq. (4.13), which obtained from analytical solution of one-line model. Moreover, as discussed

above when the value of B^* is large, the dimensionless erosion propagation distances obtained from analytical solutions of two cases are proportional to the square root of dimensionless elapsed time. It is common to observe similar process of physical phenomenon which is described by diffusion equation such as heat conduction phenomenon (e.g., Carslaw and Jaeger, 1959), viscous fluid (e.g., Schlichting and Gersten, 2000), and substance diffusion phenomenon (e.g., Crank, 1975).

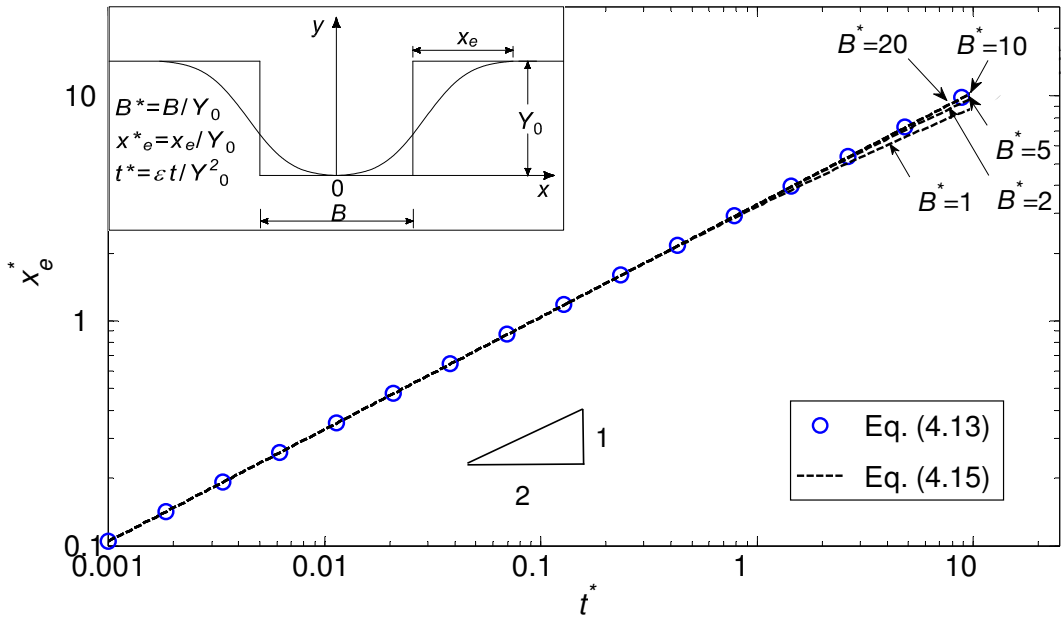

(a) Relationship between t^* and x_e^*

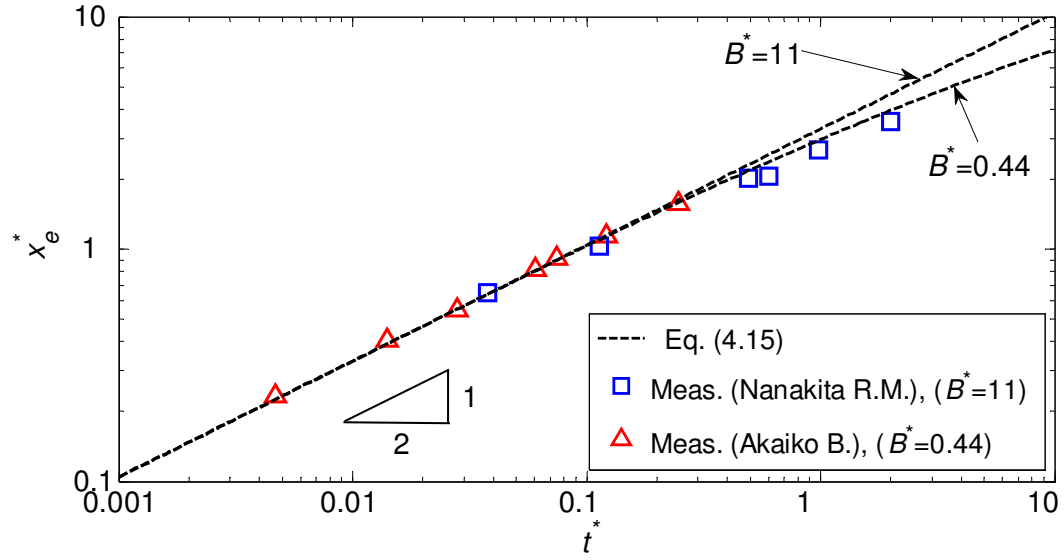

(b) Relationship between t^* and x_e^* for cases of the Nanakita River mouth and breaching at Akaiko and measured data

Fig. 4.25 Analytical solutions on the propagation of erosion

The values of Y_0 and B of each study area (concave shorelines at the Nanakita and breaching at Akaiko) are estimated from the actual conditions of concave portion right after the tsunami. The values of Y_0 of two study areas mentioned above are 95 m and 270 m, while the values of B are 1050 m and 110 m, respectively. Detailed explanation on how to obtain these two values will be given in Section 6.5. Based on the measured values presented above, the values of B^* of two study areas, concave shorelines at the Nanakita River mouth and breaching at Akaiko, obtained as 11 and 0.44, respectively. The comparison between theoretical results and measured data of two study areas are plotted together in Fig. 4.25(b). As the recovery process of concave shoreline at breaching at Akaiko is shorter than the case of concave shoreline at the Nanakita River mouth, hence its measured data of erosion propagation is also shorter. According to results shown in Fig. 4.25(b), both measured data sets are in good agreement with the theoretical relationship between t^* and x_e^* which was obtained from analytical solution of one-line model for case of rectangular cut in an infinite beach, especially in case when the value of t^* is still small. When the value of t^* becomes larger, the agreement between measured data and theoretical results for case of concave shoreline at the Nanakita River mouth becomes loser. Measured value of x_e^* tends to be smaller than theoretical value of x_e^*.

4.4.3 Estimated values of diffusion coefficient

By substituting the measured data of erosion propagation distance, x_e, and elapsed time, t, which is shown in Figs. 4.19 and 4.22, into Eq. (4.12), the average values of diffusion coefficient, ε, for two study areas are obtained. These values for the cases of the Nanakita River mouth and Akaiko breaching areas are 13 m^2/h and 14 m^2/h, respectively. The values of diffusion coefficient found in these study areas are consistent with values of this parameter found in the previous studies. Mano et al. (1996) carried out the value of dimensionless empirical proportionality coefficient in longshore sediment transport rate formula, K=0.03, for the area around Yuriage Port using the 6-year long observed shoreline position data and values of characteristics of mean wave. Kang and Tanaka (2006) calibrated the value of K (K=0.03) for Sendai Coast from Sendai Port to Yuriage Port based on yearly raw measured shoreline position data. Average wave conditions were also used in that study. Based on Eq. (3.12), the values of diffusion coefficient of these two studies are 12 m^2/h. This value is consistent with values carried out in the current study. In addition, Dean (2003) documented the values of diffusion coefficient for

the beaches in the State of Florida, the U.S. The values of diffusion coefficient vary from 10 m^2/h to 40 m^2/h for the beach facing to the Gulf of Mexico, whereas it is in wider range for the beach facing to the Atlantic Ocean (6.7-50 m^2/h). Although the characteristics of waves and sediment between the two coasts would be different, values of diffusion coefficient for Sendai Coast carried out in this study are in the range of values of diffusion coefficient of Florida Coast. That would be an interesting fact.

4.5 Discussion on the classification of morphology recovery with regarding to the temporal and spatial scales and the frame work of the dissertation

As introduced in Chapter 1, this study presents the recovery of morphology in terms of temporal and spatial scales. The following discussion makes clear about the demarcations of temporal scale (short-term and long-term) and spatial scale (small area and large area) as well as the frame work of this dissertation.

It has been reported in the early part of this chapter that during the recovery process, sandy coasts adjacent to both sides of the concave shoreline were eroded. The erosion was propagating along sandy coasts. The propagated distance is proportional to square root of elapsed time, Eq. (4.12). After a certain elapsed time, the erosion propagation would reach the coastal structures (e.g., breakwaters, jetty) which are considered as rigid boundaries (no sediment going through). Another possible case is that after a certain elapsed time, the erosion propagation from two concave shorelines is confluent. Either the case of coastal structure or confluent point is considered as the spatial demarcation (small and large areas). Small area would be solely the river mouth, the breaching of sandy coast, whereas the large area would be sandy coast that can include small areas. The time, when the erosion propagation has just reached the spatial demarcation, is considered as the temporal demarcation (short-term and long-term).

In this study, several shoreline data sets with different time series are utilized. The ones of cases the Nanakita River mouth, and breaching at Akaiko and Yamamoto are plotted in Fig. 4.26. There are two data sets at each study area are plotted except the case of breaching at Yamamoto. In Fig. 4.26, L_{EP} is the average distance from concave portion to the adjacent coastal structures (or confluent point). If any shoreline data set crosses the relationship (solid line) obtained from Eq. (4.12), it means that the erosion has reached the coastal structure or confluent point. So, it will be considered as the long-term data set. Otherwise, it will be classified as the short-term data set. Therefore, all the cases showing

in Fig. 4.26 match well with the classification above except the case of breaching at Akaiko. There is a jetty locating about 800 m on the right side of this breaching, whereas there is the long breakwater of Yuriage Port locating about 6000 m on the left side (Fig. 4.27). The breaching is rather narrow, only 110 m wide; hence the rigid boundary

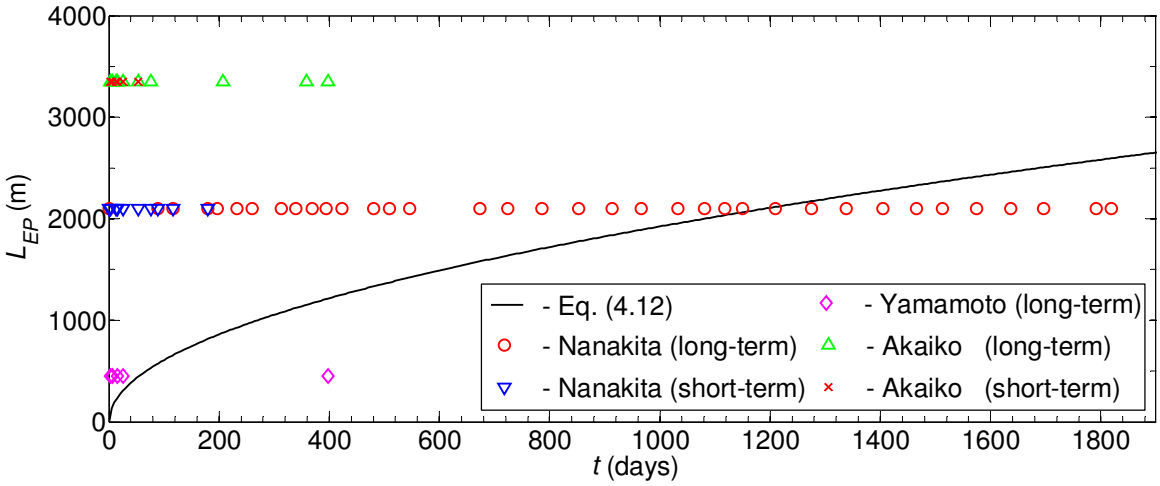

Fig. 4.26 Classification the short-term and long-term data sets for study areas on Sendai Coast (considering the average length of adjacent sandy coasts)

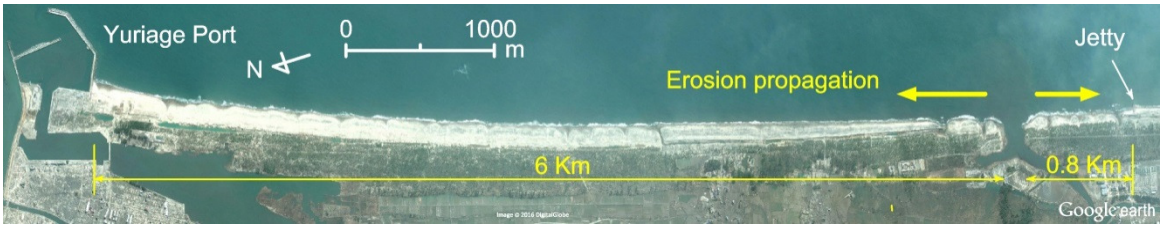

Fig. 4.27 Aerial photograph of the breaching at Akaiko (background: March 14, 2011)

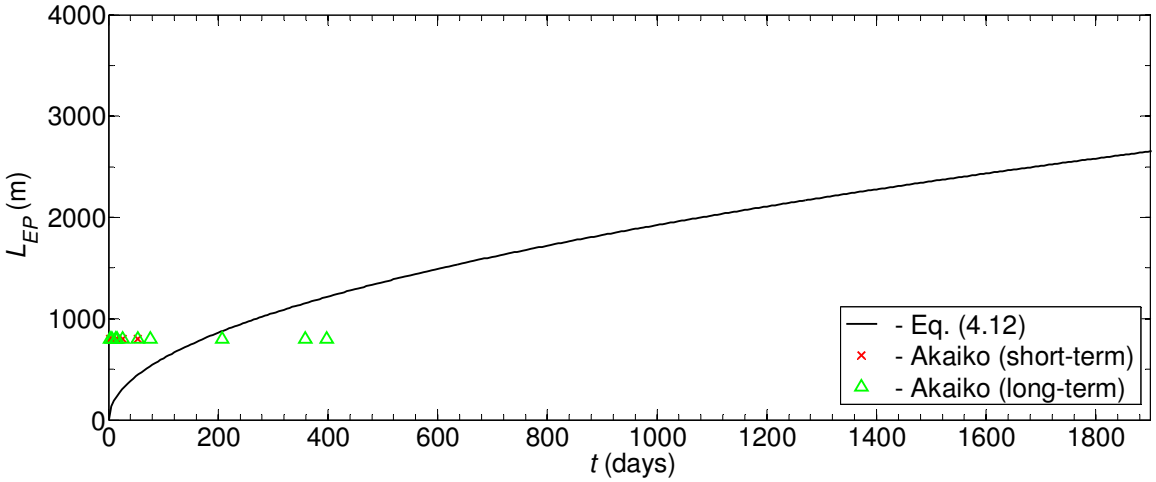

Fig. 4.28 Classification the short- and long-term data sets for the breaching at Akaiko (considering the symmetric and short length of adjacent sandy coasts)

on the left is considered too far to has influences on the evolution of shoreline at the breaching. Therefore, it is assumed that the left rigid boundary is located about symmetric with the right rigid boundary over the central line of the breaching. If applying this assumption, the results showing in Fig 4.28 confirm clearly the short-term and long-term of two data sets utilizing for the breaching at Akaiko.

According to results shown in Fig. 4.27, the demarcation time (short-term and long-term) for the northern part of Sendai Coast (including the Nanakita River mouth) is about 3 years. This demarcation will be reflected in using the shoreline position data series for studying the short-term and long-term recovery of the northern part of Sendai Coast (large area) which will be presented in Chapters 5 and 7, respectively.

Due to the severe damages, the morphology after the tsunami was in extreme disequilibrium condition, especially at the areas with formation of concave shorelines. Therefore, the recovery process at the areas with sufficient sediment supply took place right after the tsunami. The recovery process was rather fast in the early stage, and has been becoming slower after that. Because most of sediment supplying for the recovery of concave shoreline comes from adjacent sandy coasts, hence once the erosion propagation has reached coastal structures, the sediment supply is restricted. It can be said that the behavior of morphological recovery has close relationship with the elapsed time after the tsunami. The above discussion reveals the interrelationship between Chapters 4 (short-term) and 6 (long-term), and Chapter 5 (short-term) and 7 (long-term). In addition, more tight connection between these chapters can also be found. The finding from the analysis on the aerial photographs in Chapter 4 about the fast and slow recovery of morphology on the area with sufficient and sufficient sediment supply will be proven by the new developed analytical solution of one-line model in Chapter 6. On the other hand, the short-term recovery for the northern part of Sendai Coast (large area) is presented in Chapter 5, while the long-term recovery of the morphology on this sandy coast is revealed in Chapter 7. Comparative study on the results from these two chapters will clarify the similar and different behaviors of morphological recovery in short-term and long-term. Besides the short-term and long-term recovery, this study also presents the recovery of morphology with respect to the spatial scale. The tsunami caused severe damages at river mouths, breaching of sandy coasts, and barrier in front of lagoons, which are considered as small areas. The fast or slow recovery at these areas is simply related to the sediment supply from adjacent sandy coasts. Nevertheless, when considering the recovery of morphology on a large area, that could be a sandy coast including small areas

mentioned above, the influences of coastal structures, the interactions of shoreline evolution from the recovery of particular small areas on the overall recovery process are taken into account. The latter discussion indicates the interrelationship between Chapters 4 and 5, and Chapters 6 and 7. Furthermore, Chapters 4 and 6 indicate that the recovery of morphology at concave shorelines has significant recovery compared to other areas. This behavior of morphological recovery is reflected by the first component of EOF analysis in Chapters 5 and 7.

4.6 Conclusions in this chapter

This chapter has clarified the significant changes at the river mouths and breaching of sandy coasts in Miyagi Prefecture induced by the 2011 tsunami and its subsequent recovery process. Besides, the relevant phenomenon, which was raised during the recovery process, has been investigated. The following conclusions have been made.

1. The recovery of morphology of river mouths in Miyagi Prefecture, Japan has been supplemented and updated. Knowledges on the changes of morphology at the river mouths and breaching of sandy coasts and the recovery process, which are obtained from this study, will be useful for resilient and prepared plans for similar disasters in the future.

2. After the tsunami, the intrusion into river mouth of sandspit has been observed at the study river mouths. The scouring deeper the river mouth, which caused the depth of water in the river mouth greater than the depth of closure, was the cause source leading to the sandspit intrusion into river mouth area. The depth of river mouth, D_R, and the depth of closure, D_C, are important physical quantities which express the representative depths of the drift-sand system of river and littoral drift system of ocean space, respectively. These two represented depths were treated separately; however by considering them together the sandspit intrusion into river mouth can be explained comprehensively.

3. After the significant changes of river mouth morphology and forming of breaching of sandy beach, the erosion propagation occurred on the adjacent sandy coasts. The erosion propagation distance is proportional to the square root of elapsed time. The result is similar with common physical phenomenon described by diffusion equation. This appears to be a valuable finding of the current study.

4. The values of diffusion coefficient of the beaches at the Nanakita River mouth and breaching at Akaiko areas are obtained based on the analytical solutions of one-line model and the relationship between the erosion propagation distance and elapsed time. This chapter supplements a new technique to estimate the diffusion coefficient which so far is usually obtained through the empirical coefficient in longshore sediment transport rate formula, K.
5. An approach to classify the short-term and long-term, and small area and large area recovery has been given.

Chapter 4 has clarified the subsequent recovery of morphology of separated small areas that are solely the river mouths, breaching of sandy coasts and the sandy barriers in front of lagoons. However, how is the behavior of morphological recovery on a larger area which includes sandy coast and several small areas? This question would be made clearly in the next chapter.

CHAPTER 5

SUBSEQUENT RECOVERY OF MORPHOLOGY ON THE NORTHERN PART OF SENDAI COAST

5.1 Introduction

According to Chapter 4, the morphology of river mouths or breaching of sandy coasts was severely damaged by the tsunami. The breaching of sandy coasts has recovered rather quickly, whereas all the river mouths except the Nanakita River mouth had very slow recovery. That presented different manors of morphological recovery. In addition, there was phenomenon raised during the subsequent recovery process. The concern is how the behavior of morphological recovery in a large area (sandy coast) where includes the sandy beaches, river mouths and coastal structures. On the other hand, in connection with the large-scale morphological changes induced by the tsunami, the littoral system could be modified. Thus, the analysis of sediment budget of Sendai Coast (e.g., Kang and Tanaka, 2005), may need to be re-evaluated.

Accordingly, this chapter attempts to reveal the behavior of morphological recovery on Sendai Coast after the 2011 tsunami through the analyses of aerial photographs and EOF.

5.2 Overall change and subsequent recovery of morphology from aerial photograph

Figure 5.1(b) shows detected shoreline positions on the northern part of Sendai Coast, stretching from Sendai Port to the Natori River mouth. According to this figure, shoreline position in this coast was retreated a large amount, especially at the lagoon (Gamo and Idoura) and river mouth (Nanakita and Natori) areas. The accretion of shoreline position after the tsunami has different behaviors, significant accretion at the areas of the Nanakita River mouth and Gamo Lagoon and slow accretion at the areas of Natori River mouth and Idoura Lagoon. A dashed thick line, which represents mean shoreline position of after the tsunami, is also included in the figure. Figure 5.2 shows the temporal variation of shoreline positions at four places in this coast. It is noted that shoreline position data

using in this chapter was extracted from aerial photographs taken in the period from June, 2011 to Feb, 2014. In addition, for more details on the temporal variation of shoreline position, shoreline positions on Mar 6, 2011 (t=-5 day) and Mar 12, 2011 (t=1 day) are also included. According to Fig. 5.2(a), the shoreline in area updrift end of longshore sediment transport (Area (A) in Fig. 5.1(a)) was retreated about 150 m. After the tsunami, it has accreted about 100 m. In the period from around t=700 days to t=1100 days (3 years after the tsunami), shoreline position in the mentioned area has been rather stable. About 50 m of shoreline is still remained unrecovered. The shoreline in Area (B) (Fig. 5.2(b)), where is updrift of Arahama detached breakwaters, was not significantly eroded. Since the tsunami happening until Feb, 2014, the overall trend of shoreline evolution in this area has been nearly constant, although very high fluctuation can be observed. In contrast, shoreline position in the downdrift of these detached breakwaters (Area (C)) has been gradually retreated after the tsunami (Fig. 5.2(c)). High fluctuated amount of shoreline position can also be observed. Fig. 5.2(d) presents the temporal variation of shoreline position in the area of downdrift end of longshore sediment transport (Area (D)). Shoreline position in this area was eroded about 10 m to 15 m by the tsunami. In the period about 100 days after the tsunami, it was retreated further about 20m to 30m. The fluctuation of shoreline position in this area is similar at the Areas (B) and (C).

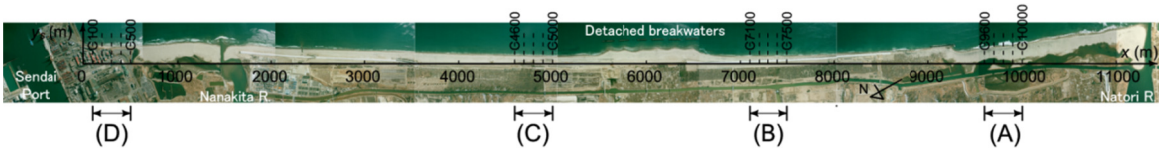

(a) Aerial photograph of the northern part of Sendai Coast after the tsunami

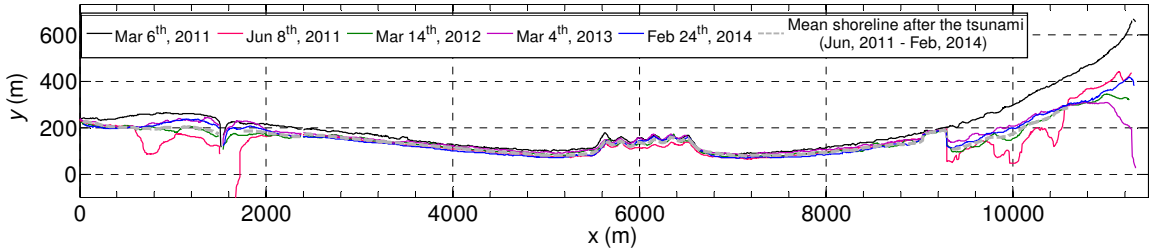

(b) Detected shoreline positions (dashed gray line is mean shoreline position, $\bar{y}(x)$, after the tsunami)

Fig. 5.1 Aerial photograph and detected shoreline positions of northern Sendai Coast

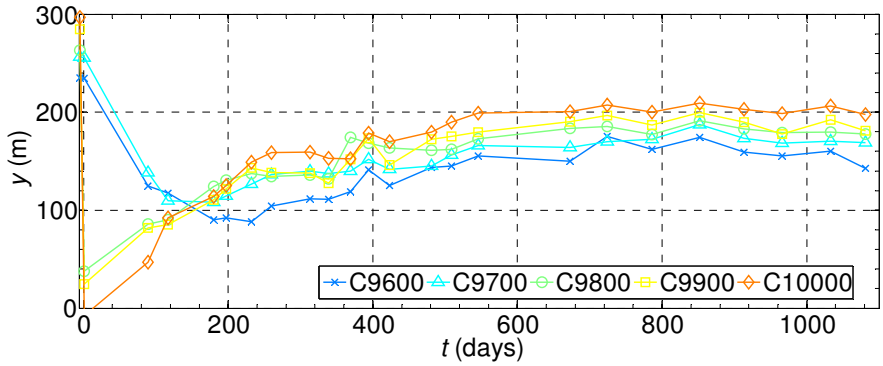

(a) Updrift end of longshore sediment transport - (Area (A) in Fig. 5.1(a))

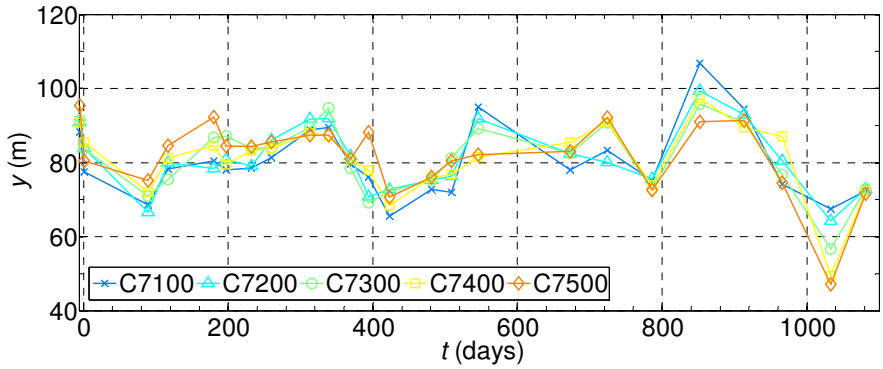

(b) Updrift of detached breakwaters - (Area (B) in Fig. 5.1(a))

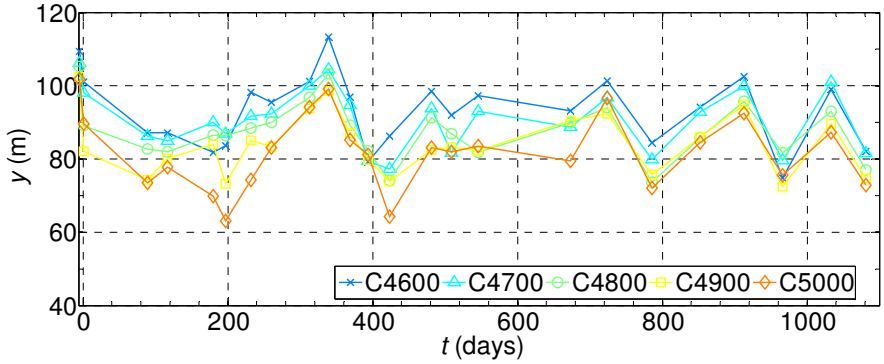

(c) Downdrift of detached breakwaters - (Area C in Fig. 5.1(a))

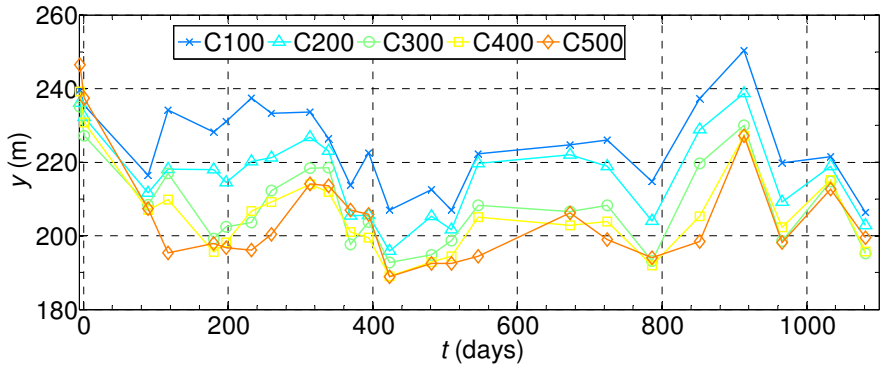

(d) Downdrift end of longshore sediment transport - (Area (D) in Fig. 5.1(a))

Fig. 5.2 Temporal variation of shoreline positions, (t is the number of days after the tsunami, from Mar 11, 2011)

Change rate of shoreline position on transections along the coast, a (m/year), is obtained by applying the simple linear approximation, $y_s=at+b$ (t is time; a and b are coefficients), on shoreline position data sets. For the period before the tsunami, the values of a were estimated based on the data set from March, 2009 to March 2011, while the data set from June, 2011 to February, 2014 was utilized for the period after the tsunami. Reflecting from demarcation time for the northern part of Sendai Coast, only shoreline position in about three years after the tsunami is utilized for the short-term recovery in this chapter. Results of shoreline change rate for both periods are shown in Fig. 5.3. According to that, before the tsunami shoreline along the coast was accretion except the area around the Nanakita river mouth, x=1000 m-2000 m. The large accretion of shoreline is in the areas of x=2500 m-4000 m, the south side of drainage jetty, and of x=6000 m-8000 m, updrift of detached breakwaters, while the small accretion is in the area around x=5000 m, downdrift of detached breakwaters. That reveals the effects of detached breakwaters. Moreover, the shoreline on the right side of wave-dissipating blocks has very small accretion, even the retreat can be also observed. The interrupting on longshore sediment supply from south by the breakwater at Yuriage Port is reason for that evolution of shoreline. After the tsunami, because of the significant recovery of morphology at river mouths, lagoons then values of shoreline change rate at these areas are very large. Besides, that value is also large at the detached breakwaters. These results are also shown clearly in results of EOF analysis in Fig. 5.8.

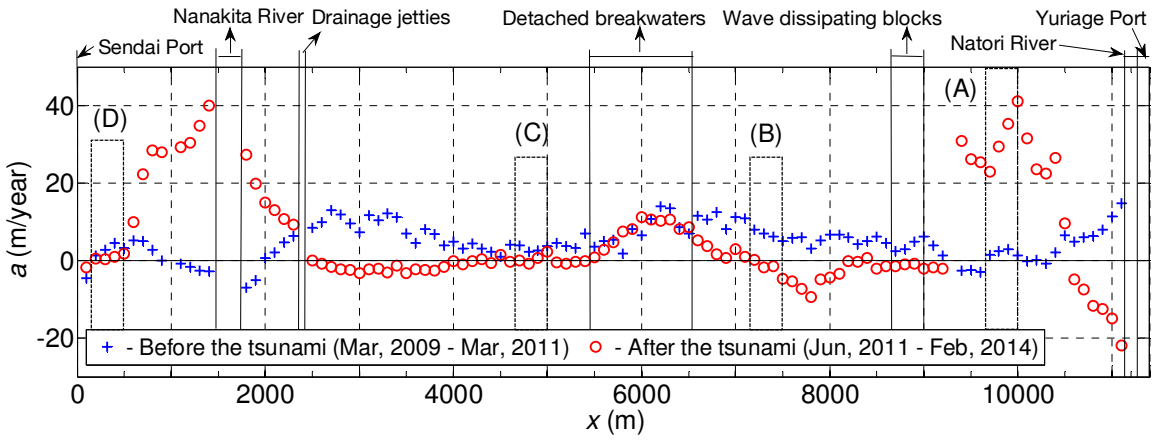

Fig. 5.3 Shoreline change rates before and after the tsunami

Shoreline change rate also indicates that the area adjacent to the Natori River mouth was significant retreated. It subjected to the intrusion of sandspit into river mouth after

the tsunami. Slight retreat of shoreline on the north (left) side of wave-dissipating blocks was also observed. Because of severe retreat at the Idoura Lagoon, after the tsunami, these blocks are facing to the shoreline (locating protrusively into the sea water body, see Fig. 5.4). That interrupts the longshore sediment transport. Hence, shoreline retreat happened on the north side of them. Another thing regarding to the existing of these blocks is that they block the sediment movement from the north side, which is considered as the source for the recovery of morphology at Idoura lagoon, fills into the lagoon area. Therefore, the significant retreat after the tsunami of shoreline on the north side of these blocks was not occurrence.

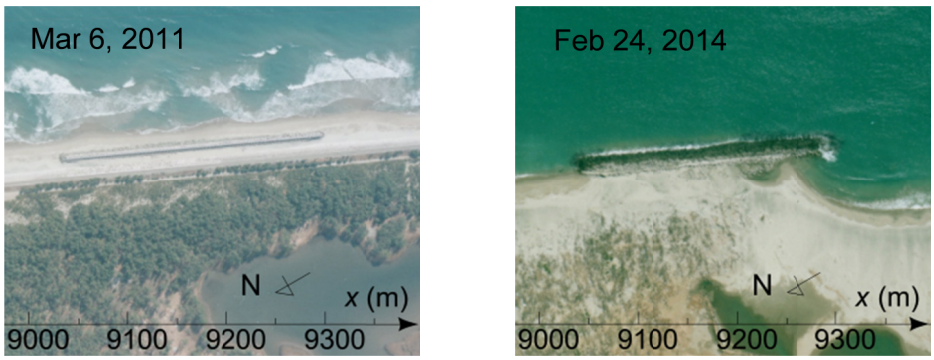

(a) Pre-tsunami (b) Post-tsunami

Fig. 5.4 Aerial photograph around the wave-dissipating blocks (x=9200 m)

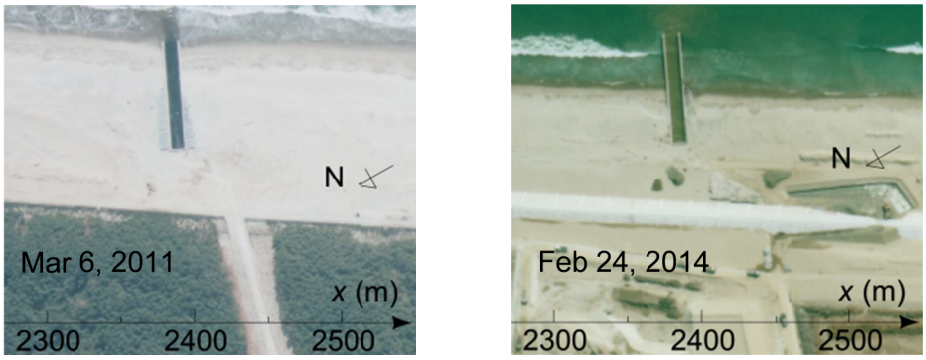

(a) Pre-tsunami (b) Post-tsunami

Fig. 5.5 Aerial photograph around the drainage jetty (x=2400 m)

Similar to situation of shoreline around the wave-dissipating blocks, the shoreline at drainage of waste water treatment plant (x=2400 m), has been retreated a large amount after the tsunami, hence the drainage is now playing the roles as jetty. Aerial photographs of the area around that location before and after the tsunami are shown in Fig. 5.5.

The average shoreline change rate from wave-dissipating blocks to drainage jetty $\bar{a}$ (m/day) and the annual average amount of sediment change dV/dt (m^3/year), which is estimated by Eq. (5.1), are presented in Table 1.

$$\frac{dV}{dt} = \bar{a} L_{WD} (D_B + D_C) \tag{5.1}$$

where L_{WD} is the distance alongshore from wave-dissipating blocks to drainage jetty (L_{WD}=6600 m); D_B is the berm height (D_B=3 m), this value was estimated by Tinh and Tanaka (2011) based on field survey data before the tsunami at the place in front of Gamo Lagoon; D_C is depth of closure (D_C=8 m, Uda, 1997).

According to the results in Table 1, before the tsunami there was sufficient sediment supply to the calculated area from longshore sediment. However, the annual amount of sediment has been reduced a lot. The interrupting of the wave-dissipating blocks on the longshore sediment from the south and the severe damages of morphology at the Natori River mouth and Idoura Lagoon would be the main reasons for that reduction.

Table 5.1 Average shoreline change rate and the annual average amount of sediment change of the coast from wave-dissipating blocks to drainage jetty (short-term)

Period	Average shoreline change rate $\bar{a}$ (m/year)	Annual average amount sediment change dV/dt (m^3/year)
Before the tsunami	6.2	4.5×10^5
After the tsunami	7.3	5.5×10^4

According to the analysis on shoreline change rate and annual sediment change for the coast, it can be said that the longshore sediment transport in this coast has supplied a large amount of sediment for the recovery morphology of lagoon areas where were significant eroded induced by the tsunami. Besides, it also shows the different aspects with the one before the tsunami. Hence, it is suggested that the coastal management planning for Sendai Coast, which was obtained based on previous sediment budget analysis, should be changed. This is another important practical finding of this study.

5.3 EOF analysis on the recovery of morphology

The Empirical Orthogonal Function (EOF) analysis is the method that can extract the dominant patterns from data sets. In coastal morphology, it can reveal the significant components of shoreline variability from several data sets. The methodology of EOF analysis has been presented in Chapter 3.

Due to the severe erosion, after the tsunami shoreline at many places along the northern part of Sendai Coast was discontinued (see Figs. 4.5, 4.6 and 4.9). Hence, the shoreline on June 8, 2011, which almost recovered to continuity status, was taken as the first shoreline data input for the EOF analysis. Moreover, in order to obtain the characteristics of overall recovery process of shoreline on entire of the coast, about 300 m of shoreline on the right side of the Nanakita River mouth and about 800 m of shoreline on the left side of the Natori River mouth, which involved into the strong fluctuation regarding to sandspit intrusion into the river mouth, were not included in the EOF analysis.

According to the results of EOF analysis, the contribution rate of the first component is 67 %, while they are 11 % and 7% for the second and third components, respectively. The contribution rates of higher components are about 4 % or less. The total contribution rate of the first three components is dominant compared to these others.

5.3.1 The first component

Figures 5.6 and 5.7 show the first three spatial eigenfunctions, $e_n(x)$, and the first three temporal eigenfunctions, $c_n(t)$, respectively. Value of the first temporal eigenfunction has decreased gradually from beginning until the time of about 800 days after the tsunami. After that, it is almost constant. On the other hand, value of the first spatial eigenfunction is high in the areas of lagoons where the tsunami induced massive morphological changes (areas around the x=1000 m and x=10000 m). Figure 5.8 shows the variability of shoreline position from average position based on the multiplication of spatial eigenfunction and temporal eigenfunction of the first component ($y_1(x, t)=e_1(x)c_1(t)$). It can be seen that the position of shoreline has increased greatly in the same range in the areas of lagoons. Accordingly, it can be said that the first component reflects the recovery process of morphology at lagoon areas (severely damaged areas). In addition, the shoreline position has also increased at central part (around the area of x=6000 m). This also indicates the recovery trend of shoreline in the area around detached breakwaters.

As mentioned above, about 70 % contribution is from the first component that reflects the recovery process of morphology after the significant changes induced by the tsunami. The massive changes of morphology had led to the extremely disequilibrium state. Therefore, the recovery took place subsequently the tsunami. However, it is still ongoing on and its influence is still dominant even approximately three years after the tsunami.

It can be observed that the value of $c_1(t)$ at around 400 days after the tsunami suddenly dropped to smaller than zero before return to the general trend of decreasing. The aerial

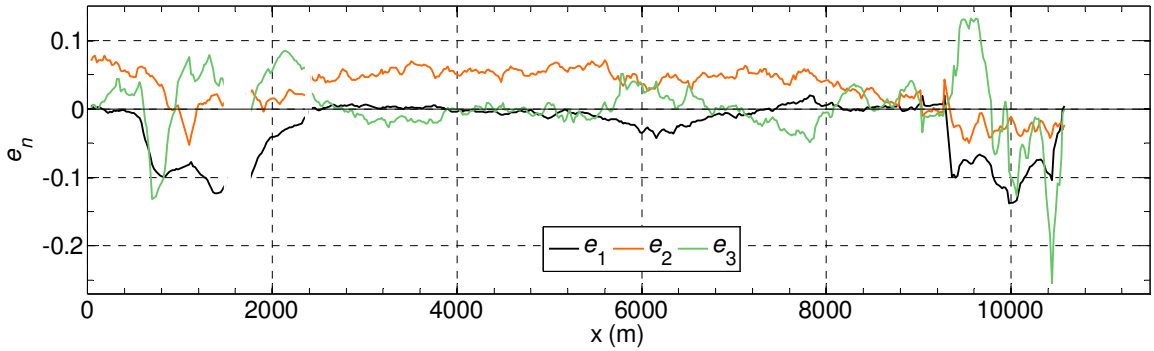

Fig. 5.6 Spatial eigenfunctions, $e_n(x)$, of the first three components

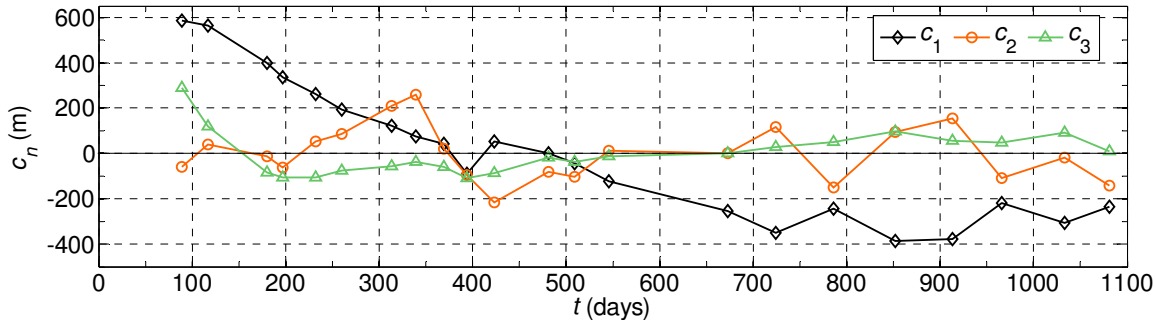

Fig. 5.7 Temporal eigenfunctions, $c_n(t)$, of the first three components

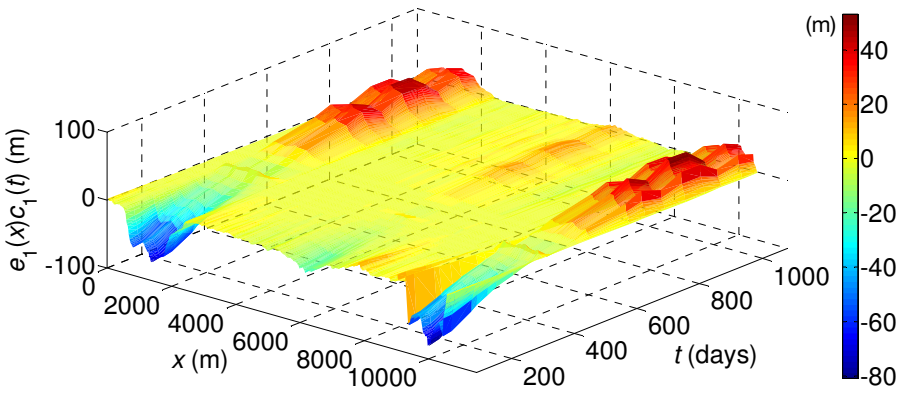

Fig. 5.8 The combination of spatial and temporal eigenfunctions of the first component, $e_1(x)c_1(t)$

photographs on that date were taken at very low tide, almost the lowest tidal level of 2012. This uncertainty indicates that the tidal correction is not always reliable. The beach slope would not be constant along the coast and would be milder than the calculated beach slope of 0.11 in this case. The corrected height of tidal level for each aerial photograph has been given in Fig. 3.8.

5.3.2 The second component

The spatial eigenfunction of the second component, $e_2(x)$, in Fig. 5.6 is all constant value along the coast except at the areas of river mouths and detached breakwaters. Its value of temporal eigenfunction after the tsunami fluctuates up down, seemly in the period of one year. The variation of shoreline position would be corresponding with the wave conditions, shoreline gets retreat during the high waves, and gets accretion during the low waves. The combination of spatial and temporal eigenfunctions in Fig. 5.9 also shows similar fluctuation. Therefore, it is supposed that the second component reflects the cross-shore movement of shoreline. However, in order to confirm that statement, the investigation on wave height need to done.

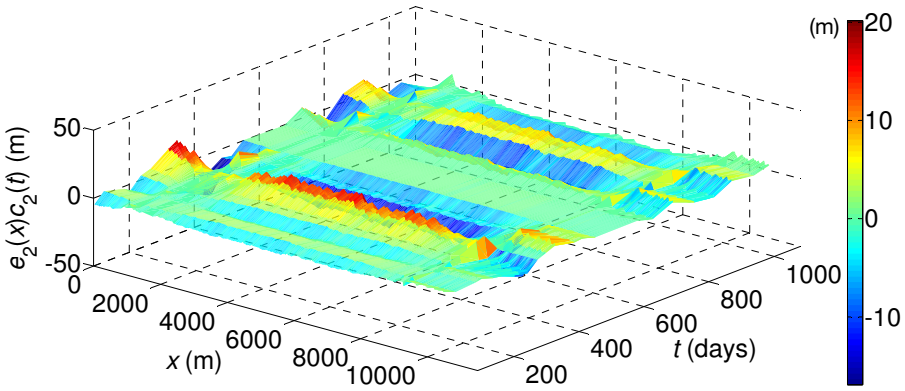

Fig. 5.9 The combination of spatial and temporal eigenfunctions of the second component, $e_2(x)c_2(t)$

Figure 5.10 illustrates the significant wave height, H_S, and the temporal eigenfunction of the second component for each year from 2012 to 2013. Because of almost constant value of spatial eigenfunction of the second component along the coast except at the severely damaged areas, only the value of temporal eigenfunction is used for the comparison. In this case, positive and negative values of temporal eigenfunction imply the shoreline is accretion and retreat, respectively. The wave height data in 2013 and late

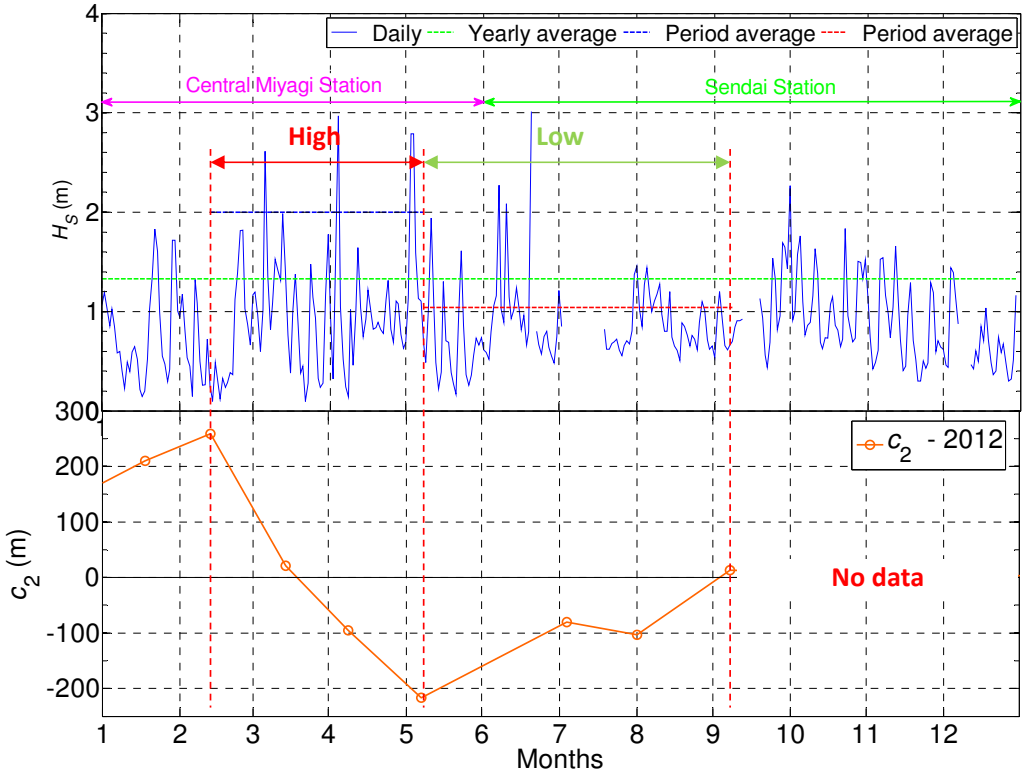

(a) 2012

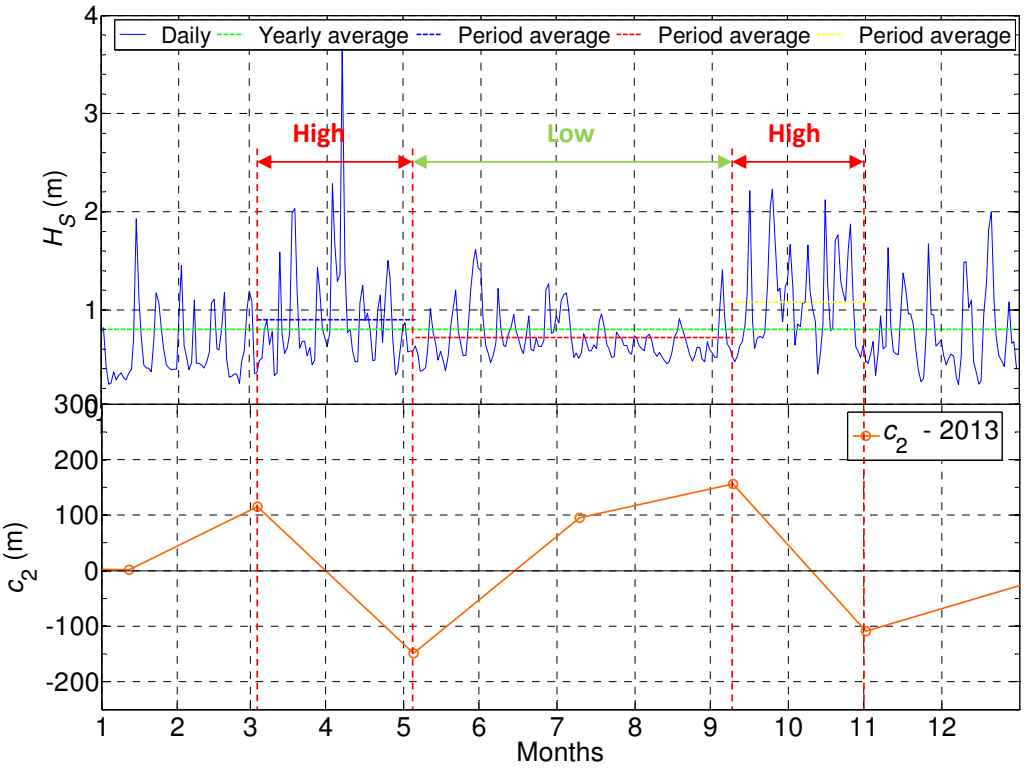

(b) 2013

Fig. 5.10 Significant wave height and temporal eigenfunction of the second component

of 2012 is the 20-minute measured wave at Sendai Station, whereas the wave height data in early 2012 is the regressed 20-minute measured wave at Central Miyagi Station. In Fig. 5.10, a green dashed line is added to represent the yearly average wave height. In addition, other lines that represent the period average wave heights are also added. These periods were defined corresponding to the periods of decreasing or increasing of the second temporal eigenvalues. According to the results showing in Fig. 5.10, it can be seen that the shoreline is accretion during the period which average wave height is lower than the yearly average wave height and vice versa. This confirms that the second component reflects the variation of shoreline position on the cross-shore direction in responding to wave conditions.

Fig. 5.11 Beach cusp formation in the area adjacent to the Natori River mouth

In addition, the fluctuation up down of value of the second component spatial eigenfunction in the area near the Natori River mouth and Idoura Lagoon is greater than other areas. The formation of the beach cusp of about several hundred meters was found in the area adjacent to the Natori River mouth after the tsunami (an example in Fig. 5.11). The troughs of the spatial eigenfunction of the second component at the Natori River mouth area are consistent with the protruding parts of shoreline which subjects to the beach cusp formation.

5.3.3 The third component

Value of the third temporal eigenfunction (Fig. 5.7) decreases in the period from 90 to about 200 days after the tsunami. It increases a small amount after that and gets zero at about 500 days. Then, its value is small and constant until the end of the computed period. Although the value of the third and the first components have different signs (+, -), in the period after 500 days, they have the same tendency. The spatial eigenfunction of the third

component has high absolute value at the severely damaged areas and at the detached breakwaters (Fig. 5.6), whereas it is almost constant and very small on the sandy beach without severe damages induced by the tsunami. Therefore, the variability of shoreline position from average position based on the multiplication of spatial eigenfunction and temporal eigenfunction of the third component ($y_3(x, t)=e_3(x)c_3(t)$) (Fig. 5.12) also has large absolute value at the severely damaged areas in the period from 90 to about 500 days after the tsunami. It has small and constant value in the other areas and in the period from 500 days onwards. Figure 5.13(b) presents the distance from average shoreline

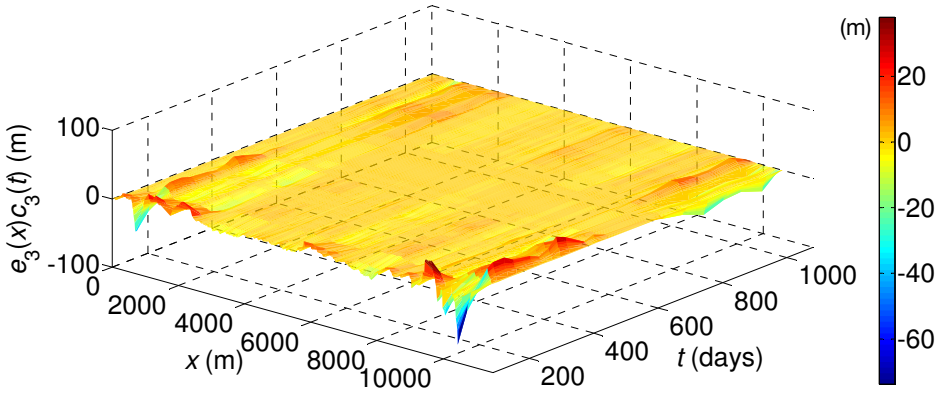

Fig. 5.12 The combination of spatial and temporal eigenfunctions of the third component, $e_3(x)c_3(t)$

position after the tsunami to four selected shorelines. The spatial eigenfunction of the third component is again shown in Fig. 5.13(a) for comparison. The trend of the shoreline position from average shoreline on June 8, 2011 (the first shoreline data in EOF analysis) is similar to the trend of spatial eigenfunction of the third component. The shoreline position on March 14, 2012 (369 days after the tsunami) shows that a large amount of shoreline retreat has recovered; however its trend is still similar to the trend of shoreline on June 8, 2011. Nevertheless, the shoreline positions on March 4, 2013 and February 24, 2014 (724 and 1081 days after the tsunami, respectively) have totally different trends with the trend of shoreline on June 8, 2011.

Accordingly, it can be said that the third component reflects the recovery of morphology at the severely damaged areas in early stage after the tsunami.

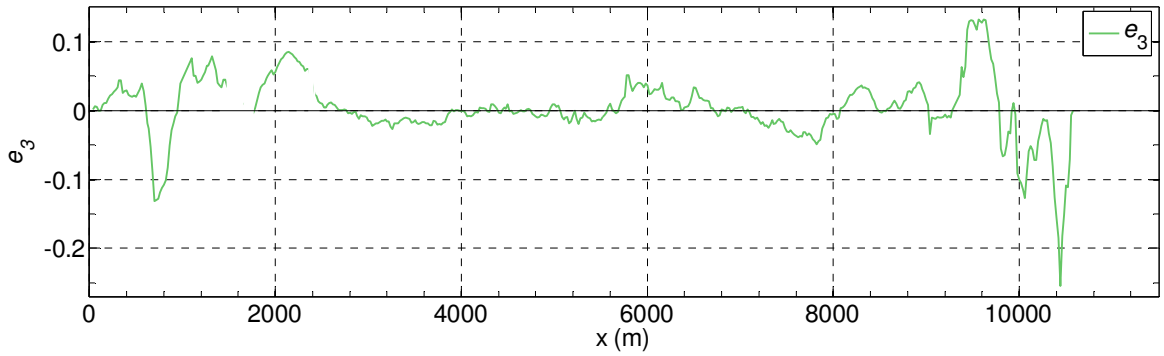

(a) Spatial eigenfunction of the third component

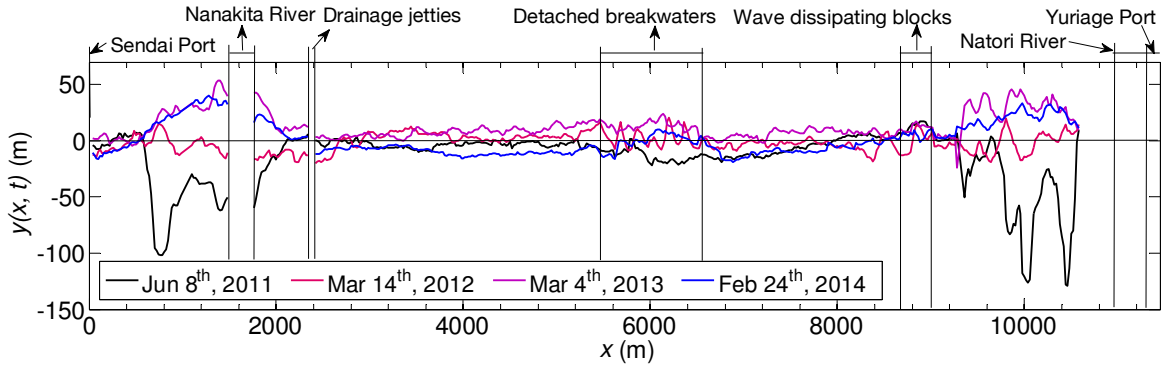

(b) The distance from average shoreline position after the tsunami to shoreline

Fig. 5.13 The spatial eigenfunction of the third component and the distance from average shoreline position after the tsunami to shoreline

In this chapter, the results of EOF analysis indicate that there is about 75 % contribution from the first and the third components which relate to the recovery process of morphology of areas with significant changes induced by the tsunami. The contribution rate of cross-shore movement is about 7 %. However, on the comparative study, the contribution rate of the cross-shore movement before the tsunami is largest, about 40 % (Kang and Tanaka, 2005). The contribution rate of the cross-shore movement has been decreased a large amount. The massive changes of morphology induced by the tsunami had led to the extremely non-equilibrium state. The recovery took place subsequently the tsunami. However, it is still ongoing on and its influence is still dominant even approximately three years after the tsunami.

5.4 Conclusions in this chapter

In this chapter, the damage of coastal and estuarine morphology induced by the tsunami and its recovery process has been assessed through the analysis of aerial photographs and EOF analysis. The following conclusions have been made.

1. The morphology of sandy beach and river mouths on Sendai Coast was severely damaged by the 2011 tsunami. The recovery process has been taking place after the tsunami but even three years after the tsunami, shoreline has not yet reached the position before the tsunami. The rate of shoreline change is completely different between before and after the tsunami. It is shown clearly that the recovery process of morphology after the significant changes induced by the tsunami has made the modification of littoral system of Sendai Coast.
2. The results of EOF analysis indicate that the first and third components reflect the recovery process of morphology at the severely damaged area such as lagoons, breaching of sandy coast. In addition, it also reflects the recovery of the shoreline at detached breakwaters. While, the second component reveals the variation of shoreline position on the cross-shore direction in corresponding to wave condition. The total contribution rate of the first and third components is about 75 % out of total.

The subsequent recovery of morphology of both small and large areas has been investigated in the Chapters 4 and 5, respectively. So, the question is how the recovery of morphology when the time going longer, in term of years? Then, the erosion propagation could reach the rigid boundaries. What are the influences of these boundaries on the recovery process? Detailed interpretations on those questions for the case of small area will be presented in Chapter 6.

CHAPTER 6

LONG-TERM RECOVERY OF TSUNAMI-INDUCED CONCAVE SHORELINE

6.1 Introduction

As pointed out in the previous chapters, one of the most common morphology formed after the 2011 tsunami was the concave shoreline. It was located around the river mouth area after the flushing of river mouth sand spit and the disappearance of adjacent sandy barrier or at the breaching of sandy coast. During the subsequent recovery process, concave morphology at some areas such as at the Nanakita River mouth, at breaching of sandy coast at Arahama and Akaiko took the recovery rather quickly, whereas it was very slow at other areas such as the Natori River mouth. As presented in Chapter 4, in connection with quick recovery, the erosion of the adjacent sandy coasts has been observed. Among them, the Nanakita river mouth and the breaching of sandy coasts at Akaiko and Yamamoto are typical cases. The erosion happened on both adjacent sandy coasts right after the tsunami, and propagated along the coasts. After a certain time, the beach erosion propagation has reached coastal structures such as breakwater, offshore breakwaters and headlands which were constructed on the coast for various purposes. During the erosion propagation process, after getting interruption of the structures, which are considered as rigid boundaries, entire sandy coast on both sides were severely and abruptly retreated. That could be seen clearer when the recovery process going longer.

As presented in Chapter 3, the analytical solutions of one-line model, which can describe various cases of shoreline variability, can be obtained when solving the simplified governing equation of one-line model with appropriate initial and boundary conditions. They have many advantages compared to the numerical solutions. According to Larson et al. (1987), the analytical solutions can provide a simple and economical means to make a quick qualitative evaluation of shoreline response under a wide range of environmental and engineering conditions. They can also eliminate the instability of the numerical solutions. In addition, the results from numerical solution can be also verified

by using the results of analytical solution. However, the analytical solutions can only handle simple cases; for cases with more complex initial and boundary conditions the numerical solutions need to be employed.

Therefore, this chapter attempts to present the long-term recovery of concave morphology after the tsunami, which the influences of coastal structures acting as rigid boundaries are also included, through analysis of aerial photographs and newly developed analytical solutions of one-line model.

6.2 Overall on the forming and recovery process of concave shorelines

As presented in Chapters 4 and 5, the concave shorelines were formed at river mouth and lagoon areas due to the flushing of sandspits and sand barriers; in addition the breaching of sandy coasts at old river mouth locations was also induced concave shorelines. Figures 6.1, 6.2, 6.3 and 6.4 present the evolution of concave shorelines after the tsunami at the Nanakita, Natori River mouths and breaching of sandy coasts at Akaiko and Yamamoto, respectively.

The baseline for shoreline measurement from aerial photographs in this chapter for cases of the Nanakita and Natori River mouth has been changes to 211.5^{O} clockwise from the north direction, whereas in these other chapters is 210^{O} clockwise from the north direction. For the cases of breaching at the Akaiko and Yamamoto, the baselines were not changed, keeping the same with other chapters, 163^{O} and 178^{O} clockwise from the north direction, respectively. The changing of baseline angle in this chapter is to make the baseline parallel to the shoreline position at the Nanakita River mouth for later calculation.

According to the figures, concave shorelines, which have sufficient long adjacent sandy coasts such as concave shorelines at the Nanakita River mouth, and at breaching of sandy coasts at Akaiko and Yamamoto, have recovered significantly, whereas it has been very slow if there are no adjacent sandy coasts as the case at the Natori River mouth. With the cases of fast recovery, the shoreline position in the concave portion gets accretion, while the one on both adjacent coasts gets retreat. (i) This is one of the indications that the longshore sediment is dominant.

About 1.5 km on the left side of the Nanakita River mouth, there is long breakwater of Sendai Port, whereas about 3.7 km on the right side there are detached breakwaters. Although these detached breakwaters are not functioned truly as rigid boundary, the mentioned breakwater and detached breakwaters are considered as rigid boundaries. They

are treated as the boundaries that can completely interrupt the longshore sediment; no longshore sediment can move in or out the bounded area. Similarly, about 800 m on the

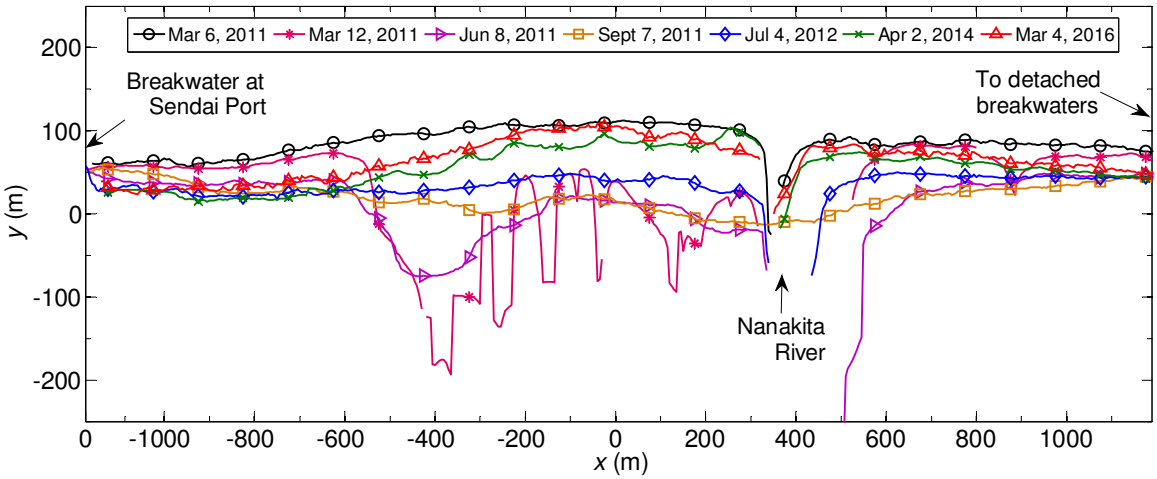

Fig. 6.1 Evolution of concave shoreline at the Nanakita River mouth after the tsunami

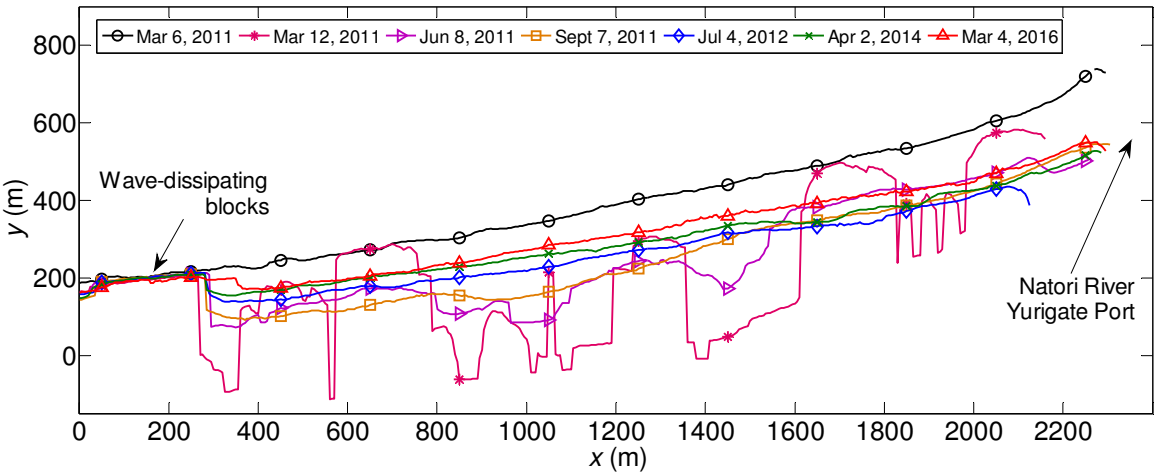

Fig. 6.2 Evolution of concave shoreline at the Natori River mouth after the tsunami

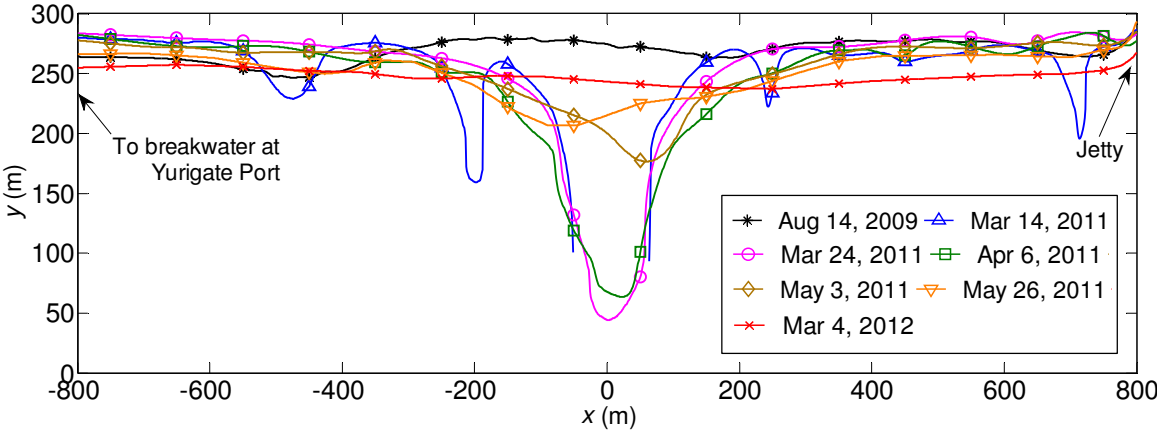

Fig. 6.3 Evolution of concave shoreline at Akaiko after the tsunami

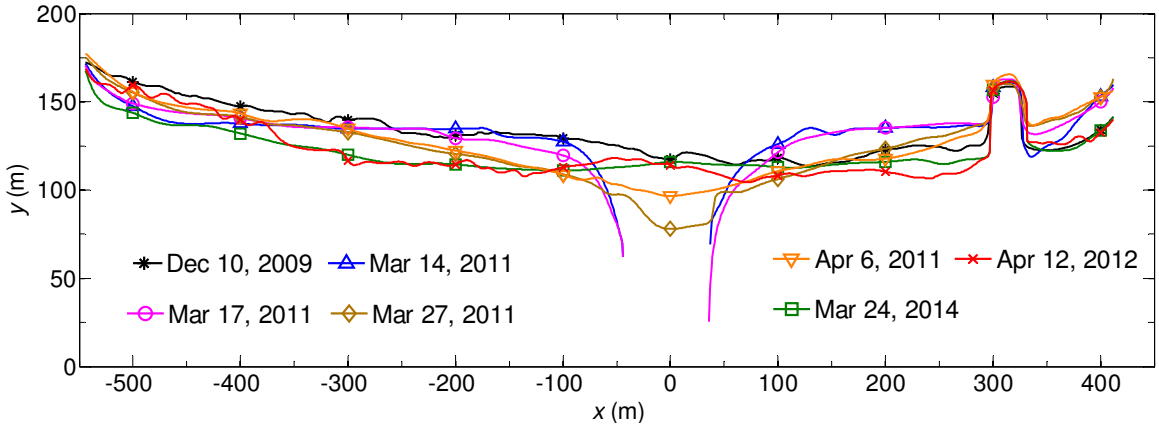

Fig. 6.4 Evolution of concave shoreline at Yamamoto after the tsunami

Fig. 6.5 Recovery of concave shoreline at the breaching of sandy coast at Yamamoto after the tsunami (background: April 2, 2011)

right side of breaching at Akaiko, there is available of a jetty, while about 6 km on the left side, there is a long breakwater of Yurigate Port. For the breaching of sandy coast at Yamamoto, the concave portion was located almost at the middle of the region bounded by headland Numbers 9 and 11.

Figure 6.5 shows an oblique photograph of the breaching at Yamamoto which was taken about 20 days after the tsunami. It confirms the connecting of the breaching and the blocking of canal by the sediment which was transported into the concave portion. Another oblique photograph is shown in Fig. 6.6(a). It indicates that the beach, which is adjacent to the breaching, was eroded (dashed circle line). It has the form of cliff beach. (ii) This is another indication of dominant longshore sediment.

Figure 6.6(b) presents the relationships between the elapsed time after the tsunami and the sediment filled area in the concave portion and the total sediment eroded area on the adjacent sandy coasts. According to these results, the filled area in the concave portion is always greater than the total eroded area on the adjacent sandy coasts, especially in the early stage. The gap becomes small in the late period. (iii) The good consistence of results in the late period can be also an important indication of dominant longshore sediment.

(a) Erosion of beach adjacent to the breaching at Yamamoto after the tsunami (cliff beach) (background: April 2, 2011)

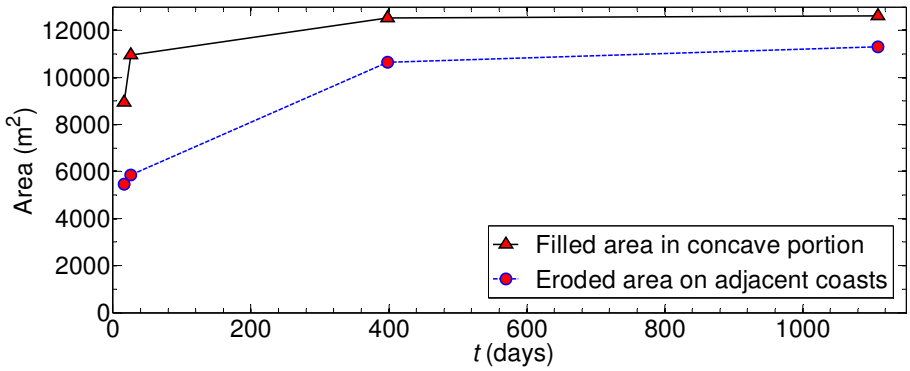

(b) Relationships between the elapsed time after the tsunami and the sediment filled area in the concave portion, and the total sediment eroded area on the adjacent sandy coasts

Fig. 6.6 Erosion of adjacent beach and the relationships between the time after the tsunami and the sediment filled and eroded areas at the breaching at Yamamoto

The worse consistence of the results in the early period can be attributed by the eroded sediment of the breaching. Udo et al. (2015) reported that more than haft of the total amount of eroded shore sand above the sea level was flushed seaward by the tsunami return flow. Some amount went to the deep area and cannot come back under the driving of waves. According to indications (i), (ii) and (iii), it can be said that during the recovery process of the concave shorelines the longshore sediment is dominant.

6.3 Analytical solutions of one-line model describing the evolution of concave shorelines without and with rigid boundaries at both ends

As discussed in latter section, during the recovery process, the longshore sediment is dominant. Thus, the theory of one-line model can be employed.

Simplified governing equation of one-line model, Eq. (3.11), is similar to governing equations (diffusion equation) which describe various physical processes such as heat conduction, fluid motion, diffusion process. By solving that equation with corresponded initial and boundary conditions, numerous analytical solutions can be obtained. Analytical solutions of diffusion equation for various cases of initial conditions and boundary conditions have been presented for a long time in textbooks (e.g., Barrer, 1941; Crank, 1975).

Larson et al. (1987) presented the analytical solution, Eq. (6.1), which can describe the evolution of concave shoreline in case without rigid boundaries at both ends, whereas this study introduces the analytical solution, Eq. (6.2), for case with rigid boundaries.

$$y = \frac{1}{2} Y_0 \left[\operatorname{erfc}\left(\frac{B-2x}{4\sqrt{\varepsilon t}}\right) + \operatorname{erfc}\left(\frac{B+2x}{4\sqrt{\varepsilon t}}\right) \right] \tag{6.1}$$

$$y = Y_0 \left[1 - \frac{B}{L} - \frac{2}{\pi} \sum_{n=1}^{\infty} \frac{1}{n} \sin\frac{n\pi B}{L} \exp\left(-\frac{4\varepsilon n^2 \pi^2 t}{L^2}\right) \cos\frac{2n\pi x}{L} \right] \tag{6.2}$$

where L is the total length of sandy coast bounded by two rigid boundaries. Those parameters, which appear in Eqs. (6.1) and (6.2), are schematically presented in Fig. 6.7.

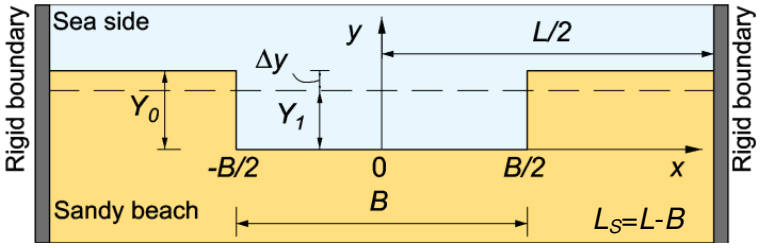

Fig. 6.7 Schematic diagram of bounded rectangular beach cut, $Y_1=Y_0(L-B)/L$

One of the distinct deference characteristics of above equations is that shoreline positions of the concave portion of cases without and with rigid boundaries approach the equilibrium state at Y_0 and Y_1 ($Y_1=Y_0(L-B)/L$), respectively.

It is interesting to note that by changing the sign of Y_0, Eq. (6.2) can be applied in engineering, for example describing the evolution of square-shaped beach nourishment on the coast bounded by coastal structures at both ends. It supplements one more solution to the solutions which have been introduced for infinite length of sandy coast (e.g., Dean, 2003).

6.4 Theoretical comparison on the analytical solutions describing the evolution of concave shoreline without and with rigid boundaries at both ends

Equations (6.1) and (6.2) above can be expressed in term of dimensionless forms as Eqs. (6.3) and (6.4), respectively.

$$y^* = \frac{1}{2}\left[\operatorname{erfc}\left(\frac{B^*-2x^*}{4\sqrt{t^*}}\right)+\operatorname{erfc}\left(\frac{B^*+2x^*}{4\sqrt{t^*}}\right)\right] \tag{6.3}$$

$$y^* = \left[1-\frac{B^*}{L^*}-\frac{2}{\pi}\sum_{n=1}^{\infty}\frac{1}{n}\sin\frac{n\pi B^*}{L^*}\exp\left(-\frac{4n^2\pi^2 t^*}{L^{*2}}\right)\cos\frac{2n\pi x^*}{L^*}\right] \tag{6.4}$$

where the dimensionless parameter is defined as following

$$L^* = \frac{L}{Y_0} \tag{6.5}$$

Figure 6.8 shows the evolution of shoreline positons of concave shoreline from both solutions, Eqs. (6.3) and (6.4), for cases of different values of B^*. An arbitrary value of L^* (L^*=5) is selected for the computation. In Fig. 6.8(a), when the value of B^* is small, shoreline positions obtained from both solutions are almost overlapping even with the large value of t^*. When the value of B^* is getting larger, in Fig. 6.8(b), they are also overlapping when the value of t^* is small; however, the difference of shoreline positions evolution can be seen when the value of t^* is getting larger. Shoreline position, which obtained from Eq. (6.3) (without rigid boundaries), tends to advance faster than the one obtained from Eq. (6.4) (with rigid boundaries). For the case of much larger value of B^*, in Fig. 6.8(c), distinct deference of shoreline positions, which obtained from above solutions, is clear to observe. Moreover, shoreline positions obtained from Eqs. (6.3) and (6.4) approach equilibrium shoreline position at y^*=1 and $y^*=Y_1/Y_0$, respectively.

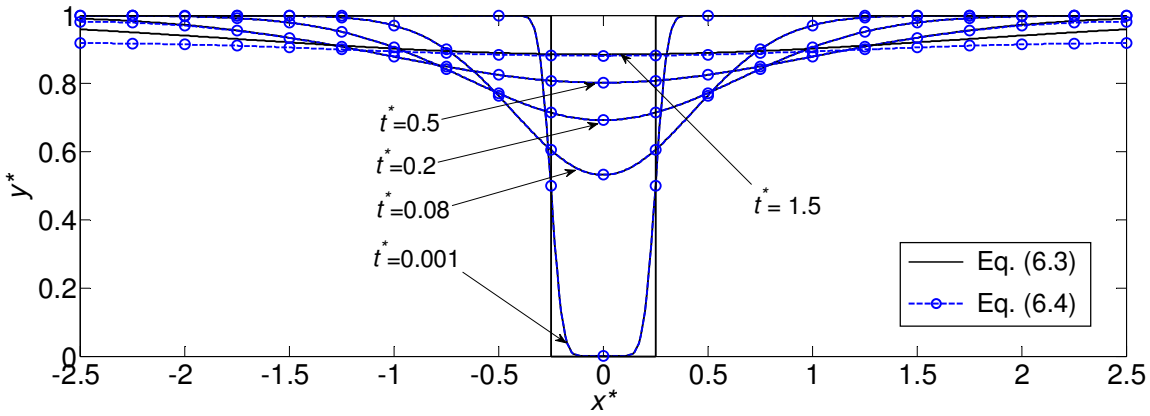

(a) B^*=0.5 (L^*=5)

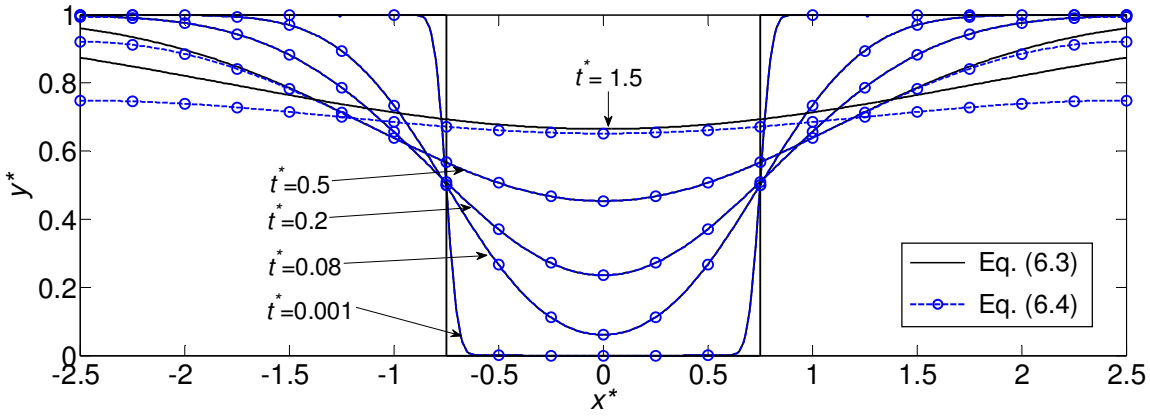

(b) B^*=1.5 (L^*=5)

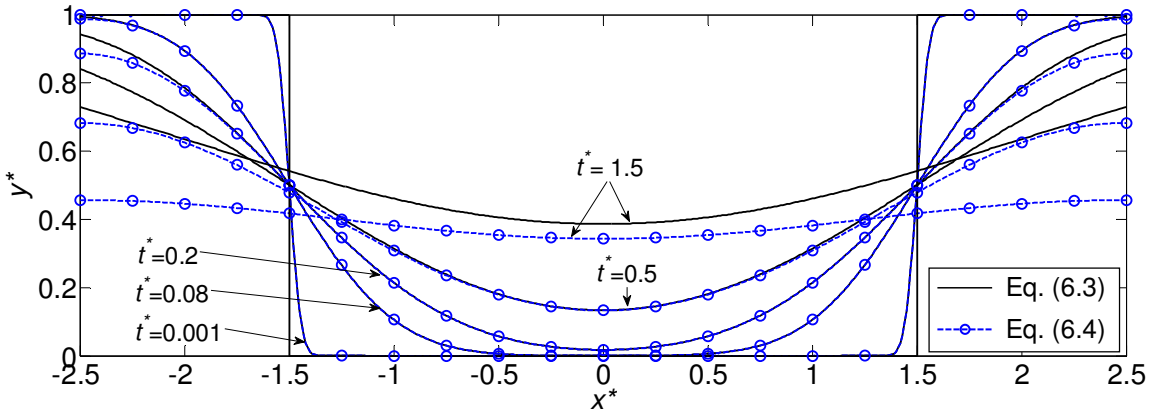

(c) B^*=3 (L^*=5)

Fig. 6.8 Shoreline evolution of initially bounded rectangular beach cut

The temporal variation of theoretical shoreline positions at the central line of concave portion (x^*=0) and at the rigid boundaries (x^*=±L/2) are shown in Fig. 6.9. At both locations, during the early stage when the evolution of shoreline has not been interrupted by the rigid boundaries, shoreline positions from both solutions are totally consistent. However, it shows distinct difference when the rigid boundaries take effect. At the central

line of concave portion, shoreline position obtained from Eq. (6.3) is going to approach the equilibrium position at 1 ($y=Y_0$), whereas shoreline position obtained from Eq. (6.4) is going to approach the equilibrium position at Y_1^*, and it has smaller accretion as compared to the one from Eq. (6.3). Meanwhile, at $x=\pm L/2$, due to the interruption of rigid boundaries on sediment supply from adjacent sandy coasts, shoreline position obtained from Eq. (6.4) has larger retreat compared to the one obtained from Eq. (6.3). This shows clearly the influences of rigid boundaries on the evolutional process of shoreline.

More theoretical comparisons on these two solutions will be given in Sections 6.6 and 6.7 which discuss about the backfilling of sediment into the concave portion.

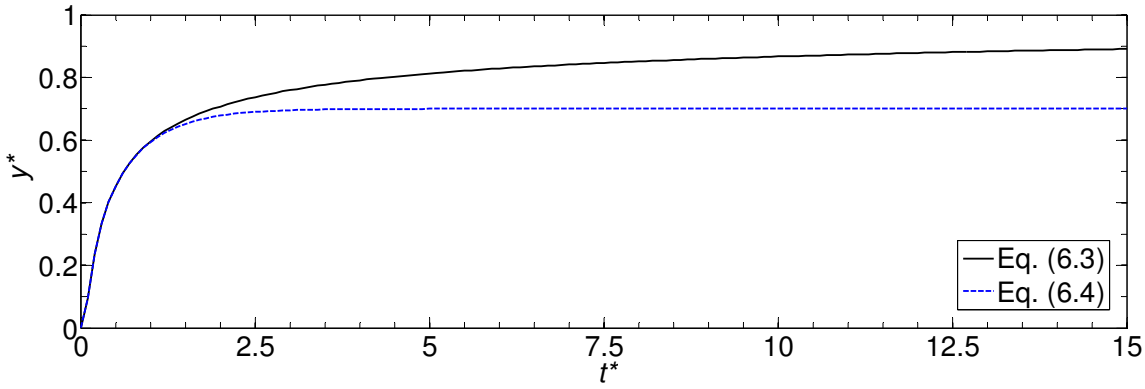

(a) At the center line of rectangular beach cut (concave portion), $x^*=0$

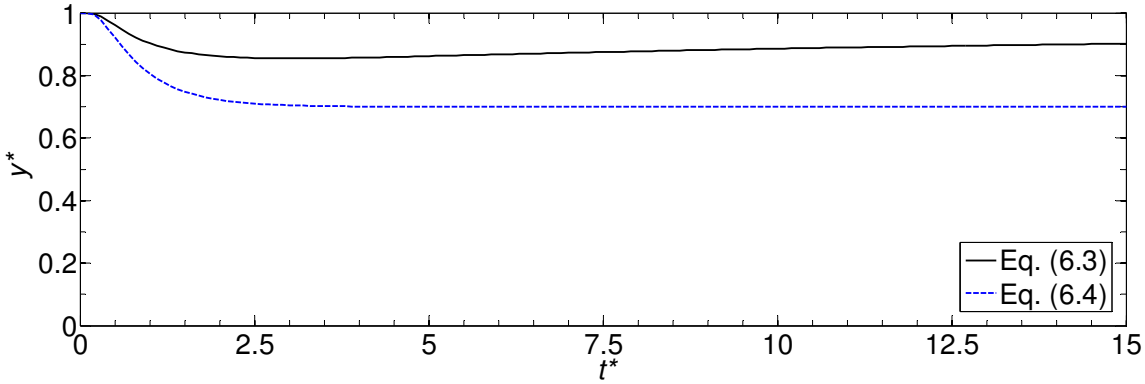

(b) At the rigid boundaries, $x^*=\pm L/(2Y_0)$

Fig. 6.9 Temporal variation of shoreline positions at the central line and at the rigid boundaries of rectangular beach cut

6.5 Relationship between the total length of adjacent sandy coasts and the recovery time

It has been pointed out in Chapter 4 that the concave shorelines, which have sufficient long of adjacent sandy coasts on both sides, have faster recovery process. Therefore, it

would be useful if the relationship between the total length of sandy coasts, L_S (Eq. 6.6) and the recovery time, T_{ER}, is given. Because the position of shoreline in Eq. (6.2) is represented by the exponential function, therefore the recovery time is defined to be the time when shoreline position at the central line of concave portion (x=0) becomes 99 % of the equilibrium shoreline position, $0.99Y_1$.

According to Fig. 6.7, the total length of adjacent sandy coasts is given by the following equation

$$L_S=L-B \tag{6.6}$$

By applying above conditions to Eq. (6.2), the relationship between recovery time and total length of adjacent sandy coasts is represented by the following equation

$$0.99\left(1-\frac{1}{L_S^*+1}\right)=1-\frac{1}{L_S^*+1}-\left[\frac{2}{\pi}\sum_{n=1}^{\infty}\frac{1}{n}\sin\frac{n\pi}{L_S^*+1}\exp\left(-4n^2\pi^2T_{ER}^*\right)\right] \tag{6.7}$$

where the dimensionless parameters are defined as follows

$$L_S^*=\frac{L-B}{B} \tag{6.8}$$

$$T_{ER}^*=\frac{\varepsilon T_{ER}}{L^2} \tag{6.9}$$

The definition of the above two dimensionless parameters have been slightly modified compared to the ones in Chapters 4 because Y_1 is a function of L and B.

Figure 6.10 illustrates the initial conditions of three concave shorelines. The estimated values of the parameters shown in the figure play very important roles for the later computation and comparison. The width of the concave shoreline is the longshore distance of the concave portion. It is easy to determine this parameter for three cases of concave shorelines in Fig. 6.10. The initial beach cut, Y_0, is the cross-shore distance of the concave portion. It stretches from initial shoreline position of the adjacent sandy coast to the end of the beach cut section (breaching). It is simple and obvious to determine this parameter for the cases of concave shorelines of the breaching at Akaiko and Yamamoto. Nevertheless, it is very complicated for the case of breaching at the Nanakita River mouth. This breaching was formed after the flushing of sandspit at the river mouth and sand barrier in front of Gamo Lagoon. The concave portion also includes the river mouth on the right side, the lagoon on behind, and some sandy island remained in the middle. Actually, it cannot apply the approach which is applied for the cases of concave shorelines of the breaching at Akaiko and Yamamoto. Therefore, it is considered that the end of beach cut section is the boundary between sandy beach and pine tree forest on the

right adjacent coast. This boundary is also coincidence with the back side (landward side) of sandy islands. Moreover, during the recovery process, the new sandy beach forming in the concave portion does not cross this boundary. Another parameter is also very important is the initial shoreline positions on the adjacent sandy coasts. It is assumed as the straight line lying on the most parts of shoreline positions of adjacent sandy coasts right after the tsunami. It is simple to determine the initial shoreline positions for the adjacent sandy coasts of concave shoreline at the Nanakita River mouth and breaching at Yamamoto.

However, it is more complicated for the case of concave shoreline at Akaiko because

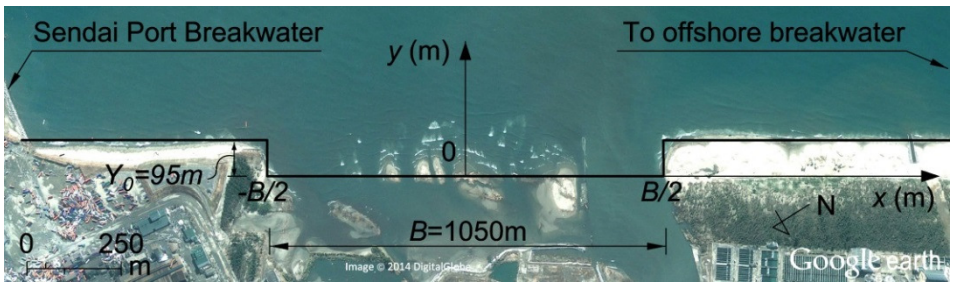

(a) Concave shoreline at the Nanakita River mouth

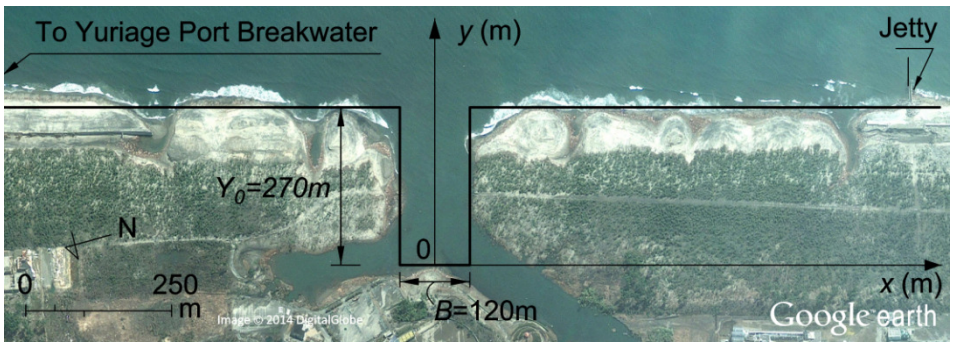

(b) Concave shoreline of the breaching at Akaiko

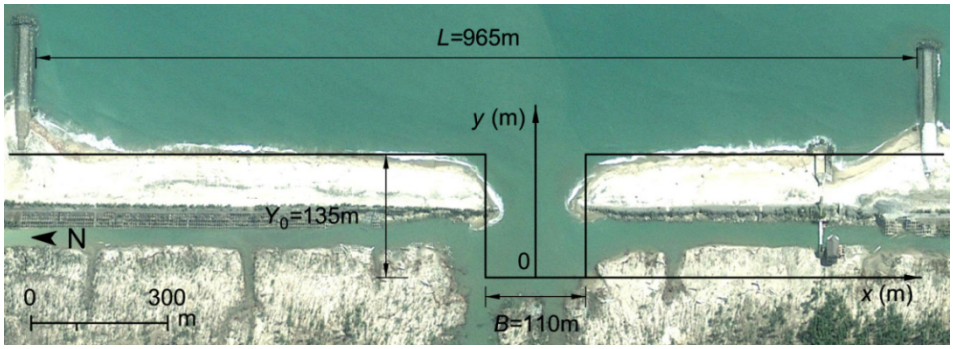

(c) Concave shoreline of the breaching at Yamamoto

Fig. 6.10 Initial conditions of concave shorelines (background: March 14, 2011)

there are some V-shaped channels cutting in the beaches right after the tsunami. These morphological damages have been mentioned in Tappin et al. (2012). The V-shaped channels were filled and smoothed right after the tsunami. However, due to more significantly damaged, the V-shaped channels on the left coast caused discontinue of erosion propagation as mentioned in Chapter 4.

Fig. 6.11 shows the relationship between T_{ER}* and L_S*. Not only the relationship for case when shoreline reaches 99 % of Y_1, but also the relationships for many other percentages of recovery are also included. According to the theoretical results, when the value of L_S* is small, T_{ER}* has high value, whereas when the value of L_S* is getting larger, the value of T_{ER}* is getting smaller. The dimensionless recovery time of morphology is depended on the ratio of total length of adjacent sandy coasts to the concave width. If the total length of adjacent sandy coasts to the concave width is large, then the dimensionless recovery time is short and vice versa.

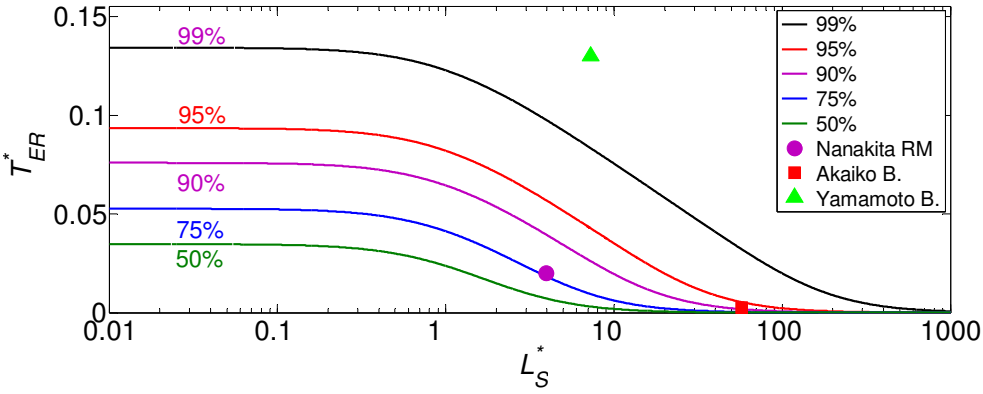

Fig. 6.11 Relationship between T_{ER}* and L_S*

The measured values of L_S* and T_{ER}* of three concave shoreline cases at the Nanakita River mouth, at the breaching of sandy coast at Akaiko and Yamamoto are also plotted in Fig. 6.11. The shoreline position at the central lines of these three case have already reached 120 %, 92 % and 96 % of the Y_1 of three cases, respectively. The concave shape of morphology on the left side of the Nanakita River mouth before the tsunami and recently (Fig. 4.5) would be the reason of the over recovery. According to the results, the measured data of the case of concave shoreline of breaching at Yamamoto has best fit with theoretical relationship from case of 99 % recovery instead of 95 %. Measured data of the case of breaching at Akaiko has good agreement with relationship of 90 % recovery. This case has the good agreement between the theoretical result and measured

data, and the best consistence among three cases. This case has long adjacent sandy coast, hence it has short recovery time. That could be the reason. The measured data of the breaching at the Nanakita River has the best fit with the relationship of case 75 % recovery, while the shoreline has reached 120 % of Y_1. The convex shape of morphology, the complex initial geometry after the tsunami and the influences of river flow to the surrounding morphology could be the reasons of inconsistence.

6.6 Backfilling of sediment into the concave portion

Backfilling is defined as the process that longshore sediment is transported into the concave portion, leading to the accretion of the shoreline position. Based on the theories proposed in the previous parts, the backfilling of sediment in the concave portion can be investigated with respect to the proportional recovery of shoreline position at the center line, y_C, and the proportional sediment filled area of concave portion, P_A.

6.6.1 The proportional recovery of shoreline position at the center line of concave portion

The backfilling of longshore sediment into the concave portion with respect to the recovery of shoreline at the central line can be expressed in terms of dimensionless parameters for the case without and with rigid boundaries as Eqs. (6.10) and (6.11), respectively. During the recovery process, shoreline position in the concave portion approaches Y_0 and Y_1 for cases with and without rigid boundaries, respectively.

$$y_C^* = \mathrm{erfc}\left(\frac{B^*}{4\sqrt{t^*}}\right) \tag{6.10}$$

$$y_C^* = 1 - \frac{B^*}{L^*} - \frac{2}{\pi}\sum_{n=1}^{\infty}\frac{1}{n}\sin n\pi\frac{B^*}{L^*}\exp\left(\frac{-4n^2\pi^2 t^*}{L^{*2}}\right) \tag{6.11}$$

where

$$y_C^* = \frac{y_C}{Y_0} \tag{6.12}$$

According to Eqs. (6.10) and (6.11), y_C^* is a function of B^* and L^*, hence an arbitrary value of B^* (B^*=1) is assumed for the computation.

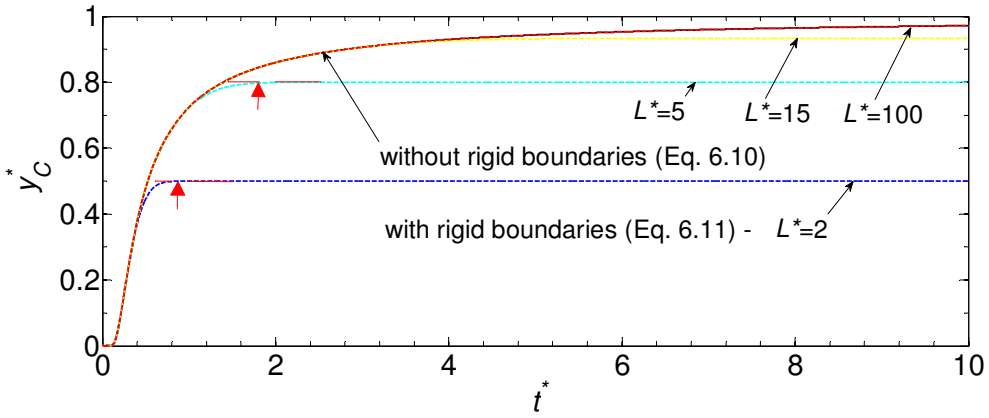

Fig. 6.12 Relationship between t^* and y_C^* (B^*=1)

Figure 6.12 shows the theoretical relationship between t^* and y_C^* for the cases without and with rigid boundaries. For the case with rigid boundaries, several values of L^* were employed for computation. According to the results, when L^* has small value, there is the distinct difference between the relationship obtained from two solutions once the value of t^* is large, although they are overlapping in the early process. There is another distinct difference between the two cases is that the relationship between t^* and y_C^* of case with rigid boundaries gets stable more early (represented by the short dashed lines and arrows) compared to the case without rigid boundary. When the value of L^* gets larger, the relationship between t^* and y_C^* from the two solutions are almost the same. For example, they are overlapping each other when the value of L^* equals to 100.

The above results supplement the understanding on the comparison between the characteristics of the two solutions which have been presented in Section 6.4.

Figure 6.13 presents the relationship between t^* and y_C^* with measured data for the concave shoreline at the Nanakita River mouth, breaching at Akaiko and Yamamoto. The actual values of L, B and Y_0 (Fig. 6.10) of each case were used for the computation. Among these cases, the consistency between theoretical results and measured data of the case breaching at Akaiko is reasonable, while they are very good and weak for the cases of the breaching at Yamamoto and the Nanakita River mouth, respectively. For the case of the breaching at Akaiko (Fig. 6.13(b)), the relationships from two solutions are overlapping each other due to value of L^*/B^* is too large. They have reasonable agreement with measured data. Hence, in this case both theories for cases without and with rigid boundaries can be used. For the case of breaching at Yamamoto (Fig. 6.13(c)), measured data has very good agreement with theoretical result of the case with rigid boundaries. The rigid boundaries of this case are really truly (clear) rigid boundaries;

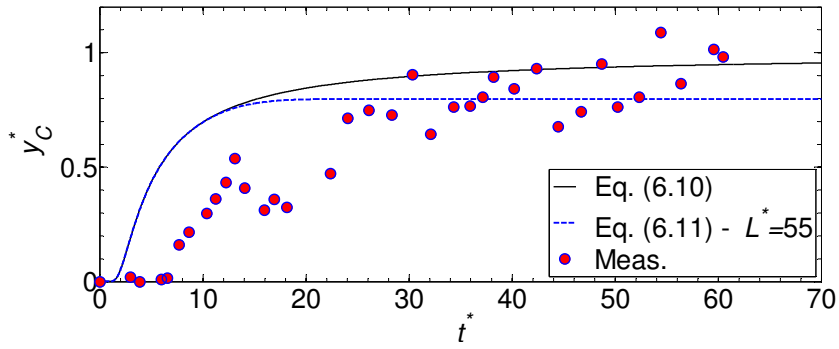

(a) Concave shoreline at the Nanakita River mouth (L*=55, B*=11)

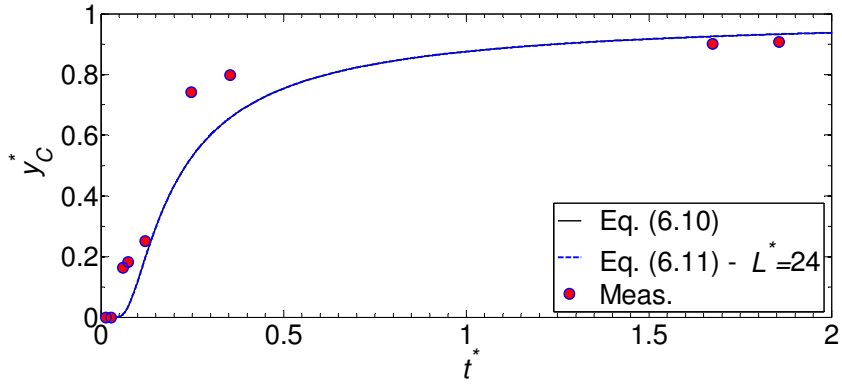

(b) Concave shoreline of breaching of sandy coast at Akaiko (L*=24, B*=0.44)

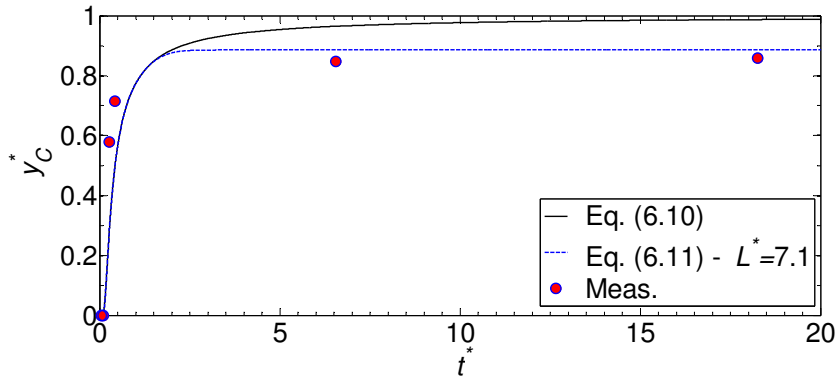

(c) Concave shoreline of breaching of sandy coast at Yamamoto (L*=7.1, B*=0.81)

Fig. 6.13 Relationship between t* and y_C* with measured data

the concave portion was located almost at the center of the bounded coast; and the value of L*/B* is not so large. They could be the explanations for the good agreement between. As a result, in this case, the theory for the case with rigid boundaries is highly recommended to utilize. The one has worst agreement among these cases is the case of concave shoreline at the Nanakita River mouth (Fig. 6.13(a)). For this case, the rigid boundary on the left side, breakwater at Sendai Port, is truly a rigid boundary; however, it is not so on the right side, six detached breakwaters. Moreover, the concave portion has very complex initial landform after the tsunami (see Figs. 4.5 and 4.17). It took some time

to smooth the shoreline after the severe damages induced by the tsunami. The result of EOF analysis (third component) in Chapter 5 has also reflected that process. The latter discussion could explain the very bad agreement in the early period (t^*<24). The agreement with the theoretical results of case with rigid boundary in the late period is much better than the other, however the fluctuation of y_C^* of measured data is large, even greater than 1. The concave portion is located next to the Nanakita River mouth. The complex hydrodynamic processes at this river mouth area could be added reason for the large fluctuation of measured y_C^*.

6.6.2 The proportional concave portion area filled by the longshore sediment

The backfilling of longshore sediment into the concave portion can also be investigated in term of the proportion of sediment filled area, P_A. This parameter represents the percentage of concave portion which has been filled by the longshore sediment from adjacent sandy coasts. Dean (2003) revealed the solution, Eq. (6.13), to obtain P_A for the case without rigid boundaries, whereas this study introduces the solution for case with rigid boundaries, Eq. (6.14). The latter equation is obtained based on Eq. (6.2) when integrating the total sediment transported into the concave portion through the boundaries between concave portion and sandy coasts.

$$P_{A1}= 1-\frac{2\sqrt{t^*}}{B^*\sqrt{\pi}}\left\{\exp\left[-\left(\frac{B^*}{2\sqrt{t^*}}\right)^2\right]-1\right\}-\mathrm{erf}\left(\frac{B^*}{2\sqrt{t^*}}\right) \tag{6.13}$$

$$P_{A2}=\frac{2L^{*2}}{B^*\left(L^*-B^*\right)\pi^2}\sum_{n=1}^{\infty}\frac{1}{n^2}\sin^2\frac{n\pi B^*}{L^*}\left[1-\exp\left(-\frac{4\varepsilon n^2\pi^2 t^*}{L^{*2}}\right)\right] \tag{6.14}$$

where the subscript "1" and "2" are denoted for cases without and with rigid boundaries, respectively.

Figure 6.14 presents the relationship between t^* and P_A for two cases. Similar to previous computation, the B^*value of 1 is again selected. According to Fig. 6.14, when the value of L^* gets larger, the relationship between t^* and P_A of the case with rigid boundaries is asymptotic with the one obtained from the case without rigid boundaries. In addition, an asymptotic line showing the relationship between t^* and P_A of the case without rigid boundaries obtained from Eq. (6.15), is also plotted in Fig. 6.13. Eq. (6.15) is obtained when taking the limit of Eq. (6.13). The asymptotic line would be useful for quick estimation the relationship between t^* and P_A, especially when the value of t^* is small, for example t^*<0.25 when B^*=1.

$$P_{A1}=\frac{2\sqrt{t^*}}{B^*\sqrt{\pi}} \tag{6.15}$$

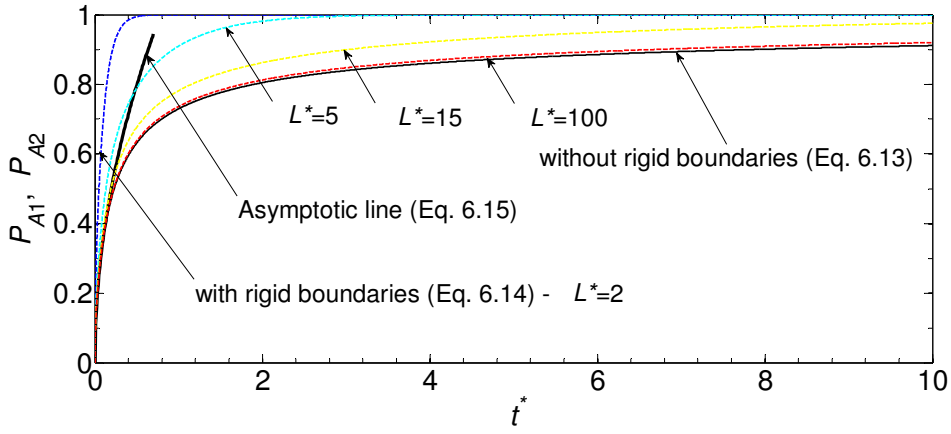

Fig. 6.14 Relationship between t^* and P_A (B^*=1)

Figure 6.15 illustrates the relationship between t^* and P_A with measured data for concave shorelines at the Nanakita River mouth, breaching at Akaiko and Yamamoto. The case of breaching at Yamamoto, Fig. 6.15(c), has very good agreement between theoretical results from the solution for case with rigid boundaries and measured data. Similarly, the case of breaching at Akaiko, Fig. 6.15(b), has also very good agreement between them except in the early period. The non-uniformed depth of concave portion could be the reason for this disagreement. When applying the analytical solution of one-line model, the depth of close of the concave portion is considered as constant and same with the depth of close of the coast. If the actual depth of close in the concave portion is smaller, the recovery of the real backfill process is faster the theoretical backfill process, and vice versa. The case of concave shoreline at the Nanakita River mouth, Fig. 6.15(a), has the worst disagreement. This is similar with the backfilling with respect to the proportional recovery of shoreline position at the central line. Nevertheless, the measured P_A is less fluctuating and has better agreement with the theoretical results from the solution for case with rigid boundaries. So, it would be recommend that when encounter a complex concave portion bounded by rigid boundaries, the relationship between t^* and P_A is more reliable than the relationship between t^* and y_C^*.

Similarly to Eq. (6.2), by making the modification of Eqs. (6.13) and (6.14), the proportion area of sediment remaining in the convex portion (beach nourishment) before shoreline position in this area reaching the equilibrium stage, P_{AN}, for cases without and with rigid boundaries, can be obtained as Eq. (6.16).

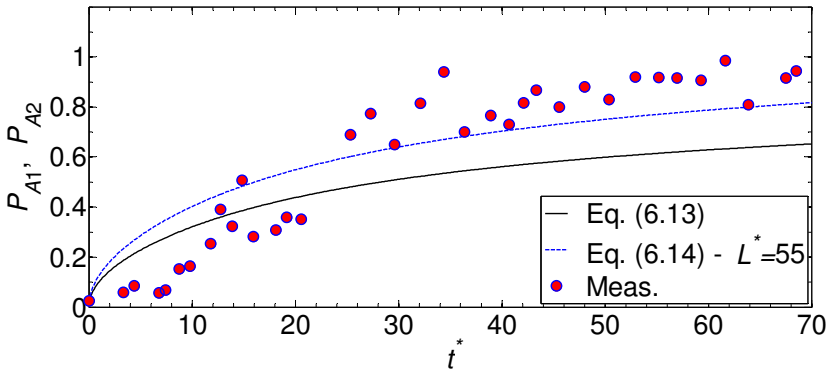

(a) Concave shoreline at the Nanakita River mouth (L*=55, B*=11)

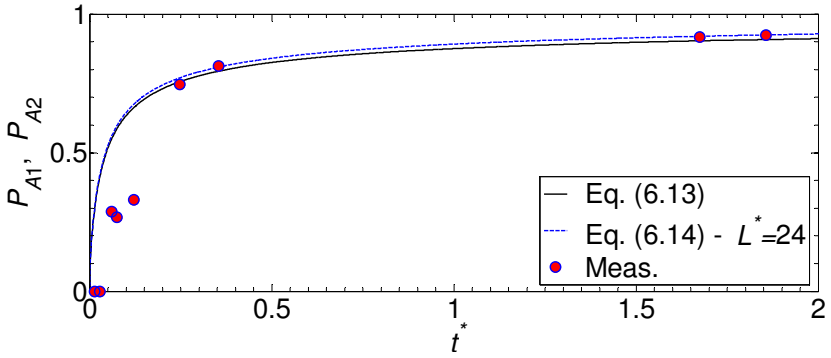

(b) Concave shoreline of breaching of sandy coast at Akaiko (L*=24, B*=0.44)

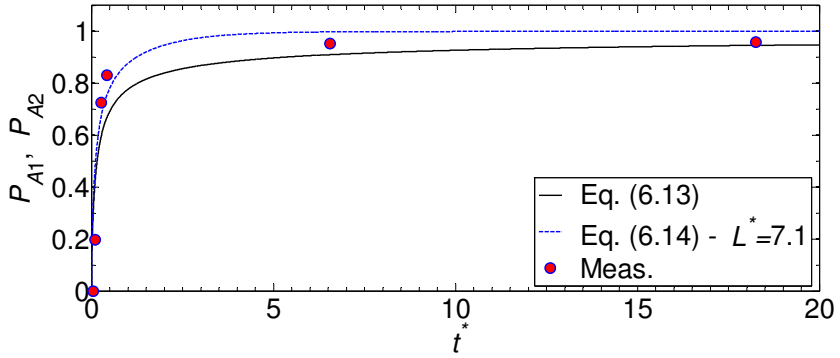

(c) Concave shoreline of breaching of sandy coast at Yamamoto (L*=7.1, B*=0.81)

Fig. 6.15 Relationship between t* and P_A with measured data

$$P_{AN} = 1 - P_A \tag{6.16}$$

6.7 Conclusions in this chapter

In this chapter, the evolution of concave shorelines formed at river mouth and lagoon areas and at breaching of sandy coasts by the tsunami has been investigated. The following conclusions have been made.

1. The coastal structures such as breakwater or jetty bounded at both ends of sandy coast have significant influences on the recovery of the morphology on Sendai Coast after the tsunami.
2. A new analytical solution of one-line model describing the evolution of rectangular beach cut (concave shoreline) bounded by the rigid boundaries has been introduced. In addition, a new analytical solution of one-line model describing the proportional sediment filled area in the concave portion has been also given. These findings are very important for not only scientific interests but also for engineering application.
3. The dimensionless recovery time of morphology, T_{ER}^{*}, which represents the recovery time when shoreline position at the central become 99 % of initial beach cut, Y_0, is depended on the total length of adjacent sandy coasts to the concave width, L_S^{*}. The larger value of L_S^{*} results in the smaller value of T_{ER}^{*}.
4. With a certain value of B^{*} and large value of L^{*}, the relationship between t^{*} and y_C^{*}, and t^{*} and P_A of the case with rigid boundaries are asymptotic with the ones of the case without rigid boundaries. The comparison between theoretical results and measured data has been made. Good agreement can be obtained for the cases of concave shorelines of the breaching of sandy coast at Yamamoto and Akaiko, however worse agreement was also obtained for the case of concave shoreline at the Nanakita River mouth which has complex concave shoreline and unclear rigid boundary.

So far, the subsequent recovery (short-term recovery) of morphology at the river mouths, the breaching of sandy coasts (small areas), or the larger area which includes small areas, have been investigated. In addition, the latter chapter also gave the investigation on the small area and long-term recovery of morphology of small area. So, the questions are how the recovery behavior of morphology on the large area when the time goes longer; what would be the similar or different evolution of shoreline in the extension of time. They will be brought clearly in the next chapter, investigation on the long-term and large area recovery.

CHAPTER 7

LONG-TERM RECOVERY OF MORPHOLOGY ON THE NORTHERN PART OF SENDAI COAST

7.1 Introduction

According to Chapter 4, the morphology at small areas such as river mouths or breaching of sandy coast was severe damaged by the tsunami. The breaching of sandy coast has recovered quite quickly, whereas all the river mouths except the Nanakita River mouth had very slow recovery. That indicates different behaviors of morphological recovery. In addition, there was phenomenon such as erosion propagation, sandspit intrusion raised up during the subsequent recovery process. Chapter 5 has given the details of the recovery of large area during the subsequent recovery (within three years after the tsunami). The littoral system has been changed significantly due to the damages induced by the tsunami. Up to this moment, five years has passed since the occurrence of the tsunami. With adding two more years of shoreline data, the different and similar behaviors of morphology recovery of a large area in the short-term and long-term periods can be revealed.

Accordingly, this chapter attempts to further analyze the behavior of long-term morphological recovery in northern part of Sendai Coast after the 2011 tsunami through the analyses of shoreline data extracted from aerial photographs and EOF.

7.2 Overall long-term recovery of morphology from aerial photograph

Some extracted shorelines are shown in Fig. 7.1(b). In addition, the mean shoreline position of the period from Jun, 2011 to Mar, 2016 is also included. It can be seen that shoreline position along the coast is still far way behind the shoreline position before the tsunami except at areas of detached breakwaters and the Nanakita River mouth. A small area on the left side of the river mouth has almost approached the position before the tsunami.

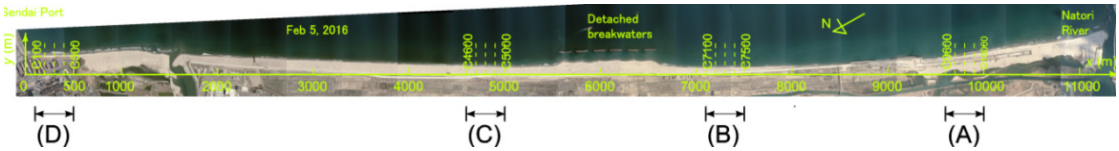

(a) Aerial photograph of Sendai Coast after the tsunami

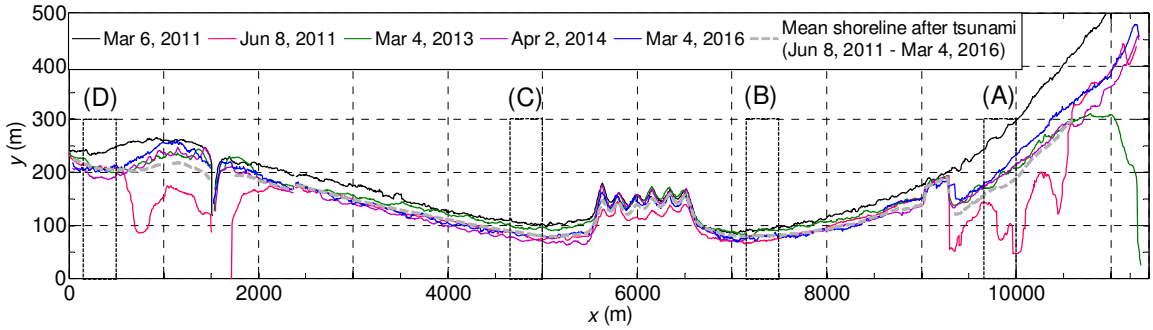

(b) Detected shoreline positions (the dashed gray line in the figure is mean shoreline positions, $\bar{y}(x)$, after the tsunami)

Fig. 7.1 Aerial photograph and detected shoreline positions of the northern part of Sendai Coast

In order to know more details on the evolution of shoreline positions, temporal variation of shoreline positions on the transections along the coast are presented in Fig. 7.2. The same transections, which were utilized in Chapter 5 (Fig. 5.2), are again selected. A vertical dashed line is also included to show the demarcation of data has shown in Chapter 5 (short-term) and new added data. More details about this demarcation time for short-term and long-term recovery can be found in Sections 4.5 and 5.2. Temporal variation of shoreline positions in the updrift end of longshore sediment transport of the coast is illustrated in Fig. 7.2(a). Shoreline position in this area is still accreting, however it still remain about 70 to 80 m behind the shoreline positions before the tsunami. In the area updrift of the detached breakwaters (Fig. 7.2(b)), shoreline position in the last two years is rather stable, there no clear retreat or accretive trends can be observed. Figure 7.2(c) shows the temporal variation of shoreline positions on the downdrift side of detached breakwaters. It is similar to the area updrift of detached breakwaters, shoreline positions in this area has been rather stable in the last two years. In the area downdrift end of longshore sediment transport, clear trend of retreat in the last one year can be observed.

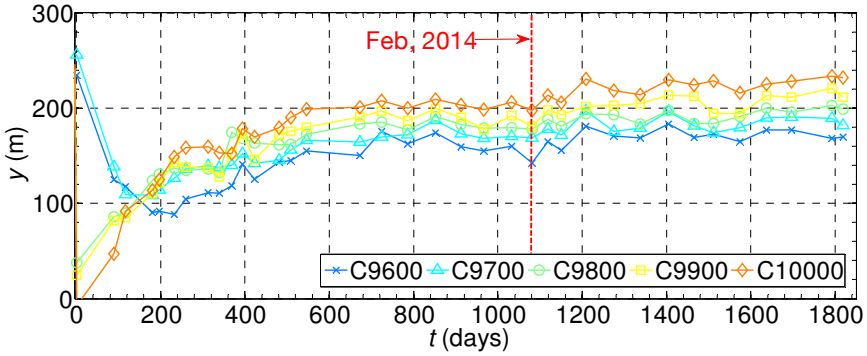

(a) Updrift end of longshore sediment transport - (Area (A) in Fig. 7.1(a))

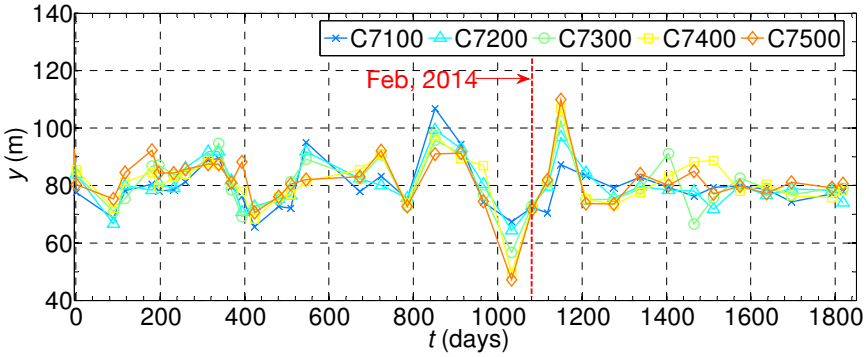

(b) Updrift of detached breakwaters - (Area (B) in Fig. 7.1(a))

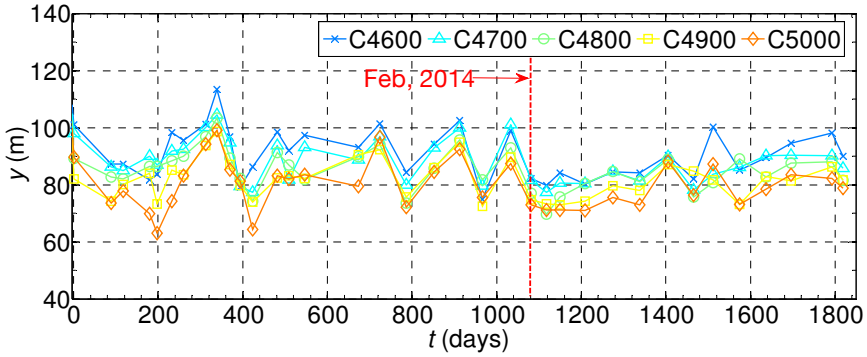

(c) Downdrift of detached breakwaters - (Area (C) in Fig. 7.1(a))

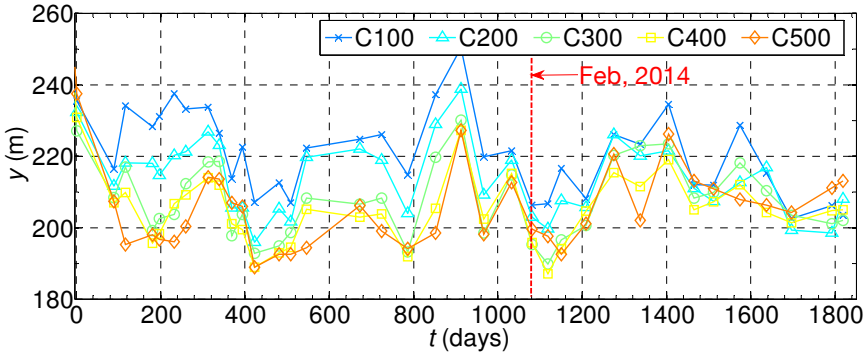

(d) Downdrift end of longshore sediment transport - (Area (D) in Fig. 7.1(a))

Fig. 7.2 Temporal variation of shoreline positions, *t* is the number of days after the tsunami (from Mar 11, 2011)

It can be observed that the shoreline position showing in Fig. 7.2 is less fluctuating in the last two years. This is the distinct difference of the recovery of morphology in the long-term and the short-term periods, especially at the areas with less damaged induced by the tsunami. In order to obtain details about that difference, the standard deviation of shoreline position is computed and illustrated in Fig. 7.3. The computation has been done for two sets of shoreline position. The first is the shoreline position extracted from aerial photographs taken in the period from June, 2011 to February, 2014 (first three years), whereas the other one is from April, 2014 to March, 2016 (last two years). According to results presented in Fig. 7.3, the standard deviation of shoreline position in the last two years is much smaller than the one of the first three years after the tsunami.

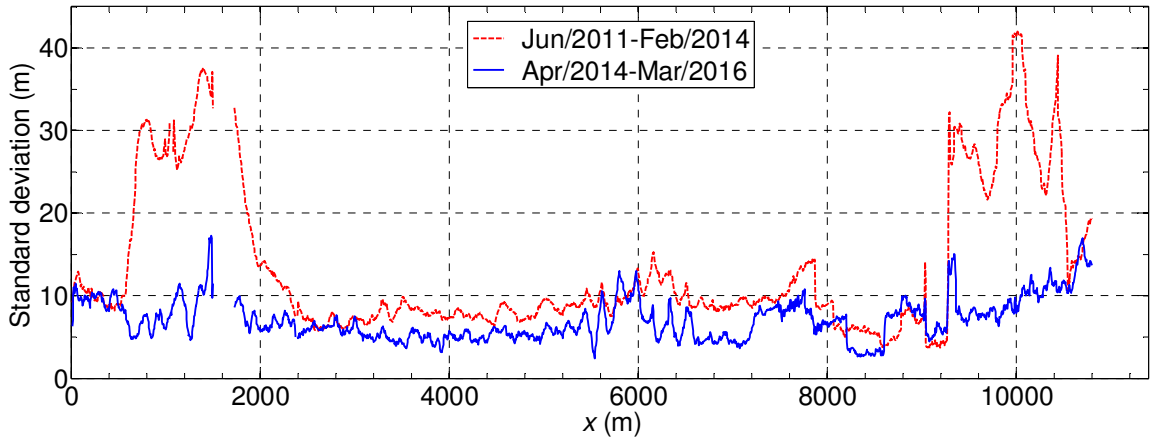

Fig. 7.3 Standard deviation of shoreline positions from the short-term and long-term data sets

The explanation, which could be appropriate for the reducing of fluctuation, is that shoreline has approached more stable condition. As mentioned before, the morphology after the tsunami was in extremely disequilibrium state; therefore the evolution of shoreline could be more active in responding to the changing wave conditions. However, after a few years with the significant recovery at many places, the morphology could be more stable and less active with the changing of wave conditions. Moreover, the reducing of shoreline position fluctuation is just clear at the areas updrift and downdrift of detached breakwaters, where have suffered less severe changes than these other areas. This is could be the added clue for the above discussion.

Change rates of shoreline position on transections along the coast for the periods after the tsunami, from June, 2011 to February, 2014 (hereafter referred as short-term data set)

and from June, 2011 to March, 2016 (hereafter referred as long-term data set), are shown in Fig. 7.4. The results obtained from the 2-year shoreline data from March, 2009 to March, 2011 (hereafter referred as data set before the tsunami) before the tsunami, which have been presented in Chapter 5, are also re-included in Fig. 7.4. It can be seen that the change rate obtained from the long-term data after the tsunami is totally different with the change rate generated from data set before the tsunami. If making comparison between the values of shoreline change rate after the tsunami obtained from short-term and long-term data sets, distinct deference can also be found. At the detached breakwater the change rate of long-term data has reduced much its value. In addition, the similar reduction of shoreline change rate also occurred at the severely damaged area adjacent to the Nanakita and Natori River mouths, although it is still positive at both areas.

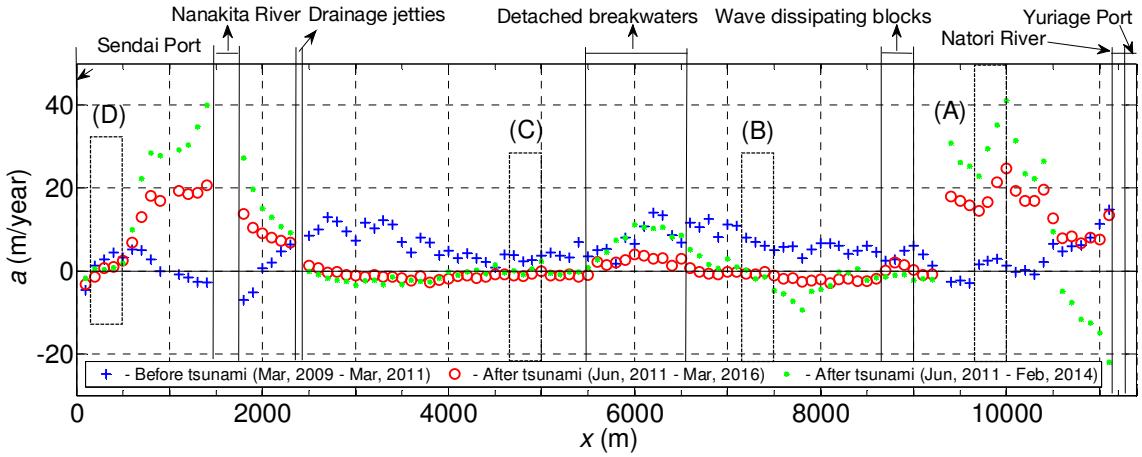

Fig. 7.4 Shoreline change rates before and after the tsunami

The change rate of long-term data in the areas updrift and downdrift of the detached breakwaters becomes negative value almost.

The average shoreline change rate from wave-dissipating blocks to drainage jetty $\bar{a}$ (m/year) and the annual average amount of sediment change dV/dt (m^3/year) for the long-term data set, which is estimated using Eq. (5.1), are updated in Table 7.1 along with the results of these other data sets.

Table 7.1 Average shoreline change rate and the annual average amount of sediment change of the coast from wave-dissipating blocks to drainage jetty (long-term)

Period	Average shoreline change rate, $\bar{a}$ (m/year)	Annual average amount sediment change, dV/dt (m^3/year)
Before the tsunami	6.2	4.5×10^5
Short-term recovery (Chapter 5)	7.3	5.5×10^4
Long-term recovery (current chapter)	-0.47	-3.5×10^4

According to the results in Table 7.1, the value of average shoreline change rate has reduced much, dropping from 7.3 m/year of short-term data set to -0.47 m/year of the long-term data set. On the other hand, the latter value is completely different with the value before the tsunami. The value of annual average amount of sediment change has dropped to negative value. It means that the sediment of the coast from wave-dissipating blocks to drainage jetty was transported out the area. The dominant of longshore sediment transport of the coast is from south to north; hence the mentioned sediment would be transported to the coast around the Nanakita River mouth, and result in the significant recovery of shoreline position at this area.

According to above discussion, it can be said that littoral system on the northern part of Sendai Coast has been significantly changed after the tsunami. In addition, if consider in term of short-term and long-term recovery, the littoral system also got the difference.

On the northern part of Sendai Coast, there are two river mouths, the Nanakita and the Natori. As mentioned in Chapter 2, river mouth can play the role of sediment sink or sediment source. When river flow is low, river mouth has the same function of tidal inlet, playing sink effect (formatting flood-tidal shoal). In addition, river mouth can also play the sink effect once the intrusion of sandspit happens, for example, the sandspit intrusion after the 2011 tsunami which has been presented in Chapter 4. However, river also supplies a lot of sediment to the coastal area. River flow (especially during high flood) transports sediment along the river, sediment at the river mouth area and the sediment of sandspit to the sea area and forms the sand terrace. Under the actions of waves, the sediment at sand terrace will be transported to the adjacent sandy beaches. The annual sediment supply from Nanakita River and Natori River are 2000 and 10000 m^3/year,

respectively. The amount of sediment supply from Nanakita River and the eroded sediment from adjacent sandy coasts led to fast recovery of the concave shoreline at that river mouth. However, the sediment supply from the river in one year is rather small compared to the eroded sediment which has been indicated as longshore sediment. The amount of sediment supply from Natori River is much greater than the one of Nanakita River. That would significantly lead to the accretion of shoreline. The long breakwater at the Yuriage Port totally interrupts the sediment supply from the south. In addition, the wave-dissipating blocks (Fig. 5.5) interrupt to the longshore sediment to the north (left), and also block eroded sediment from the adjacent sandy coast on the north side supplying to the concave portion. Hence, it can be said that the sediment supply from Natori River was the main sediment source for the accretion of shoreline at the area around Natori River mouth and Idoura Lagoon. Another source of sediment on the northern part of Sendai Coast was supplying from the eroded sediment of the coastal area next to Sendai Port. The ground elevation of that area is much higher than the elevation of berm. After the tsunami, that area has been eroding hence the amount eroded sediment from this area would be larger than normal. The sediment sink and source regarding to rivers and sediment supply from the erosion of high elevation area can contribute effects to the conventional theory of one-line model using in Chapters 4 and 6 which does not consider sediment sink and source. Another effect of the river is that river flow can partly interrupt the longshore current (especially at the Nanakita River mouth), cause deposition on the updrift side and erosion on the downdrift side. More details on the evolution of shoreline around the Nanakita and Natori River mouth after the tsunami with discussion on the influences of the river mouths can be found in Hoang et al. (2014).

On Nanakita and Natori Rivers, there have been usually big floods which followed the typhoons. The typhoons and floods have caused significant changes of morphology of these two river mouths. A typical case is that strong typhoon and flooding event occurred in early September, 2015. It caused significant changes of morphology at the Nanakita and Natori River mouths. The sandspits were flushed; the river mouths became wider and deeper; the sandy barrier in front of Idoura Lagoon was also severely eroded. After that event, sediment from the beach on the left side of the Nanakita River mouth was significantly eroded and transported to the river mouth area. That caused serious retreat of shoreline position on the left side of the river mouth. The phenomenon of sandspit intrusion could observe again. More details morphological changes and recovery can be found in Tanaka et al. (2016).

As mentioned in Chapter 3 that shoreline aerial photographs have been taken in every one or two months. Therefore, sometime it could be taken before and after the time when the big floods happen. These floods happen in a short-term and cause severe morphological changes at river mouths. The changes would have influences on the long-term morphological recovery of the coast. However, these influences cannot be reflected in the results of current EOF. In order to take into account that more frequent aerial photographs (taken before and after each event) or using video monitoring system at the river mouth are required.

7.3 Results of EOF analysis on the long-term recovery of morphology

The EOF analysis, which was utilized in Chapter 5, is again employed in this chapter to express the behaviors of long-term morphological recovery. Two years of shoreline data is added into the computation. Hence, the EOF analysis results showing below could make clear the evolution of shoreline on the northern part of Sendai Coast in a long-term period after the tsunami.

The first three spatial eigenfunctions $e_n(x)$ and the first three temporal eigenfunctions $c_n(t)$ are presented in Figs. 7.5 and 7.6, respectively. According to the results showing in Fig. 7.5, the spatial eigenfunction of the first component has changed the sign of value compared to the one of short-term data; however, the temporal eigenfunction has changed the sign too. Therefore, the combination of the spatial and temporal eigenfunction would have same sign with the one of short-term data. The spatial and temporal and eigenfunctions of the second and third components have the same trends with the ones of the second and third components of the short-term data. If paying attention on the variation of temporal eigenfunction of the second component (Fig. 7.6), it can be recognized that the fluctuation of value is gradually reducing from beginning to the end. Especially, it is very small in the last two years. This is consistent with the more stable condition of shoreline position in the less severely damaged areas. Besides, this also confirms the discussion in the latter section about the more stable condition of shoreline recently.

Figures 7.7, 7.8 and 7.9 present the combination spatial and temporal eigenfunctions of the first three components extracted from the long-term data set. Generally, the component orders and shapes in these figures are similar to the ones extracted from short-term data set. Figure 7.7 indicates that the values of the combination at the severely

damaged areas are still getting bigger. It means that the recovery of morphology at the severely damaged areas is still going on and dominant compared to among other processes. The contribution rate of this component is 71 %. The fluctuation of value of the combination in the last two years of the second component is much smaller and more stable than the one in the first three years. The contribution rate of this component is 7 %. The combination of the spatial and temporal eigenfunctions of the last two years of the third component is similar to what is in the second and third years. Moreover, in short-term recovery, this component has been reported to reflect the recovery of morphology at the severely damaged area in the early stage after the tsunami. As a result, its effects should be weaker when longer time passing. Therefore, its contribution rate has dropped to 4 %. From the above results and discussion, the first three components extracted from long-term data set reflect the same processes with what were obtained from short-term data set in Chapter 5. However, their contribution rates have been changed.

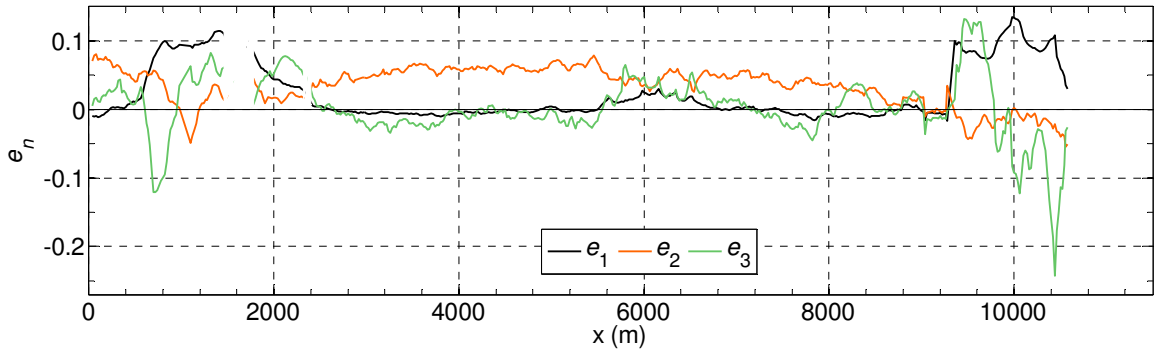

Fig. 7.5 Spatial eigenfunctions, $e_n(x)$, of the first three components

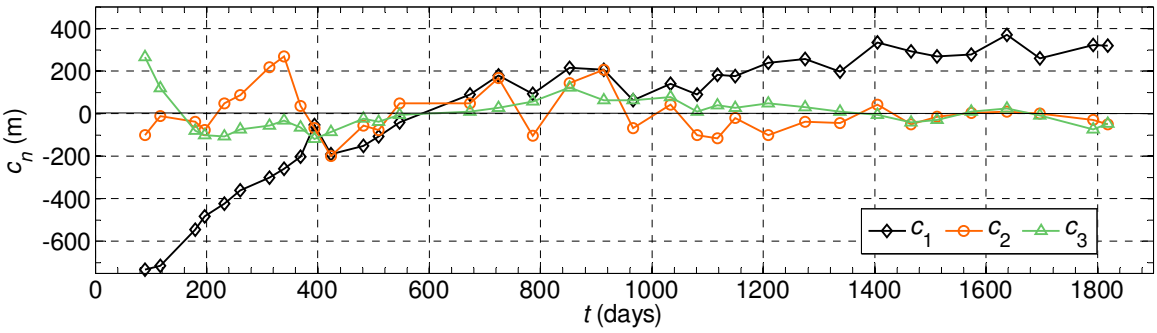

Fig. 7.6 Temporal eigenfunctions, $c_n(t)$, of the first three components

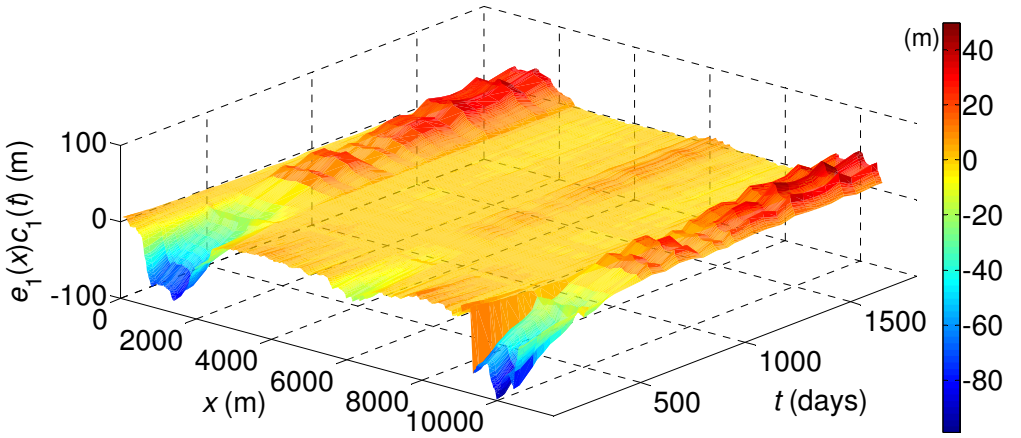

Fig. 7.7 The combination of spatial and temporal eigenfunctions of the first component, $e_1(x)c_1(t)$

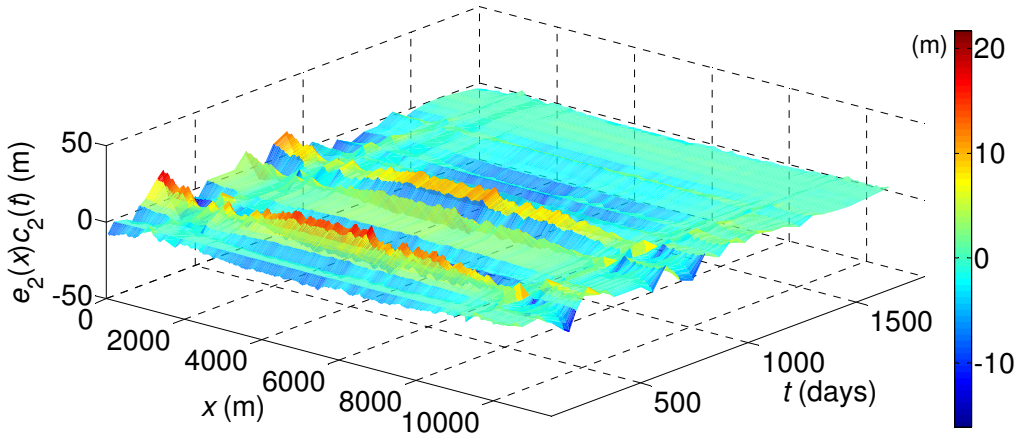

Fig. 7.8 The combination of spatial and temporal eigenfunctions of the second component, $e_2(x)c_2(t)$

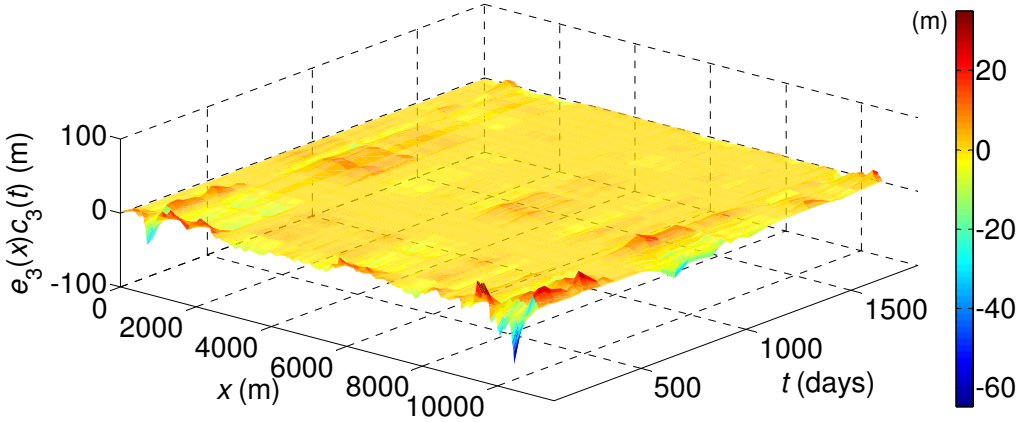

Fig. 7.9 The combination of spatial and temporal eigenfunctions of the third component, $e_3(x)c_3(t)$

7.4 Discussion on the evolution of morphology before and after the tsunami

The contribution rates and the reflected processes from studies before and after the tsunami are presented in Table 7.2. Kang and Tanaka (2005) applied the EOF analysis for the same study area with the present study with the shoreline data set from 1996 to 2003. They reported that the most dominant component of shoreline change is cross-shore variability of shoreline position, whereas the second component reflects the evolution of shoreline position regarding to the longshore sediment transport. Before the tsunami, shoreline has been in quasi-equilibrium state; hence the evolution of shoreline was most significantly driven by cross-shore movement of sediment in responding to the changing of wave conditions, i.e. wave height increasing during the storm, etc. However, the contribution rates of these two components are only about a couple times difference. In the contrary, the evolution of shoreline after the tsunami has been completely changed due to the extremely imbalance of morphology. The most dominant evolution of shoreline position in both short-term and long-term consideration is the accretion of shoreline positions at the severely damaged areas. As presented in Chapters 4 and 6 that recovery was mostly contributed by longshore sediment from adjacent sandy coasts. The contribution rates of the first component obtained from short and long-term data are all about 70 %.

Table 7.2 Contribution rates of the components and reflected processes

Period	Component and Contribution rate	Reflected process
1996～2003	1st: 39 %	Cross-shore variability of shoreline
(Kang and Tanaka, 2005)	2nd: 18 %	Longshore sediment transport
	1st: 67 %	Recovery of severely damaged areas
6/2011～2/2014	2nd: 11 %	Cross-shore variability of shoreline
(Short-term recovery)	3rd: 7 %	Recovery of severely damaged areas in the early stage after the tsunami
	1st: 71 %	Recovery of severely damaged areas
6/2011～3/2016	2nd: 8 %	Cross-shore variability of shoreline
(Long-term recovery)	3rd: 4 %	Recovery of severely damaged areas in the early stage after the tsunami

After the tsunami, the evolution of shoreline driving by the cross-shore sediment movement became the second component, and the contribution rate has dropped to about 10 % or smaller. It means the littoral system of the coast has been significantly modified compared to the period before the tsunami. If comparing the results of EOF analysis on the short-term and long-term shoreline data set, the order and the reflected processes of the long-term data analysis remain similarly to the ones of the short-term data analysis. Nevertheless, the contribution rates have changed. In the long-term data analysis, the contribution rate of the first component has increased, while the contribution rates of the second and third components have decreased. As discussed in the Section 7.2, shoreline position in the last two years (2014 and 2015) was rather stable, especially at the places out of the severely damaged areas. Hence, the contribution from cross-shore movement, which leads to the large amount and speedy shoreline position change, has reduced slightly.

7.5 Conclusions in this chapter

In this chapter, the recovery of the morphology on the northern part of Sendai Coast in long-term period has been analyzed. The following conclusions have been made.

1. Shoreline position has not been reached the equilibrium state, although five years have been passed since the occurrence of the tsunami, and the more stable behavior can be observed.
2. Shoreline change rates along the coast of the period five years after the tsunami have been changed significantly compared to the period before the tsunami and comparatively changed compared to the period three years after the tsunami. It means that the littoral system on this coast has been also changed.
3. The first three dominant components of the long-term recovery reflect the same physical processes compared with what were found in the short-term recovery; however the contribution rates have been changed.

The significant changes and the subsequent and long-term recovery of morphology along the coast of Miyagi Prefecture have been presented in Chapters 4 to 7. The overall findings, conclusions on the mentioned topics and recommendations for engineering application and further studies will be given in the next chapter.

CHAPTER 8

CONCLUSIONS AND RECOMMENDATIONS

8.1 Conclusions

Throughout the previous chapters in this study, the results on the significant changes and recovery process of morphology along the coast in Miyagi Prefecture have been presented and discussed. The followings overall conclusions have been made.

- The estuarine and coastal morphologies along the coast of Miyagi Prefecture have been significantly changed by the 2011 tsunami. The recovery process has soon started at the areas with sufficient sediment supply from adjacent sandy coasts, while it has been slow or no recovery with the ones having insufficient sediment supply.
- During the subsequent recovery process, the sandy coasts adjacent to concave shorelines of severely damaged areas were eroded. The erosion propagated along the coast in proportional to square root elapsed time since the tsunami occurrence.
- A new approach to evaluate diffusion coefficient is introduced. The values of diffusion coefficient for areas at the Nanakita River mouth and the breaching at Akaiko are 13 m^2/h and 14 m^2/h, respectively.
- The intrusion of sandspit into all studied river mouths after the tsunami has been observed. The scouring river mouth bed deeper than the depth of closure induced by the tsunami waves and return flow has been pointed out as the cause of the sandspit intrusion.
- The recovery of concave shorelines at severely damaged areas can be described by the analytical solutions of one-line model. A new analytical solution describing the evolution of concave shoreline bounded by the coastal structures, which are considered as the rigid boundaries, has been introduced. In addition, a new analytical solution describing the proportional backfilled area in the concave portion has been revealed too.

- With large value of dimensionless length of the bounded coast, L^*, the relationship between dimensionless elapsed time, t^*, and proportional recovery of shoreline at the central line of concave portion, y_C^*, and the relationship between dimensionless elapsed time, t^*, and the proportional of backfilled area, P_A, of the case with rigid boundaries are asymptotic with the ones of the case without rigid boundaries.
- The dimensionless morphological recovery time of concave shoreline after the tsunami, T_{ER}^*, is depended on the dimensionless total length of adjacent sandy coasts to the width of concave portion, L_S^*. The larger value of L_S^* results in the smaller value of T_{ER}^*.
- On the subsequent recovery process of morphology on the northern part of Sendai Coast, the recovery at the places such as the river mouths, breaching of sandy coasts and the flushing of sandy barriers in front of lagoon, where were severely damaged by the tsunami, was dominant compared to among other processes. When considering the recovery on the long-term scale, the order and the reflected processes of the dominant components are the same; however their contribution rates have changed.
- The littoral system of the northern part of Sendai Coast has been modified significantly since the tsunami induced the massive changes of morphology. Shoreline position of the coast has not been in equilibrium condition yet, although five years has passed since the occurrence of the 2011 tsunami.

8.2 Recommendations

The following recommendations have been made from the present study.

- The approach of classification small and large areas, short- and long-term in this study would be useful to apply in other areas which have similar characteristics.
- When the sand spit intrusion into river mouth after the tsunami, that indicates the boundary between fresh-sea water also moves further upstream, hence when implementing out the design of river structures, wave forces need to be taken into account.

- This study carried out the values of diffusion coefficient for the coasts at the Nanakita River mouth and breaching at Akaiko after the tsunami. These values could be utilized in engineering.
- The introduced analytical solutions of one-line model describing the evolution of concave shoreline bounded by rigid boundaries could be also applied in engineering. By making slight modification, it can describe the evolution of rectangular planform beach nourishment in the coastal area bounded by the jetties or groins at both ends.
- The introduced analytical solution of one-line model so far can only be applied for the simple initial bounded concave shoreline that has symmetric length of adjacent sandy coasts on both sides. Hence, further development on the analytical solution of one-line model to describe the evolution of bounded concave shoreline, that has asymmetric length of adjacent sandy coasts on both sides of the concave portion, or has the non-uniform of depth of closure, or has the complex shape of initial shoreline and concave portion, is highly necessary.
- The recovery of morphology in this study has been mainly discussed based on the variation of shoreline position itself. The cross-shoreline movement of sediment was neglected. Hence, the study on the recovery of morphology in connection with bathymetry change is useful and highly required. In addition, the sediment budget analysis will need to be carried out too.
- The results of EOF analysis cannot reveal the influences of short-term shoreline changes at the river mouth induced by big floods on the long-term recovery of morphology on the northern part of Sendai Coast. It is necessary to improve that by input more shoreline position data, especially taking before and after the flood events or extracting from images of video monitoring camera system.
- The recovery of morphology is important for the resilient and prepared plans for the future similar disasters. This study has presented the recovery process in the past five years. However, the behavior of shoreline evolution in the future is also highly important. Hence, the numerical model to predict the evolution of shoreline position in the future may need to be developed.

References

Aarninkhof, S. G. J., Turner, I. L., Dronkers, T. D. T., Caljouw, M. and Nipius, L. (2003). A video-based technique for mapping intertidal beach bathymetry. *Coastal Engineering, Vol. 49*(4), pp. 275-289.

Aarninkhof, S. G. J., Ruessink, B. G. and Roelvink, J. A. (2005). Nearshore subtidal bathymetry from time-exposure video images. *Journal of Geophysical Research, Vol. 110*(C06011).

Ali, P. Y. and Narayana, A. C. (2015). Short-term morphological and shoreline changes at Trinkat island, Andaman and Nicobar, India, after the 2004 tsunami. *Marine Geodesy, Vol. 38*(1), pp. 26-39.

Anders, F. J. and Byrnes, M. R. (1991). Accuracy of shoreline change rates as determined from maps and aerial photographs. *Shore and Beach, Vol. 59*(1), pp. 17-26.

Armaroli, C. and Ciavola, P. (2011). Dynamics of a nearshore bar system in the northern Adriatic: A video-based morphological classification. *Geomorphology, Vol. 126*(1-2), pp. 201-216.

Bagus, M. A. and Tanaka, H. (2013). Shoreline changes at Sendai Port due to the Great North East Japan, Taunami of 2011. *Proceedings of the 7th International Conference on Coastal Dynamics*, pp. 63-72.

Bakker, W. T. and Edelman, T. (1965). The coastline of river deltas. *Proceedings of the 9th Coastal Engineering Conference*, pp. 199-218.

Bakker, W. T. (1969). The dynamics of a coast with a groin system. *Proceedings of the 11th Coastal Engineering Conference*, pp. 492-517.

Barrer, R. M. (1941). *Diffusion in and through solids*: Cambridge University Press, 464 p.

Boak, E. H. and Turner, I. L. (2005). Shoreline definition and detection: A review. *Journal of Coastal Research, 21*(4), pp. 688–703.

Bowen, A. J. and Inman, D. L. (1966). Budget of littoral sand in the vicinity of point arguello, California. *Technical Memorandum, No. 19*, U.S. Army Coastal Engineering Research Center, 56 p.

Carslaw, H. and Jaeger, J. (1959). *Conduction of Heat in Solids*: Clarendon Press, 510 p.

Catalán, P. A., Cienfuegos, R. and Villagrán, M. (2014). Perspectives on the long-term equilibrium of a wave dominated coastal zone affected by tsunamis: the case of central Chile. *Journal of Coastal Research, Vol. 71*, pp. 55-61.

Choowong, M., Phantuwongraj, S., Charoentitirat, T., Chutakositkanon, V., Yumuang, S. and Charusiri, P. (2009). Beach recovery after 2004 Indian Ocean tsunami from Phang-nga, Thailand. *Journal of Geomorphology, Vol. 104*(3-4), pp. 134-142.

Cienfuegos, R., Villagran, M., Aguilera, J. C., Catalán, P., Castelle, B. and Almar, R. (2014). Video monitoring and field measurements of a rapidly evolving coastal system: the river mouth and sandspit of the Mataquito River in Chile. *Journal of Coastal Research, Proceedings of the 13th International Coastal Symposium, Vol. 70*, pp. 639-644.

Cohen, J. E., Small, C., Mellinger, A., Gallup, J. and Sachs, J. (1997). Estimates of coastal populations. *Science, Vol. 278*(5341), pp. 1209-1213.

Crank, J. (1975). *The Mathematics of Diffusion* (2nd Ed.): Clarendon Press, 414 p.

Dean, R. G. (1989). Measuring longshore transport with traps. *Nearshore Sediment Transport, ed., Seymour R. J., Plenum Press*, pp. 313-336.

Dean, R. G. and Work, P. A. (1993). Interaction of navigational entrances with adjacent shorelines. *Journal of Coastal Research, Vol. 18*(special issue), pp. 91-110.

Dean, R. G. and Dalrymple, R. A. (2002). *Coastal processes with engineering applications*: Cambridge University Press, 471 p.

Dean, R. G. (2003). *Beach Nourishment -Theory and Practice*: World Scientific, 420 p.

Deguchi, I. and Sawaragi, T. (1988). Effects of structure of discharged sediment around river mouth. *Proceedings of the 21st International Conference on Coastal Engineering*, pp. 1573-1587.

del Valle, R., Medina, R. and Losada, M. A. (1993). Dependence of coefficient *K* on grain size. *Technical Note No. 3062, Journal of Waterways, Port, Coastal, and Ocean Engineering, Vol. 119*(5), pp. 568-574.

Dolan, R., Hayden, B. and Heywood, J. (1978). A new photogrammetric method for determining shoreline erosion. *Coastal Engineering, Vol. 2*, pp. 21-39.

Dolan, R., Hayden, B., May, P. and May, S. (1980). The reliability of shoreline change measurements from aerial photographs. *Shore and Beach, Vol. 48*(4), pp. 22-29.

Dolan, T. J., Castens, P. G., Sonu, C. J. and Egense, A. K. (1987). Review of sediment budget methodology: Oceanside littoral cell, California. *Proceedings of the Coastal Sediments '87*, pp. 1289-1304.

Elizabeth, H. B. and Ian, L. T. (2005). Shoreline definition and detection: A review. *Journal of Coastal Research, Vol. 21*(4), pp. 688-703.

Fairbridge, R. W. (1980). *The estuary: its definition and geo-dynamic cycle*: Cambridge University Press, 623 p.

Feyisaa, G. L., Meilbya, H., Fensholtb, R. and Proud, S. R. (2014). Automated Water Extraction Index: A new technique for surface water mapping using Landsat imagery. *Remote Sensing of Environment, Vol. 140*, pp. 23-35.

FitzGerald, D. M. (1988). Shoreline erosional-depositional processes associated with tidal inlets *Hydrodynamics and Sediment Dynamics of Tidal Inlets, Vol. 29*, pp. 186-225.

FitzGerald, D. M. (2005). Tidal inlets. *in Schwartz, M. L., (Ed.), Encyclopedia of coastal science*: Springer, pp. 958-965.

Ford, M. (2013). Shoreline changes interpreted from multi-temporal aerial photographs and high resolution satellite images: Wotje Atoll, Marshall Islands. *Remote Sensing of Environment, Vol. 135*, pp. 130-140.

García-Rubio, G., Huntley, D. and Russell, P. (2015). Evaluating shoreline identification using optical satellite images. *Marine Geology, Vol. 359*, pp. 96-105.

Goto, K., Hashimoto, K., Sugawara, D., Yanagisawa, H. and Abe, T. (2014). Spatial thickness variability of the 2011 Tohoku-oki tsunami deposits along the coastline of Sendai Bay. *Marine Geology, Vol. 358*, pp. 38-48.

Grijm, W. (1961). Theoretical forms of shoreline. *Proceedings of the 7th Coastal Engineering Conference*, pp. 197-202.

Grijm, W. (1965). Theoretical forms of shoreline. *Proceedings of the 9th Coastal Engineering Conference*, pp. 219-235.

GSI. (2016). List of variation of coastal observation stations. Retrieved from *http://www.gsi.go.jp/common/000136983.pdf*.

Hanslow, D. J. (2007). Beach erosion trend measurement: A comparison of trend indicators. *Proceedings of the 9th International Coastal Symposium*, pp. 588–593.

Hanson, H. and Kraus, N. C. (1989). GENESIS: Generalized model for simulating shoreline change, Report 1: Technical Reference. *Technical Report CERC-89-19*, U.S. Army Engineer Waterways Experiment Station, Coastal Engineering Research Center.

Hoang, V. C., Mitobe, Y. and Tanaka, H. (2014). Analysis of shoreline behavior on Sendai Coast before and after the 2011 tsunami. *Proceedings of the 34th International Conference on Coastal Engineering*.

Hoang, V. C., Tanaka, H. and Mitobe, Y. (2016). Post-tsunami lagoon morphology restoration. *in Santiago-Fandino, V., Tanaka, H., Spiske, M., (Eds.), Tsunami and Earthquake Impact on Coastal Environments: Significance and Restoration*: Springer, pp. 153-166.

Hoang, V. C., Tanaka, H., Mitobe, Y., Udo, K. and Mano, A. (2017). The Yamamoto Coast over 5 years; the reconstruction of an embankment with tsunami-induced embayment. *in Santiago-Fandino, V., Sato, S., Maki, N., Iuchi, K., (Eds.)*, Springer, Under preparation.

Holland, K. T., Holman, R. A., Lippmann, T. C. and Haines, J. W. (1997). Practical use of video imagery in nearshore oceanographic field studies. *IEEE Journal of Oceanic Engineering, Vol. 22*(1), pp. 81-92

Holman, R. A. and Stanley, J. (2007). The history and technical capabilities of Argus. *Coastal Engineering, Vol. 54*(6-7), pp. 477-491.

Hunt, I. A. (1959). Design of seawalls and breakwaters. *Journal of Waterway and Harbors Division, Vol. 85*(3), pp. 123-152.

ITIC. List of tsunamis. Retrieved from *http://itic.iocunesco.org/index.php?option=com_content&view=category&layout=blog&id=1160&Itemid=1077*.

Jarrett, J. T. (1977). Sediment budget analysis: Wrightsville Beach to Kure Beach, N.C. *Proceedings of the Coastal Sediments '77*, pp. 986-1005.

Johnson, H. K. and Kamphuis, J. W. (1988). N-line model for a large initially conical sand island. *Proceedings of the IAHR Symposium on Mathematical Modelling of Sediment Transport in the Coastal Zone, Copenhagen*, pp. 275-289.

Kaminsky, G. M., Ruggiero, P., Buijsman, M. C., McCandless, D. and Gelfenbaum, G. (2010). Historical evolution of the Columbia River littoral cell. *Marine Geology, Vol. 273*(1-4), pp. 96-126.

Kamphuis, J. W. (1991). Alongshore sediment transport rate. *Journal of Waterway, Port, Coastal and Ocean Engineering, Vol. 117*, pp. 624-640.

Kana, T. W., Hayter, E. J. and Work, P. A. (1999). Mesoscale sediment transport at southeastern U.S. tidal inlets: Conceptual model applicable to mixed energy settings. *Journal of Coastal Research, Vol. 15*(2), pp. 303-313.

Kang, H. and Tanaka, H. (2005). Monitoring of long-term shoreline evolution on Sendai Coast. *Proceedings of the 4th Congress of Environmental Hydraulics and the 14th APD-IAHR Congress*, pp. 1101-1107.

Kang, H. and Tanaka, H. (2006). Influence of cross-shore sediment movement on long-term shoreline change simulation *Proceedings of the 4th IAHR Symposium on River, Coastal and Estuarine Morphodynamics, RCEM 2005, in Parker, G. and Garcia, M. H., River, Coastal and Estuarine Morphodynamics, (Eds.)*: Taylor & Francis, pp. 343-348.

Kang, H. (2006). Study on beach topography change and evaluation of sediment budget on Sendai Coast. *Doctoral dissertation, Tohoku University,* (in Japanese).

Komar, P. D. and Inman, D. L. (1970). Longshore sand transport on beaches. *Journal of Geophysical Research, Vol. 75*(30), pp. 5514-5527.

Kraus, N. C. and Harikai, S. (1983). Numerical model of the shoreline change at Oarai beach. *Coastal Engineering, Vol. 7*(1), pp. 1-28.

Kraus, N. C., Larson, M. and Wise, R. A. (1999). Depth of closure in beach-fill design. *Proceedings of the 1999 National Conference on Beach Preservation Technology*, pp. 268-280.

Kraus, N. C. (2002). Reservoir model for calculating natural sand bypassing and change in volume of ebb-tidal shoals, part I: Description. *ERDC/CHL CHETN-IV-39*, U.S. Army Engineer Research and Development Center.

Kraus, N. C. and Wamsley, T. V. (2003). Coastal barrier breaching, Part 1: Overview of breaching processes. *ERDC/CHL CHETN-IV-56,* U.S. Army Engineer Research and Development Center.

Kraus, N. C. (2010). Engineering of tidal inlets and morphologic consequences. *in Kim, Y. C. (Ed), Handbook of coastal and ocean engineering*: World Scientific, pp. 867-900.

Kuleli, T., Guneroglu, A., Karsli, F. and Dihkan, M. (2011). Automatic detection of shoreline change on coastal Ramsar wetlands of Turkey. *Ocean Engineering, Vol. 38*(10), pp. 1141-1149.

Kuriyama, Y. (2003). Sediment budget analysis with aerial photographs. *Proceedings of the Coastal Sediments '03*, CD-ROM.

Larson, M., Hanson, H. and Kraus, N. C. (1987). Analytical solutions of the one-line model of shoreline change, *Technical Report CERC-87-15*, U.S. Army Engineer Waterways Experiment Station.

Larson, M., Hanson, H. and Kraus, N. C. (1997). Analytical solutions of one-line model for shoreline change near coastal structures. *Journal of Waterway, Port, Coastal, and Ocean Engineering, Vol. 123*(4), pp. 180-191.

Leatherman, S. P. (1983). Shoreline mapping: A comparison of techniques. *Shore and Beach, Vol. 51*, pp. 28-33.

Leatherman, S. P., Davison, A. T. and Nicholls, R. J. (1994). Coastal geomorphology. *in Environmental Science in the Coastal Zone: Issues for Further Research, National Research Council*, 182pp.

Liew, S. C., Gupta, A., Wong, P. P. and Kwoh, L. K. (2010). Recovery from a large tsunami mapped over time: The Aceh coast, Sumatra. *Journal of Geomorphology, Vol. 114*(4), pp. 520-529.

Lippmann, T. C. and Holman, R. A. (1989). Quantification of sand bar morphology: a video technique based on wave dissipation. *Journal of Geophysical Research, Vol. 94*(C1), pp. 995-1001.

Lippmann, T. C. and Holman, R. A. (1990). The spatial and temporal variability of sand bar morphology. *Journal of Geophysical Research, Vol. 94*(C7), pp. 11575-11590.

Maekawa, K. (2010). Chapter 9 Mogami. *in Sawamoto, M. , Mano, A., Tanaka, H., (Eds.), Estuaries in Japan*, pp. 83-93 (in Japanese).

Mano, A., Sawamoto, M. and Nagao, M. (1994). Response characteristics of river mouth topography in wide time scale range. *Proceedings of 24th International Conference on Coastal Engineering*, pp. 3126-3138.

Mano, A., Muhammad, H. and Sawamoto, M. (1996). Annual mean waves for the littoral drift formula. *Proceedings of Civil Engineering in the Ocean, Vol. 12*, pp. 55-59 (in Japanese).

Mano, A., Iida, T., Udo, K. and Tanaka, H. (2013). Breaking process and mechanism of coastal levees on Sendai Bay Coast hit by the 2011 mega tsunami. *Journal of Coastal Research*, pp. 772-777.

Masselink, G. and Gehrels, W. R. (2014). *Coastal environments and global change*: Wiley Works, 448 p.

Miller, J. K. and Dean, R. G. (2007a). Shoreline variability via empirical orthogonal function analysis: Part I temporal and spatial characteristics. *Coastal Engineering, Vol. 54*(2), pp. 111-131.

Miller, J. K. and Dean, R. G. (2007b). Shoreline variability via empirical orthogonal function analysis: Part II relationship to nearshore conditions. *Coastal Engineering, Vol. 54*(2), pp. 133-150.

Minoura, K., Imamura, F., Sugawara, D., Kono, Y. and Iwashita, T. (2001). The 869 Jōgan tsunami deposit and recurrence interval of large-scale tsunami on the Pacific

coast of northeast Japan. *Journal of Japan Society for Natural Disaster, Vol. 23*, pp. 83-88.

Moore, L. J. (2000). Shoreline mapping techniques. *Journal of Coastal Research, Vol. 16*(1), pp. 111-124.

Moore, R. D., Wolf, J., Souza, A. J. and Flint, S. S. (2009). Morphological evolution of the Dee Estuary, Eastern Irish Sea, UK: A tidal asymmetry approach. *Geomorphology, Vol. 103*(4), pp. 588-596.

Mori, F., Mitobe, Y. and Tanaka, H. (2015). Environmental variation of sediment transport due to tsunami around detached breakwaters. *Journal of JSCE, Ser. B3 (Ocean Engineering), Vol. B3-71*, CD-ROM (in Japanese).

Mori, N., Takahashi, T., Yasuda, T. and Yanagisawa, H. (2012). Survey of 2011 Tohoku earthquake tsunami inundation and run-up. *Geophysical Research Letters, Vol. 38*(7), pp. L00G14 (6 pages).

Munoz-Perez, J. J., Medina, R. and Tejedor, B. (2001). Evolution of longshore beach contour lines determined by the EOF method. *Scientia Marina, Vol. 65*(4), pp. 393-402.

NCEI, NGDC/WDS global historical tsunami database. Retrieved from *https://www.ngdc.noaa.gov/hazard/tsu_db.shtml*.

Overton, M., Petrina, C. and Fisher, J. (1996). Determining shoreline position using historical photography and digital softcopy photogrammetry. *ASPRS/ACSM Annual Convention And Expo, Technical Paper, Vol. 1*, pp. 512-513.

Overton, M., Grenier, R., Judge, E. and Fisher, J. (1999). Identification and analysis of coastal erosion hazard areas: Dare and Brunswick Counties, North Carolina. *Journal of Coastal Research, Special Issue No. 28*, pp. 69-84.

Pardo-Pascual, J. E., Almonacid-Caballer, J., Ruiz, L. A. and PalomarVázquez, J. (2012). Automatic extraction of shorelines from Landsat TM and ETM+ multi-temporal images with subpixel precision. *Remote Sensing of Environment, Vol. 123*, pp. 1-11.

Paris, R., Wassmer, P., Sartohadi, J., Lavigne, F., Barthomeuf, B., Desgages, E., Grancher, D., Baumert, P., Vautier, F., Brunstein, D., Gomez, C. (2009). Tsunamis as geomorphic crises: Lessons from the December 26, 2004 tsunami in Lhok Nga, West Banda Aceh (Sumatra, Indonesia). *Geomorphology, Vol. 104*(1-2), pp. 59-72.

Patsch, K. and Griggs, G. (2008). A sand budget for the Santa Barbara littoral cell, California. *Marine Geology, Vol. 252*(1-2), pp. 50-61.

Pelnard-Considere, R. (1956). Essi de theorie de l'evolution des formes de ravage en plages de sables et de galets. *Societe Hydrotechnique de France, IV'eme Journee de L'Hydraulique Question III, Rapport, Vol. 1*, pp. 74-71-10

Perlin, M. and Dean, R. G. (1983). A numerical model to simulate sediment transport in the vicinity of coastal structures. *Report MR-83-10,* US. Army Corps of Engineer, Coastal Engineering Research Center.

Pradjoko, E. and Tanaka, H. (2010). Aerial photograph of Sendai Coast for shoreline behavior analysis. *Proceedings of the 32nd International Conference on Coastal Engineering*.

Rosati, J. D. and Kraus, N. C. (1997). Even-odd function analysis of shoreline position and volume change. *Coastal Engineering Technical Note, CETN IV-10,* U.S. Army Engineer Waterways Experiment Station.

Rosati, J. D. and Kraus, N. C. (1999). Formulation of sediment budgets at inlets. *Coastal Engineering Technical Note CETN-IV-15*, U.S. Army Engineer Research and Development Center, 20 p.

Rosati, J. D. (2005). Concepts in sediment budgets. *Journal of Coastal Research, Vol. 21*(2), pp. 307-322.

Ryu, J.-H., Won, J.-S. and Min, K. M. (2002). Waterline extraction from Landsat TM data in a tidal flat: A case study in Gomso Bay, Korea. *Remote Sensing of Environment, Vol. 83*(3), pp. 442-456.

Sana, A. and Tanaka, H. (2007). Full-range equation for wave boundary layer thickness. *Coastal Engineering, Vol. 54,* pp. 639-642.

Sato, S. and Tanaka, N. (1962). Sand motion on the horizontal bottom under waves. *Proceedings of the 9th Japanese Conference on Coastal Engineering*, pp. 95-100 (in Japanese).

Schlichting, H., Gersten, K. (2000). *Boundary-Layer Theory*. Translated by Mayes, C.: Springer, 801p.

Smith, G. L. and Zarillo, G. A. (1988). Short-term interactions between hydraulics and morphodynamics of a small tidal inlet, Long Island, New York. *Journal of Coastal Research, Vol. 4*(2), pp. 301-314.

Stafford, D. B. (1971). An aerial photographic technique for beach erosion surveys in North Carolina. Washington DC. *Technical Memorandum, No. 36*, U.S. Army Corps of Engineers, Coastal Engineering Research Center, 115 p.

Takashimizu, Y., Urabe, A., Suzuki, K. and Sato, Y. (2012). Deposition by the 2011 Tohoku-oki tsunami on coastal lowland controlled by beach ridges near Sendai, Japan. *Sedimentary Geology, Vol. 282*(0), pp. 124-141.

Tanaka, H. and Takahashi, A. (1995). Short-term shoreline change on Sendai Coast. *Computer Modelling of Seas and Coastal Regions II*, pp. 205-212.

Tanaka, H., Tinh, N. X., Umeda, M., Hirao, R., Pradjoko, E., Mano, A. and Udo, K. (2012). Coastal and estuarine morphology changes induced by the 2011 Great East Japan earthquake tsunami. *Coastal Engineering Journal, Vol. 54*(1), pp. 1250010 (25 pages).

Tanaka, H., Adityawan, M. B. and Mano, A. (2014a). Morphological changes at the Nanakita River mouth after the Great East Japan Tsunami of 2011. *Coastal Engineering, Vol. 86*, pp. 14-26.

Tanaka, H., Adityawan, M. B., Udo, K. and Mano, A. (2014b). Breaching and tsunami water drainage at old river mouth locations during the 2011 tsunami. *Proceedings of the 34th International Conference on Coastal Engineering*.

Tanaka, H., Mitobe, Y. and Hoang, V. C. (2016). Estuarine morphological changes due to the 2015 Kanto-Tohoku Heavy Rainfall and their subsequent recovery. *Tohoku Journal of Natural Disaster Science, Vol. 52*, pp. 67-72 (in Japanese).

Tappin, D. R., Evans, H. M., Jordan, C. J., Richmond, B., Sugawara, D. and Goto, K. (2012). Coastal changes in the Sendai area from the impact of the 2011 Tōhoku-oki tsunami: Interpretations of time series satellite images, helicopter-borne video footage and field observations. *Sedimentary Geology, 282*(30), pp. 151-174.

Thanh, T. M., Mitobe, Y., Hoang, V. C., Viet, N. T. and Tanaka, H. (2015). Coastal morphology change and its relationship with climate characteristics on Nha Trang Coast, Vietnam. *Proceedings of the 5th International Conference on Estuaries and Coasts,* USB.

Thieler, E. R. and Danforth, W. W. (1994). Historical shoreline mapping (I): Improving techniques and reducing positioning errors. *Journal of Coastal Research, Vol. 10*(3), pp. 549-563.

Thomas, R. C. and Frey, A. E. (2013). Shoreline change modeling using one-line models: General model comparison and literature review. *ERDC/CHL CHETN-II-55,* U.S. Army Engineer Research and Development Center.

Tinh, N. X. and Tanaka, H. (2011). Discussion of overwash prevention construction on the northern part of Sendai Coast. *Proceedings of 6th International Conference on Coastal Structures, Yokohama*, CD-ROM.

Tobler, W., Deichmann, U., Gottsegen, J. and Maloy, K. (1995). The global demography project (Technical Report 95-6). *National Center for Geographic Information and Analysis, University of California*.

Townsend, K. E., Thomas, R. C. and Frey, A. E. (2014). Shoreline change modeling using one-line models: Application and comparison of GenCade, Unibest, and Litpak. *ERDC/CHL CHETN-IV-102,* U.S. Army Engineer Research and Development Center.

U.S. Army Corps of Engineers (1984). Shore protection manual. Department of the Army, Waterways Experiment Station, Coastal Engineering Research Center.

U.S. Army Corps of Engineers (2002). *Coastal engineering manual 1110-2-1100, Part III, Chapter 2*, U.S. Army Corps of Engineers.

U.S. Army Corps of Engineers (2006). Map reading and land navigation. *FM 3-25.26,* Headquarters Department of the Army.

Uda, T. and Hashimoto, H. (1982). Description of beach changes using an empirical predictive model of beach profile changes *Proceedings of the 18th International Conference on Coastal Engineering*, pp. 1405-1418.

Uda, T. (1997). *Beach erosion in Japan*: Sankaido Press, 442 p. (in Japanese).

Udo, K., Sugawara, D., Tanaka, H., Imai, K. and Mano, A. (2012). Impact of the 2011 Tohoku earthquake and tsunami on beach morphology along the northern Sendai Coast *Coastal Engineering Journal, Vol. 54*(01), pp. 1250009 (15 pages).

Udo, K., Takeda, Y., Takamura, M. and Mano, A. (2015). Serious erosion of the southern Sendai Coast due to the 2011 Tohoku Earthquake Tsunami and its recovery process. *in Santiago-Fandino, V., Konta, Y. A., Kaneda, Y., (Eds.), Post-Tsunami Hazard - Reconstruction and Restoration, Vol. 44*: Springer, pp. 225-236.

Udo, K., Tojo, K., Takeda, Y., Tanaka, H. and Mano, A. (2016). Characteristics of shoreline retreat due to the 2011 Tohoku Earthquake and Tsunami and its recovery after three years. *in Santiago-Fandino, V., Tanaka, H., Spiske, M., (Eds.), Tsunami and Earthquake Impact on Coastal Environments: Significance and Restoration*: Springer, pp. 113-123.

Valle-Levinson, A. (2010). Definition and classification of estuaries. *in Valle-Levinson, A., (Ed.), Contemporary Issues in Estuarine Physics*: Cambridge University Press, pp. 1-11.

van Rijn, L. C. (1997). Sediment transport and budget of the central coastal zone of Holland. *Coastal Engineering, Vol. 32*(1), pp. 61-90.

Villagran, M., Caamaño, D. and Cienfuegos, R. (2014). Hydrodynamics of a river-associated tidal inlet and maintenance of dynamic equilibrium: preliminary findings. *Journal of Coastal Research*, pp. 592-597.

Walton Jr, T. L. and Chiu, T. Y. (1979). A review of analytical techniques to solve the sand transport equation and some simplified solutions. *Proceedings of Coastal Structures '79*, pp. 809-837.

Walton Jr, T. L. (2002). Even–odd analysis on a complex shoreline. *Ocean Engineering, Vol. 29*(6), pp. 711-719.

Walton Jr, T. L., Dean, R. G. and Rosati, J. D. (2012). Sediment budget possibilities and improbabilities. *Coastal Engineering, Vol. 60*, pp. 323-325.

Winant, C. D., Inman, D. L. and Nordstrom, C. E. (1975). Description of seasonal beach changes using empirical eigenfunctions. *Journal of Geophysical Research, Vol. 80*(15), pp. 1979-1986.

Wright, L. D. (1976). Morphodynamics of a wave-dominated river mouth. *Proceedings of the 15th Coastal Engineering Conference*, pp. 1721-1737.

Work, P. A. and Dean, R. G. (1990). Even/odd analysis of shoreline changes adjacent to Florida's tidal inlets. *Proceedings 20th Coastal Engineering Conference*, pp. 2522-2535.

Yamada, F., Kobayashi, N., Shirakawa, Y. and Sakanishi, Y. (2010). Sediment budgets based on the mass of silt and clay on intertidal flat adjacent to river mouth. *Proceedings of the 32nd International Conference on Coastal Engineering*.